
[All ETDs from UAB](#)

[UAB Theses & Dissertations](#)

1999

An analysis of components influencing the outcome of defibrillation shocks.

James Bradley White
University of Alabama at Birmingham

Follow this and additional works at: <https://digitalcommons.library.uab.edu/etd-collection>

Recommended Citation

White, James Bradley, "An analysis of components influencing the outcome of defibrillation shocks."
(1999). *All ETDs from UAB*. 6417.
<https://digitalcommons.library.uab.edu/etd-collection/6417>

This content has been accepted for inclusion by an authorized administrator of the UAB Digital Commons, and is provided as a free open access item. All inquiries regarding this item or the UAB Digital Commons should be directed to the [UAB Libraries Office of Scholarly Communication](#).

INFORMATION TO USERS

This manuscript has been reproduced from the microfilm master. UMI films the text directly from the original or copy submitted. Thus, some thesis and dissertation copies are in typewriter face, while others may be from any type of computer printer.

The quality of this reproduction is dependent upon the quality of the copy submitted. Broken or indistinct print, colored or poor quality illustrations and photographs, print bleedthrough, substandard margins, and improper alignment can adversely affect reproduction.

In the unlikely event that the author did not send UMI a complete manuscript and there are missing pages, these will be noted. Also, if unauthorized copyright material had to be removed, a note will indicate the deletion.

Oversize materials (e.g., maps, drawings, charts) are reproduced by sectioning the original, beginning at the upper left-hand corner and continuing from left to right in equal sections with small overlaps.

Photographs included in the original manuscript have been reproduced xerographically in this copy. Higher quality 6" x 9" black and white photographic prints are available for any photographs or illustrations appearing in this copy for an additional charge. Contact UMI directly to order.

**Bell & Howell Information and Learning
300 North Zeeb Road, Ann Arbor, MI 48106-1346 USA
800-521-0600**

UMI[®]

**AN ANALYSIS OF COMPONENTS INFLUENCING THE OUTCOME OF
DEFIBRILLATION SHOCKS**

by

JAMES BRADLEY WHITE

A DISSERTATION

**Submitted to the graduate faculty of The University of Alabama at Birmingham,
in partial fulfillment of the requirements for the degree of
Doctor of Philosophy**

BIRMINGHAM, ALABAMA

1999

UMI Number: 9956759

UMI[®]

UMI Microform 9956759

Copyright 2000 by Bell & Howell Information and Learning Company.

**All rights reserved. This microform edition is protected against
unauthorized copying under Title 17, United States Code.**

**Bell & Howell Information and Learning Company
300 North Zeeb Road
P.O. Box 1346
Ann Arbor, MI 48106-1346**

**ABSTRACT OF DISSERTATION
GRADUATE SCHOOL, UNIVERSITY OF ALABAMA AT BIRMINGHAM**

Degree Ph.D. Program Physiology & Biophysics

Name of Candidate James Bradley White

Committee Chair Raymond E. Ideker

Title An Analysis of Components Influencing the Outcome of Defibrillation Shocks

Sudden cardiac death precipitated by ventricular fibrillation is one of the leading causes of mortality in developed countries. The only effective method for treating ventricular fibrillation is by the application of an electric shock across the heart, known as defibrillation. Numerous studies have examined the characteristics of defibrillation shocks and the mechanisms by which these shocks affect the heart, but the exact mechanism by which a defibrillation shock works remains unclear. The main purpose of this dissertation was to further the understanding of defibrillation by examining some of the components that influence defibrillation.

The first study in this dissertation began with an analysis of defibrillation waveforms delivered transthoracically. In this study, we hypothesized that defibrillation success can be reliably predicted using a mathematical membrane model. By using both animal and passive mathematical models, the shape, amplitude, duration, and number of phases of the defibrillation waveforms were varied to determine the effect each has on defibrillation success. The animal and passive mathematical models were then compared to assess the robustness of the mathematical model's predictive power. The method by which these and other shock waveforms alter myocardial activation patterns to produce successful defibrillation shocks was examined in the second and third study with a multichannel epicardial mapping system. Myocardial lesions were created in ventricular

and atrial tissue to ascertain the ability of these lesions to alter the spatial distribution of shock-induced activations. The shock strengths required to activate resting tissue or cardiovert fibrillating tissue were analyzed in conjunction with the activation patterns recorded from the lesion sites.

The results of the first study confirm previous studies showing that waveform shape, duration, amplitude, and number of phases affects the defibrillation threshold. Furthermore, the model used was able to predict the relative defibrillation efficacies of the defibrillation shocks delivered in animals. In the second study, shocks delivered in ventricular tissue with and without an artificially created lesion produced dramatically different activation patterns after the shock. In the presence of the lesion, the area of tissue that is directly activated is greater than the area of tissue activated by the same shock strength before the lesion. Finally, application of lesions to the atria during defibrillation shocks produced a marked decrease in the defibrillation threshold after the shock. In addition to the reduced threshold, the lesion appeared to increase the organization of the atrial fibrillation.

Our data indicate that the simple mathematical model used in our study is applicable to both transthoracic defibrillation and internal defibrillation. Furthermore, it is robust even when comparing waveforms of different shapes and sizes. The activations created in response to shocks in the presence of large myocardial lesions placed in the ventricles provide evidence for myocardial discontinuities in defibrillation. In addition to activations produced as a result of large lesions, the application of lesions to the atria appears to reduce the defibrillation threshold by prompting an increase fibrillatory organization.

DEDICATION

To Mom and Dad, who have continually supported, loved, and understood.

ACKNOWLEDGMENTS

There is a multitude of people, too many to name, that have very unselfishly contributed to this work. Undoubtedly, many of the key figures are the “members” of the Cardiac Rhythm Management Laboratory. The opportunity to work with this world-class group was a tremendous blessing. I am grateful to each and every person that took the time and mustered the patience to work with a non-engineer in an engineering-laden environment.

At the forefront of this work is my mentor, Dr. Raymond E Ideker. He continually challenged me and instilled in me the necessity of pragmatic-scientific thought. I feel very indebted to him for his guidance and the wealth of opportunity that he has provided. I also wish to thank my committee members, Drs. Kathleen H. Berecek, Jack M Rogers, James A Schafer, and Gregory P Walcott, for their dedication of time. A great thanks goes to Dennis Rollins, James Wayland, and Liu Zhu for their much-needed assistance with the mapping systems.

I would like to thank Dr. Nipon “Toon” Chattipakorn for making a great study partner through classes during our first two years. Our conversations, arguments, and travels have been many. It has also been a pleasure to work with Fred Evans and Philip Johnson. Fred has always been a source of humor and provides me with some repose in knowing that someone else in this world shares my unique sense of humor. I thank Philip for teaching me “EE101.” Learning the ins and outs of all those “electrical things” was greatly facilitated by his knowledge.

It is difficult, if not impossible, to find the perfect way to thank my family. My mother and father, Dr. Mary E. White and James H. White, and my brother, Wilson C. White, have always been an inspiration and source of continued support. In addition to teaching me the importance of education, perseverance, and humility, they have always believed in me and provided for me, often with great sacrifice. For all that they have done, I am forever grateful. My last thank you is extended to my dear wife, Abigail Charlotte White. She has always supported me, loved me, and understood me. She is the source of my happiness and the best friend everyone seeks. I love her dearly.

TABLE OF CONTENTS

	<i>Page</i>
ABSTRACT.....	ii
DEDICATION.....	iv
ACKNOWLEDGMENTS.....	v
LIST OF TABLES.....	ix
LIST OF FIGURES.....	xi
LIST OF ABBREVIATIONS.....	xiv
INTRODUCTION AND BACKGROUND.....	1
Introduction.....	1
Shock Characteristics of Defibrillation.....	3
Waveform Duration.....	4
Number of Phases.....	5
Mathematical Models of Defibrillation.....	6
Myocardial Responses to Electric Shocks.....	9
Potential Gradients.....	9
Transmembrane Voltage Changes.....	10
Mechanisms of Defibrillation.....	12
Detrimental Effects of Shocks.....	14
Research Aims.....	15
PREDICTING THE RELATIVE EFFICACY OF SHOCK WAVEFORMS FOR TRANSTHORACIC DEFIBRILLATION IN DOGS.....	26
MYOCARDIAL DISCONTINUITIES: A SUBSTRATE FOR PRODUCING VIRTUAL ELECTRODES THAT DIRECTLY EXCITE THE MYOCARDIUM BY SHOCKS.....	69
MARKED REDUCTION IN ATRIAL DEFIBRILLATION THRESHOLDS BY A SINGLE LINEAR ABLATION LESION.....	107

TABLE OF CONTENTS (Continued)

	<i>Page</i>
SUMMARY AND FUTURE RESEARCH.....	148
Limitations.....	150
Research Implications.....	151
Future Research.....	152
LIST OF REFERENCES.....	154
APPENDIX: ANIMAL USE APPROVAL.....	161

LIST OF TABLES

<i>Table</i>	<i>Page</i>
MYOCARDIAL DISCONTINUITIES: A SUBSTRATE FOR PRODUCING VIRTUAL ELECTRODES THAT DIRECTLY EXCITE THE MYOCARDIUM BY SHOCKS	
1 Minimum Current Required to Activate All Columns of the Mapped Area, mA.....	76
2 Minimum Current Required to Activate Area Adjacent to Transmural Incision, mA.....	77
3 Interval from Beginning of S1 Stimulus to Activation at Electrode #254, ms.....	78
4 Interval from Beginning of S2 Stimulus to Activation at Electrode #254, ms.....	79
5 Parameters for Simulations.....	88
MARKED REDUCTION IN ATRIAL DEFIBRILLATION THRESHOLDS BY A SINGLE LINEAR ABLATION LESION	
1 ADFT Comparisons for Animals Before and After RF Application.....	119
2 Quantification of AF on Left Atrium Before and After LA Lesion.....	120
3 Quantification of AF on Left Atrium Before and After RA Lesion.....	121
4 Quantification of AF on Right Atrium. Before and After RA Lesion (vs LA, Table 3).....	122
5 Postshock Activations Following Successful and Failed ADFT Shocks.....	123
6 Earliest Postshock Activation Times on Left Atrium Before and After LA Lesion.....	124
7 Earliest Postshock Activation Times on Left Atrium Before and After RA Lesion.....	125

LIST OF TABLES (Continued)

<i>Table</i>	<i>Page</i>
8 Earliest Post-Shock Activation Times on Right Atrium. Before and After RA Lesion.....	126

LIST OF FIGURES

<i>Figure</i>	<i>Page</i>
INTRODUCTION AND GENERAL BACKGROUND	
1 Illustrations of the waveforms used for defibrillation—a historical perspective.....	18
2 The strength-duration relationship for current, energy, and charge for square waves.....	19
3 Monophasic versus biphasic shocks.....	20
4 Conditions necessary for producing critical point reentry.....	21
5 The graded response produced by an S2 stimulus generating a potential gradient of 8.4 V/cm oriented along the long axis of the myofibers.....	22
6 The mean and standard deviation of the peak ΔV_m during shocks delivered during the action potential plateau.....	23
7 The effect of myocardial discontinuities on current flow.....	24
8 Transmembrane isopotential contours in response to an extracellular cathodal current (4 mA/mm) derived from the bidomain model.....	25
PREDICTING THE RELATIVE EFFICACY OF SHOCK WAVEFORMS FOR TRANSTHORACIC DEFIBRILLATION IN DOGS	
1 The model response to 3 monophasic waveform shapes with a time constant equal to 2.8 ms.....	47
2 The model responses for 3 biphasic waveforms with the membrane time constant equal to 2.8 ms.....	49
3 Strength-duration curves for peak current and energy.....	51

LIST OF FIGURES (Continued)

<i>Figure</i>	<i>Page</i>
4 Monophasic waveform strength-duration relationships determined experimentally in part 1 of the study.....	53
5 Experimental thresholds plotted against the model thresholds for peak current and energy for the monophasic waveforms in part 1 of the study.....	55
6 Effect of the membrane time constant on the summed square error of the model data compared with the experimental data.....	57
7 Strength-duration relationships for the biphasic waveforms studied in Part 2 of the study.....	59
8 The experimental DFTs in part 2 plotted against the decrease in the model response during the second phase expressed as a percent of the peak model response during the first phase.....	61
9 Strength-duration relationships for the biphasic waveforms studied in part 3 of the study.....	63
10 Experimental thresholds obtained in part 3 plotted against the second-phase model response.....	65
11 Mean DFTs and second phase model responses for the biphasic waveforms that had a first phase equal to a 30-ms ascending ramp and a second phase equal to a descending ramp in parts 2 and 3 of the study.....	67
MYOCARDIAL DISCONTINUITIES: A SUBSTRATE FOR PRODUCING VIRTUAL ELECTRODES THAT DIRECTLY EXCITE THE MYOCARDIUM BY SHOCKS	
1 Illustration of the effect of an intracellular discontinuity on intracellular current flow.....	94
2 A representation of the mapped area on the right ventricle.....	96
3 Isochronal maps representing activation patterns arising from cathodal stimuli for one animal.....	97
4 Electrogram tracings recorded from row 6 of electrodes during activation sequences in Figure 3.....	99

LIST OF FIGURES (Continued)

<i>Figure</i>	<i>Page</i>
5 Isochronal maps representing activation patterns arising from anodal stimuli for one animal.....	101
6 Electrogram tracings recorded from row 5 of electrodes during the activation sequences in Figure 5.....	103
7 Results from bidomain simulations.....	105
MARKED REDUCTION IN ATRIAL DEFIBRILLATION THRESHOLDS BY A SINGLE LINEAR ABLATION LESION	
1 A depiction of the location of the recording plaques with respect to the atria.....	136
2 Activation maps illustrating the 4 types of postshock activation Patterns.....	138
3 Activation maps of epicardial activations recorded from the LA before and after a linear lesion was created in the LA.....	140
4 Activation maps of epicardial activations recorded from both the LA and RA before and after RFA in the RA.....	142
5 A scatter plot indicating the relationships between postshock interval, shock strength, and shock outcome.....	144
6 ERPs recorded before and after administration of acetyl β -methylcholine.....	146

LIST OF ABBREVIATIONS

ADFT	Atrial defibrillation threshold
AF	Atrial fibrillation
DFT	Defibrillation threshold
ERP	Effective refractory period
IAD	Internal atrial defibrillator
ICD	Implantable cardioverter-defibrillator
LA	Left atrium
LAL	Left atrial lesion
LV	Left ventricle
RA	Right atrium
RAL	Right atrial lesion
RC	Resistor-capacitor
RFA	Radiofrequency ablation
SVC	Superior vena cava
VF	Ventricular fibrillation
V_m	Transmembrane potential

INTRODUCTION AND BACKGROUND

Introduction

One of the leading health threats in the industrialized world is sudden cardiac death. Sudden cardiac death is defined as the unexpected natural death from a cardiac cause within a short period of time, generally ≤ 1 hour from the onset of symptoms.¹ The primary culprit in sudden cardiac death, ventricular fibrillation (VF), is characterized as the onset of electrical instability within the ventricular myocardium resulting in the heart's inability to maintain a normal perfusing pressure. The subsequent lack of systemic circulation produces an immediate deprivation of oxygen to the brain, followed by death in minutes.

VF is thought responsible for approximately 1000 deaths each day.² It is the most common and often the first manifestation of coronary artery disease and is responsible for nearly 50% of the mortality from cardiovascular disease in the United States.³ There are numerous other predisposing factors commonly leading to VF; an incomplete list includes age, race, gender, hypertension, diabetes, and smoking.³

Since the discovery of VF, two primary treatments have dominated the management of VF—pharmacological therapy for the prevention of onset of VF and electric countershock, or defibrillation for restoration of sinus rhythm once arrhythmia onset has occurred. As both of these treatment modalities have evolved, superiority of defibrillation over antiarrhythmic drug regimens has been demonstrated.^{4,5} However, despite recent successes in defibrillation therapy such as the implantable cardioverter defibrillator

(ICD) and the automatic external defibrillator, defibrillation remains poorly understood, and the challenges to improve defibrillation are great.

In addition to the challenges associated with VF, an equally perplexing problem is atrial fibrillation (AF). AF is one of the most commonly diagnosed arrhythmias, and, although not necessarily lethal, AF is associated with an increased risk for stroke. AF, like VF, can be terminated by electric countershock. One obstacle preventing the widespread implantation of atrial defibrillators, however, is the pain experienced by the awake patient when receiving the electric shock. Consequently, efforts to eliminate this shock-associated pain have become a main focus of AF research.

For decades, efforts have focused on improving the efficacy of a defibrillation shock while reducing the strength needed to deliver the shock. Among some of the avenues of exploration are waveform design, pacing therapy,⁶ electrode placement, and multiphasic shocks.⁷ Many studies have attempted to clarify some of the underlying mechanisms of defibrillation, yet no clear answer has evolved. Many theories exist and some hypotheses have been demonstrated experimentally; however, no one hypothesis is capable of fully explaining the means by which a shock defibrillates.

Therefore, in an attempt to remove an inch from the mile of complexity associated with defibrillation, the work in this dissertation was designed to address some of the unknowns. To completely appreciate the individual contribution of each study and the congruence among them, a review of the less intuitive concepts is provided.

Shock Characteristics of Defibrillation

Shock characteristics important for defibrillation include those dealing with the waveform and those dealing with the electrodes through which the waveform is delivered. Waveform characteristics include shape, duration, and number of phases. Electrode characteristics include number, location, size, and material. For the purpose of this dissertation, a review is offered of waveform characteristics and of how the electric field generated by shocks delivered through the electrodes influences the transmembrane potential leading to defibrillation.

The first human defibrillation by internal and external electrodes was delivered with 60-Hz alternating current,^{8,9} the same type of current now frequently used to induce fibrillation. Subsequent waveforms for external defibrillation included the underdamped and critically damped sinusoids.¹⁰⁻¹² These waveforms require large inductors and therefore are impractical for ICDs, even though some of these waveforms may have a lower defibrillation threshold than a biphasic truncated exponential waveform.¹³ The straight capacitor discharge waveform¹⁴ does not require an inductor, but its prolonged voltage tail was thought to reinduce fibrillation.¹⁵ To circumvent this problem, the truncated capacitor discharge waveform was introduced in which shock delivery is halted before the exponentially decaying voltage becomes very low. As a result, the biphasic truncated exponential waveform has subsequently become the waveform of choice for defibrillation (Figure 1).

Waveform Duration

The significance of waveform duration as it applied to electrical stimulation was first characterized by Hoorweg¹⁶ and Weiss.¹⁷ They constructed linear charge and hyperbolic current and energy strength-duration curves based on monophasic rectangular pulses. Lapicque further distinguished these electrical phenomena by introducing the “rheobase” and “chronaxie”.¹⁸ Koning et al,¹⁹ however, were the first to publish the strength-duration relationship for defibrillation (Figure 2), substantiating the qualitative similarity between stimulation and defibrillation. The relationship between shock strength and duration for both monophasic (single phase) and biphasic (dual phase) waveforms has since been studied extensively.¹⁹⁻²²

Monophasic waveforms tested experimentally^{14,21} exhibit strength-duration characteristics similar to those first produced by Koning. Curves for current require a larger strength to defibrillate at shorter durations than at longer durations. Energy curves are also duration dependent with energy high at very short and long durations (Fig 2) but low at the chronaxie. The strength-duration characteristics of the monophasic waveforms have also been tested using mathematical models introduced by Kroll²³ and Walcott et al²⁴ (discussed below). These models were able to predict the relative defibrillation efficacy of waveforms as capacitance and waveform time constant were varied.

When the second phase is held constant, the first phase of the biphasic waveform generates strength-duration curves that are comparable to those of the monophasic waveform. A second phase duration that is equal to or less than the duration of the first phase is often more efficient at defibrillating than waveforms with second phase durations longer than the first.^{22,25,26}

Number of Phases

Most of the experimental evidence suggests that the biphasic waveform defibrillates at lower strengths than equivalent monophasic waveforms.²⁷⁻²⁹ Factors that can influence the efficacy of the biphasic waveform are the duration ratio of the second phase to the first phase, the tilt of each phase, and the magnitude of each phase.

A monophasic shock has been shown to alter activation fronts by creating new action potentials or extending the duration of existing action potentials. These shock-induced changes are thought responsible for creating the conditions necessary for successful defibrillation. Some of the theories constructed to explain these changes are the critical mass hypothesis³⁰ and the upper limit of vulnerability hypothesis.³¹ The critical mass hypothesis states that to successfully defibrillate, a shock must halt activation fronts only within a critical mass of fibrillating tissue. The upper limit of vulnerability hypothesis, however, states that shocks must not only stop activation fronts throughout the myocardium, but they must also prevent the formation of new activation fronts that could reinitiate fibrillation. The biphasic waveform has also been applied to these hypotheses, although some controversy exists over which phase of the biphasic waveform is the defibrillating phase. One theory suggests that the first phase of the biphasic waveform actually serves to defibrillate and that the second phase removes the excess voltage from the cell membrane.^{24,32} Removing the residual charge, or “burping” the membrane, is believed to prevent refrillation by removing the slow decay of the transmembrane potential after a monophasic waveform (Figure 3A).³² Other evidence suggests that the second phase of the biphasic waveform defibrillates the heart.^{33,34} These studies indicate that the first phase is a preconditioning period that hyperpolarizes the membrane to

prepare the sodium channels for activation by the second phase. For monophasic and biphasic shocks delivered at the same coupling interval, Jones et al³⁵ have shown that the biphasic waveform will elicit an action potential before the monophasic waveform (Figure 3B), although earlier studies by Daubert et al³⁶ contradict these findings. Regardless of whether the second phase serves to restore membrane voltage or defibrillate the heart, recent work in both animals²² and humans³⁷ has shown that it may be the amplitude of this phase that is more critical for successful defibrillation than the duration.

Triphasic waveforms were introduced with the idea that the first two phases would have the increased defibrillation efficacy of biphasic waveforms and that the third phase would reduce the detrimental effects of the shock.³⁸ Yet, studies by Dixon et al²⁵ and Chapman et al³⁹ showed that the triphasic waveforms required higher strength shocks for defibrillation than did the biphasic waveform. However, Huang et al^{40,41} have recently shown that triphasic waveforms at certain tilts and durations have defibrillation thresholds that are equal to or lower than some biphasic waveforms.

Mathematical Models of Defibrillation

Models that simulate defibrillation are constantly evolving as more information is gained from experimental studies. Active membrane models include the dynamic components of the heart such as the flux of membrane currents. These models can be constructed in multiple dimensions and are often complex and computationally intensive. On the other hand, passive membrane models can be as simple as a mere representation of the capacitive and resistive aspects of the cell. Often, passive models are presented as a single unit that is assumed to represent the behavior of the entire heart. The simplistic

nature of these models make them easier to use and interpret. For this dissertation, only the passive model was used, and the ensuing discussion on mathematical models is confined to these models.

The mathematical models of defibrillation were based on the earlier models of stimulation because the strength-duration relationship of stimulation and defibrillation were found to be qualitatively similar.²⁴ Kroll²³ was one of the first to apply the earlier models of stimulation to defibrillation. Using the Weiss-Lapique models of stimulation, the equations were solved for an effective current that was equal to the rheobase current:

$$I_e = \frac{I_{AVE}}{1 + \frac{d_c}{d}} \quad (1)$$

where I_e = the effective current, I_{ave} = current averaged over the pulse duration, d_c = chronaxie; and d = pulse duration. Using this formula while making other mathematical substitutions, Kroll²³ was able to define “optimal” parameters for pulse duration (2.83 ms), tilt (73%), and capacitance (43uF) for monophasic waveforms.

Kroll³² further extended the monophasic model to incorporate biphasic waveforms. The main idea behind the biphasic model was that the second phase of the biphasic waveform serves to remove excess charge that was deposited on the cell membrane by the first phase. The first phase of this model is created mathematically just as the monophasic waveform was in the monophasic model, by using the Weiss-Lapique hyperbolic formula. In this model, the second phase serves to restore the membrane voltage to near zero after the first phase. The optimal duration that meets that criterion is computed in this model with the following equation:

$$d_2(\text{opt}) = \left[\frac{\tau_s \tau_m}{\tau_s - \tau_m} \right] \ln \left\{ 2 - \left[\frac{e^{-\frac{d}{\tau_m}}}{e^{-\frac{d}{\tau_s}}} \right] \right\} \quad (2)$$

where τ_s = shock time constant, τ_m = membrane time constant, and d = first phase duration. The second-phase equation takes into account both the passive response of the membrane after the first phase the active response generated by the second phase.

Walcott et al²⁴ have also generated a mathematical model for defibrillation based on earlier stimulation formulations. Using concepts of Blair,⁴² this defibrillation model was presented as a parallel RC circuit that described the cell membrane averaged across all or part of the heart. Unlike the model produced by Kroll, which uses a hyperbolic relationship, this model uses an exponential relationship where the first phase model response is defined

$$V(t) = \frac{I_o \gamma}{C_m} e^{-\frac{t}{\tau}} (e^{\frac{d}{\tau}} - 1) \quad (3)$$

where I_o = leading edge current, τ_m = membrane time constant, C_m = network capacitance, and $\gamma = \tau_s \tau_m / (\tau_s - \tau_m)$. As in Kroll's model, the second phase of the biphasic waveform for this model is optimal if it returns $V(t)$ to its starting point at the time the shock was given.

One difference in this model from the Kroll model is that this model incorporates the waveform time constant into the equations rather than making approximations for waveform shape as does the Kroll model. Furthermore, this model, like all passive models, makes many assumptions about the state of tissue during the shock. This model assumes that the membrane is in a single state and that both phases of the biphasic waveform are delivered during that state. Other groups have since used both the Kroll

model and the Walcott model for defibrillation studies, some with minor modifications.^{43,44}

Myocardial Responses to Electric Shocks

Potential Gradients

Electrical shocks produce a distribution of potential gradients throughout the heart.⁴⁵ The potential gradient is greatest near the defibrillating electrodes and lowest at some distance away from the electrodes. For a defibrillation shock to be effective, it is thought that a certain minimum potential gradient must be achieved throughout the heart.⁴⁵ Experiments have shown this minimum gradient to be different for different waveforms. For a typical monophasic waveform, it is around 6 V/cm, and for an efficacious biphasic waveform it is lower, near 4 V/cm.⁴⁶

The strength of the potential field generated by a defibrillation shock not only determines whether a defibrillation shock succeeds or fails, but also determines the sites of early activation after the shock and their subsequent propagation. For shocks that produce very low potential gradients throughout the heart, there can be multiple sites of activation, both far away from and near the defibrillating electrodes.⁴⁷ These sites of activation may contribute to failed defibrillation by creating reentrant loops via a critical point mechanism (Figure 4). Critical points are generated by the intersection of a critical state of tissue recovery with a critical potential gradient resulting in tissue states that establish unidirectional block and unidirectional propagation conducive to circuitous movement.⁴⁸ As shock strengths are increased, the sites of early activation are shown to move away from the stimulating electrodes toward the lower potential gradient. Eventu-

ally, a shock strength is reached that removes the critical gradient needed to form critical points, thereby resulting in successful defibrillation. There is some evidence that suggests biphasic waveforms are superior to monophasic waveforms because they produce critical points under a different set of circumstances than do monophasic waveforms.⁴⁹ Efimov et al⁵⁰ have shown that some biphasic waveforms may eliminate conditions necessary for critical point reentry by reducing the large gradients of polarization produced by monophasic shocks. It has been demonstrated that the second phase of the biphasic waveform removes the large polarization gradient created by the first phase. Because monophasic waveforms lack the second phase, the large polarization gradients created by these waveforms can lead to reentry via the creation of phase singularities (critical points).

Transmembrane Voltage Changes

To understand the means by which the electric field produces the changes in tissue refractoriness, it is important to understand how the shock affects the action potential. If a cell is recovered at the time of the shock, a new action potential will be elicited. This will occur near the electrodes and at distances away from the electrodes if the potential gradient reaches a minimum threshold. For those cells that are not fully recovered, there may or may not be a change in the action potential. Cells that have just fired are completely refractory and as such are incapable of an active response because the ionic channels responsible for depolarization of the cell are inactive. As the cell begins to repolarize, as occurs during the relative refractory period, more depolarizing currents become available, and if the shock strength is great enough, depolarization may

again occur during that time. This depolarization occurring before the action potential has fully recovered is termed the graded response,⁵¹ which is accompanied by an extension of refractoriness (Figure 5).⁵² This extension of refractoriness is thought to occur only for shocks that exceed the minimum potential gradient for defibrillation. As such, the mechanism of defibrillation has been closely linked to the ability of a shock to create new action potentials and to cause the extension of refractoriness in existing action potentials.^{53,54}

The changes in the action potential in response to a shock have been shown to be polarity dependent. Directly under a stimulating electrode, cathodal stimuli depolarize tissue, whereas anodal stimuli hyperpolarize tissue. The magnitude of these polarizations initially increases with increases in shock strength. As shock strengths are increased further, changes in V_m plateau, indicating that the strength of the electric field is not linearly related to the change in the transmembrane potential. Furthermore, these changes with polarity have been shown to be asymmetrical when delivered during the plateau phase of the action potential--an anodal shock will produce a larger hyperpolarization than will the same strength cathodal shock produce a depolarization (Figure 6). It is possible that the asymmetric response of the tissue is due to the direction of net current flow across the membrane during the time of stimulation, with a higher impedance to current flow in one direction compared with the other across the cell membrane.⁵⁵ It is also possible that in addition to charging the membrane, a shock may alter the active processes in the membrane, such as the conductivities of the ionic channels, leading to a larger hyperpolarization than depolarization.

Changes in the transmembrane potential under stimulating electrodes are well understood and have been characterized by numerous theoretical and experimental studies. For defibrillation, however, changes in the transmembrane potential must also occur far away from the defibrillating electrodes. The mechanism by which this occurs is less well understood. Two prominent theories exist that may provide a plausible explanation for these changes—they are the secondary source model and the bidomain formulation.

Mechanisms of Defibrillation

Secondary source model. The secondary source model suggests that areas of polarization resulting from changes in the transmembrane potential arise where the myocardium is discontinuous. Discontinuities, whether physiological or pathological, interrupt the intracellular space, forcing current to redistribute across the membrane (Figure 7). These changes in current flow produce virtual electrodes that, if of sufficient magnitude, can directly activate tissue in the polarized region. Since current redistributes across the membrane on both sides of the discontinuity, hyperpolarization and depolarization would be expected at the discontinuity. One of the earliest studies to incorporate the concept of secondary sources was that of Plonsey and Barr.⁵⁶ Through mathematical simulations, they proposed that changes in the transmembrane potential occur at cell boundaries because of high resistance gap junctions. During a shock, it was postulated that these “saw-tooth”-like changes occur throughout the myocardium, providing near-field and far-field cellular alterations in the transmembrane potential. Thus far, this model of defibrillation has not been observed experimentally. More recent models have

suggested that the periodic polarization observed with the saw-tooth concept may occur at bundles of tissue produced by larger tissue inhomogeneities such as interstitial septa.⁵⁷ Using optical mapping techniques, secondary sources have been verified adjacent to intercellular clefts in neonatal myocytes.⁵⁸ The dimensions of the cleft determined the strength of the secondary source, suggesting that some cellular interruptions may produce regions of secondary sources throughout the heart during a defibrillation shock. In addition to naturally occurring tissue discontinuities, pathological interruptions may also contribute to defibrillation success.

Bidomain model. The bidomain formulation is a model based on the anisotropic nature of the heart. It depends on the differences in electrical conductivity between the intracellular and extracellular space both along and across fibers. The anisotropy of both compartments is quite different, with the intracellular space having a conductivity that is about ten times higher in the longitudinal direction than in the short axis of the fiber. The extracellular space has a longitudinal conductivity that is only twice that of the short axis. It is the difference in the anisotropy ratios that leads to some of the unusual transmembrane changes observed during and after a shock. Unlike the secondary source model, the bidomain theory accounts for polarizations that occur with changes in fiber orientation and potential gradient distribution. As fibers curve, the magnitude of external current flowing along the fiber is different at every point, thus preventing the equilibration between intracellular and extracellular currents and causing continuous current redistribution and subsequent transmembrane potential changes. A similar explanation can be used to describe changes that occur as a result of spatially nonuniform potential

gradients—the magnitude of current at points along fibers is different due to a nonuniform electric field. Using bidomain theory, Sepulveda and others⁵⁹ were able to show areas of depolarization and hyperpolarization both under and adjacent to stimulating electrodes (Figure 8). This “dog bone” pattern of polarization was subsequently shown experimentally for both point^{60,61} and line⁶² stimulation. The dog-bone patterns of polarization have since been used to describe make-and-break excitation⁶¹ as well as stimulus induced reentry.⁶³ More recently, bidomain effects have been implicated in a mechanism for failed defibrillation.⁶⁴ It has been suggested that dog bone-like patterns created by stimuli produce a dispersion of polarizations near the stimulating electrodes that can then lead to reentry.⁶⁴

The mechanisms responsible for defibrillation are surely complex and are not likely due to any one model. In truth, it is probably the combination of these models that contribute to the transmembrane changes associated with defibrillation shocks. Recent work, both theoretical^{57,65} and experimental,^{66,67} has begun to consider the probable synergistic relationship of the bidomain model and secondary source model in constructing a realistic representation of defibrillation.

Detrimental Effects of Shocks

Since the potential gradient distribution through the heart is highly uneven, in order to exceed the minimum potential gradient where the shock field is weakest on the heart, high potential gradients are created near the defibrillation electrodes. These strong shock strengths have numerous detrimental effects including bradycardia,⁶⁸ atrioventricular block,⁶⁹ conduction block,⁷⁰ tachyarrhythmias,⁷¹ fibrillation,⁷² necrosis,⁷³ and

death.⁷⁴ Studies have shown that once the potential gradient exceeds 50 V/cm, temporary conduction block occurs.⁷⁵ As the gradients are increased to 100 V/cm or greater, ectopic beats have been shown to arise that may reinduce fibrillation.⁷⁰ As the strength is increased further, the cell is incapable of repairing itself and, therefore, necrosis or cell death occurs.

Responsible for many of the detrimental effects of electrical shocks may be pores that are formed in the membrane as a result of electroporation. Shown to occur at transmembrane potentials greater than $\pm 200\text{mV}$,⁷⁶ these pores permit the passive flow of ions and current across the membrane that would otherwise be impermeable. The passage of these electrical components may then alter excitability, resulting in abnormal electrical events. Near the defibrillating electrodes, electroporation is thought responsible for the saturation of the transmembrane potential that was shown to occur in isolated preparations.⁷⁷ Theoretical models have since supported this notion and further suggested that electroporation may improve defibrillation by reducing the unequal distribution of charge near the shocking electrodes.^{78,79} Aside from cell damage occurring from electroporation, formation of free radicals⁸⁰ and sterical changes to ionic pumps⁸¹ have also been isolated as sources of cell damage.

Research Aims

The overall goal of this dissertation was to provide a clearer understanding of the characteristics associated with defibrillation shocks and how those shocks affect the myocardium.

The first study was an external defibrillation study that utilized animal models and a computer model to assess the effectiveness of different shock waveforms on the outcome of defibrillation. Previous internal defibrillation studies demonstrated the ability of a simple computer model to predict the optimal waveforms for defibrillation. We hypothesized that the same computer model used to reliably predict waveforms for internal defibrillation could also reliably predict the relative defibrillation efficacy for shock waveforms delivered transthoracically. Therefore, using a simple computer model designed to mimic the passive properties of the heart, waveforms were predicted and compared with the experimental outcomes of those waveforms to determine the model's power of prediction.

The means by which a delivered shock, external or internal, affects the transmembrane potential is not completely understood. The purpose of the second study was to broaden this understanding. Using the secondary source model of defibrillation as our paradigm, we hypothesized that an artificially created discontinuity would produce activations at the time of the shock near the discontinuity. We further proposed that activations created via a secondary source mechanism would enhance shocks by increasing the area of the myocardium affected by the shocks. Based on the activations observed from the electrical recordings, we were then able to infer changes that occur to the transmembrane potential and deduce possible mechanisms by which the shock-induced activations arose.

The second study determined the effect of a large discontinuity on activation patterns when shocks were delivered in diastole. The goal of the final study was to assess any changes that occur to activation patterns before, during, and after atrial defibrillation

shocks are delivered in the presence of a discontinuity strategically placed in the atrial myocardium. In addition to activation pattern analysis, the effect of a large lesion on the atrial defibrillation threshold was also investigated. We hypothesized that a large lesion placed in the atria could simplify activation patterns and reduce atrial defibrillation thresholds. To test this hypothesis, we chose a clinically relevant scenario that utilizes radio frequency ablation to create a discontinuity in the atria. Determining the changes in the atrial defibrillation threshold and the AF activation patterns may provide evidence for the role of discontinuities in defibrillation.

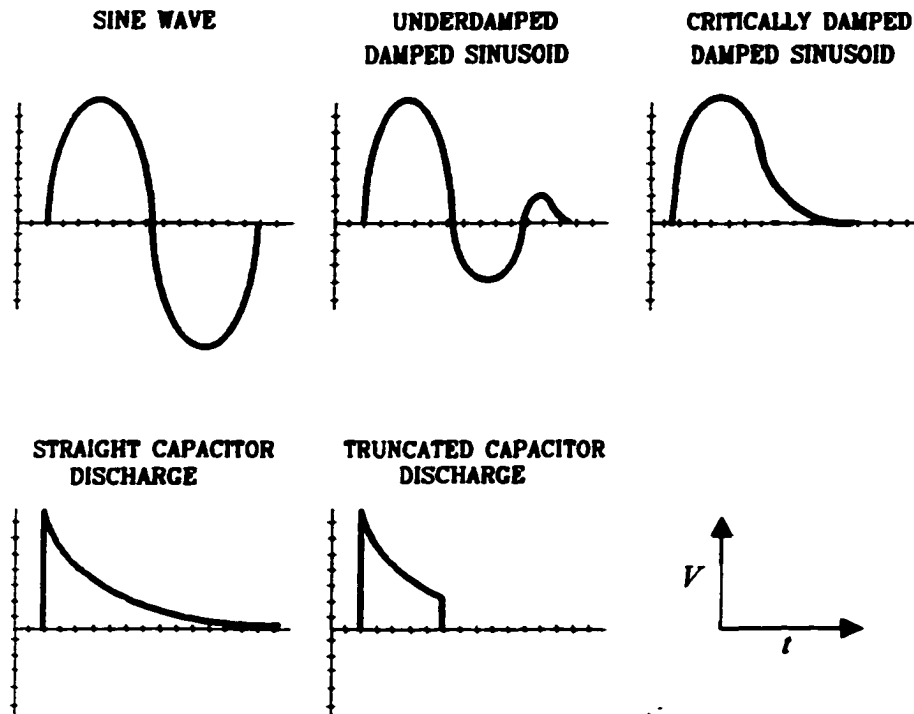


Figure 1. Illustrations of the waveforms used for defibrillation—a historical perspective. The sine wave waveform was one of the first defibrillation waveforms used. The underdamped and critically damped sinusoids were among the next generation of defibrillation waveforms. The straight capacitor discharge waveform was created to eliminate the need for inductors in defibrillation. And finally, the truncated capacitor discharge waveforms evolved to eliminate the low voltage tail associated with the earlier waveforms. (Figure modified with permission from Troup, PJ. Implantable Cardioverters and Defibrillators. Current Problems in Cardiology. Year Book Medical: page 730, 1989.)

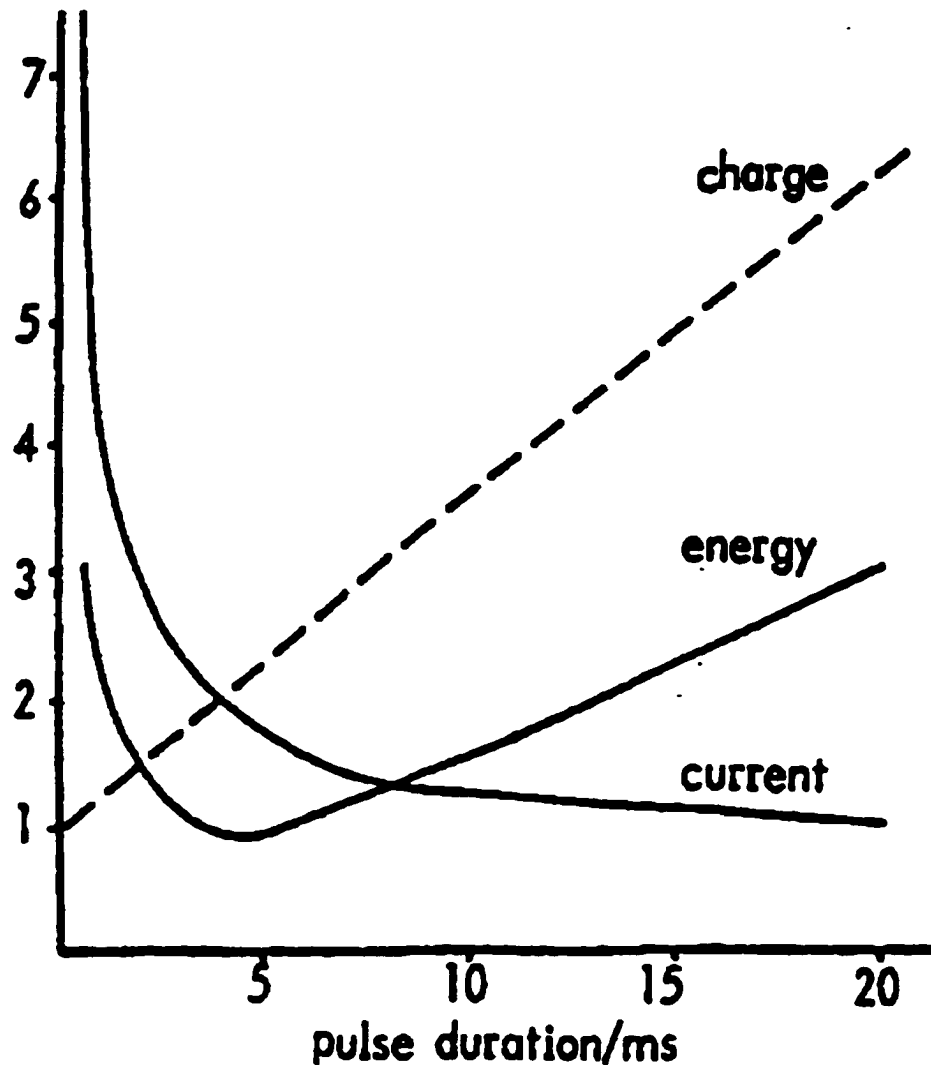


Figure 2. The strength-duration relationship for current, energy, and charge for square waves. Minimum intensities I_{\min} : current = 11 mA/g; energy = 8 mJ/g; Charge = 40 μ C/g. The current on the y axis is normalized by dividing by I_{\min} . The rheobase is defined as the threshold current for an infinitely long duration pulse. Chronaxie is defined as the duration for a current pulse of twice rheobase intensity. (Figure with permission from Koning G, Schneider H, Hoelen AJ et al.: Amplitude-duration relation for direct ventricular defibrillation with rectangular pulses, Med Biol Eng, vol 13, page 389, 1975.)

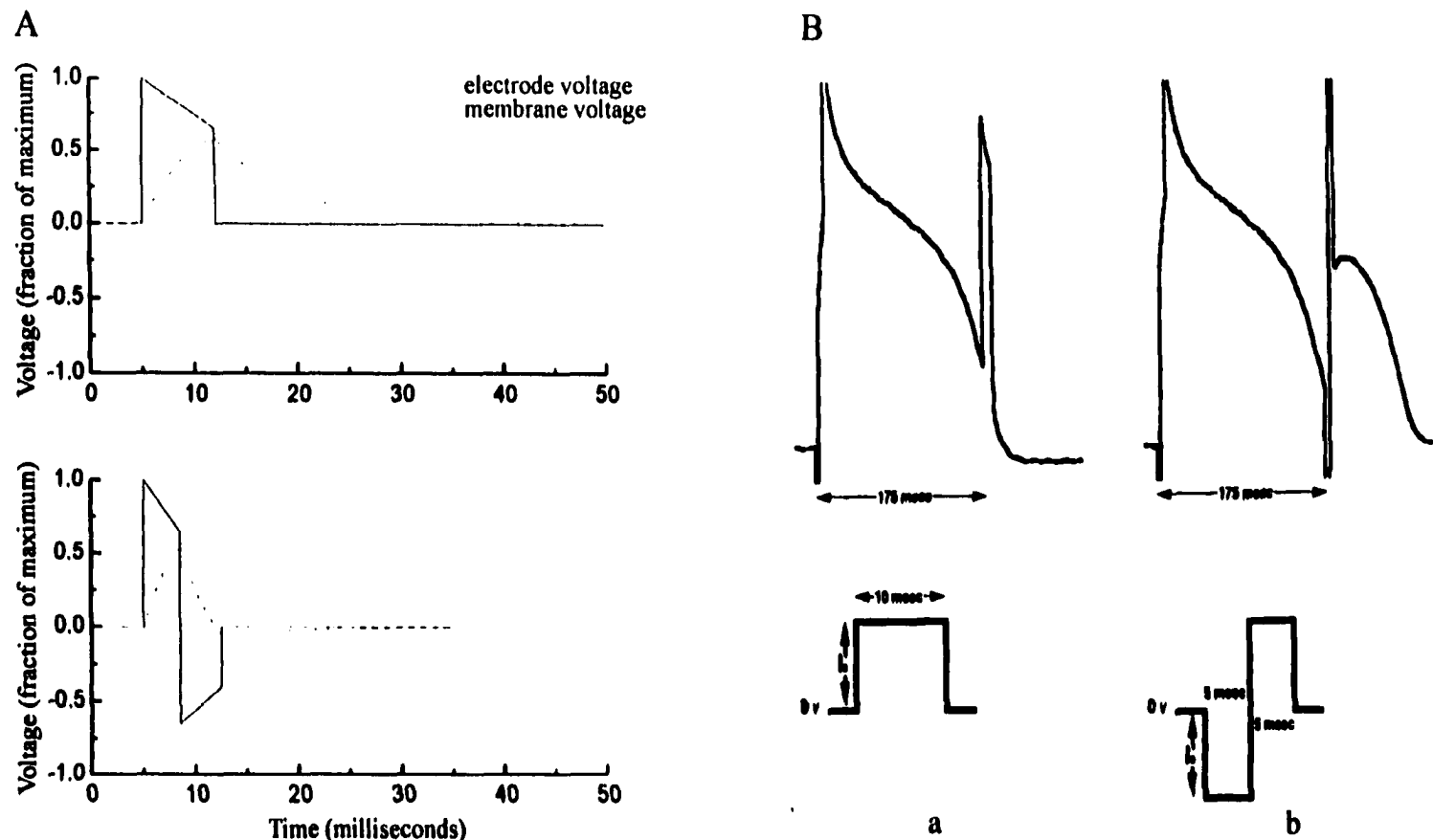


Figure 3. Monophasic versus biphasic shocks. A, top, Electrode and membrane voltages for a 7.5 msec monophasic (top) and a 3.5/3.5 msec biphasic (bottom) waveform from a 150-uF capacitor and 50-Ohm electrode resistance. For the same waveform total duration, the biphasic waveform forces the membrane voltage to baseline more quickly than the membrane naturally decays to baseline following the monophasic waveform. B, Postshock responses produced by a 10-ms monophasic (left) and a 5/5-ms biphasic (right) electric field stimulus delivered at 1.5 times diastolic threshold. Because the first phase of the biphasic waveform is thought to restore sodium channels, the second phase is capable of eliciting an action potential whereas the monophasic waveform is not. (Panel A modified with permission from Kroll MW: A minimal model of the single capacitor biphasic defibrillation waveform, PACE, vol 17, page 1783, 1994. Panel B with permission from Jones JL and Tovar OH: The mechanism of defibrillation and cardioversion, Proc IEEE, vol 84, page 396, 1996.)

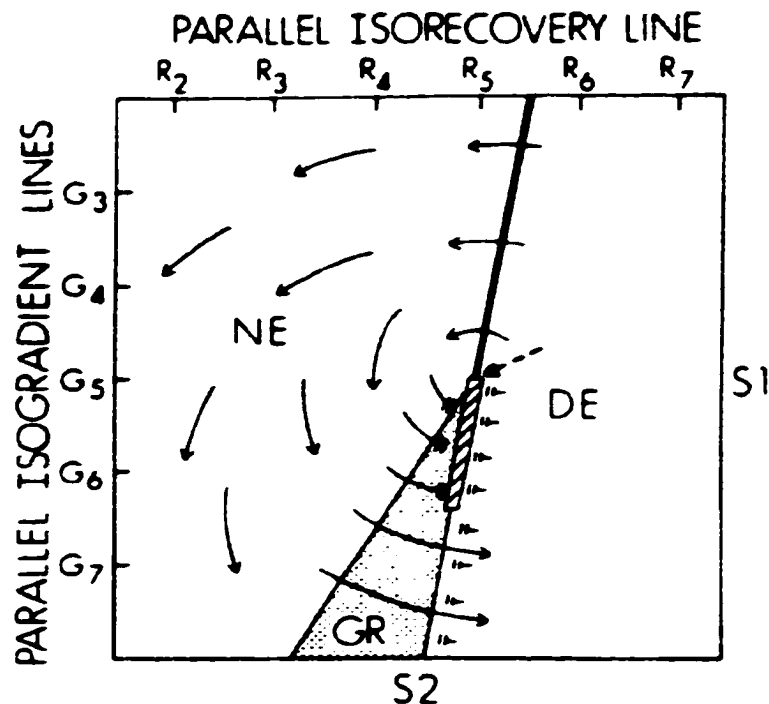


Figure 4. Conditions necessary for producing critical point reentry. The confluence of various states of recovered tissue (R_2 - R_7) with a range of shock potential gradients (G_3 - G_7) that fall off with distance from the shocking electrodes (S_2 at bottom) result in the formation of a critical point (dashed arrow). After the delivery of the S_2 stimulus, tissue will experience direct excitation (DE), no excitation (NE), or a graded response (GR) with prolongation of the refractory period. The coexistence of these three states of excitation provides a substrate for reentry (solid arrows) around the critical point. (Figure with permission from Frazier DW, Wolf PD, Wharton M et al.: Stimulus-induced critical point: Mechanism for electrical initiation of reentry in normal canine myocardium, *J Clin Invest*, vol 83, page 1049, 1989.)

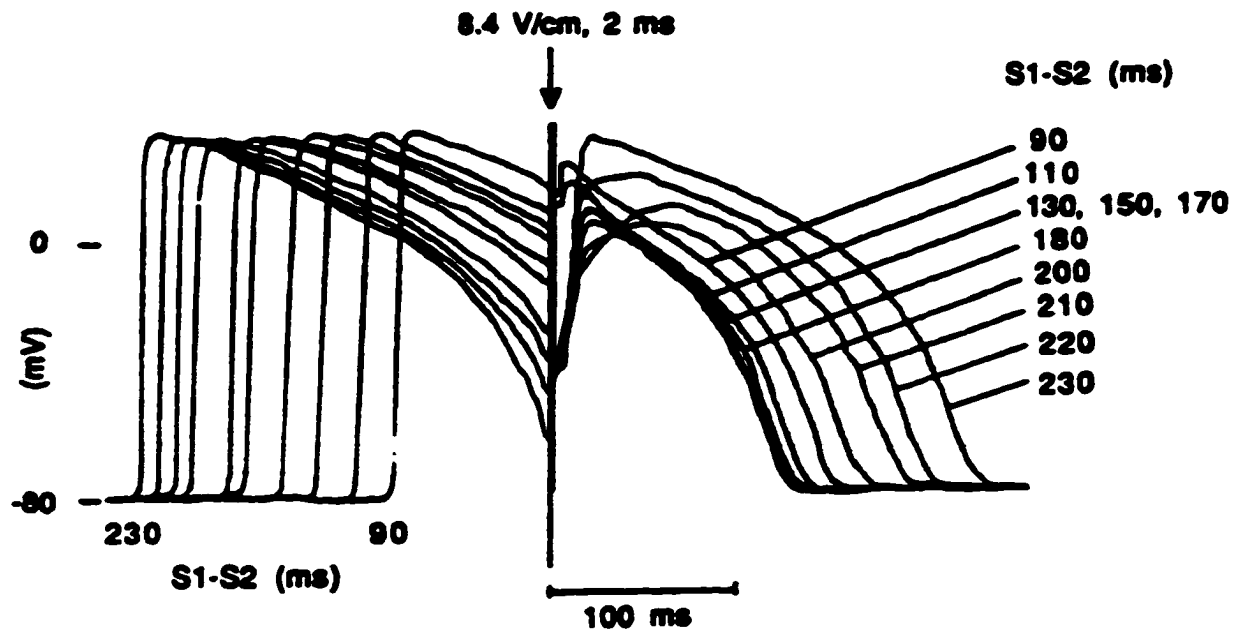


Figure 5. The graded response produced by an S2 stimulus generating a potential gradient of 8.4 V/cm oriented along the long axis of the myofibers. The action potential recordings, obtained from one cellular impalement, are aligned with the S2 time. The longest and shortest S1-S2 intervals tested, 230 and 90 ms, are indicated beneath their respective phase-zero depolarizations. The S1-S2 intervals for each response after S2 are indicated to the right. With some variation, the duration of the graded response tends to increase as the S1-S2 interval increases. (Figure with permission from Knisley SB, Smith WM, Ideker RE: Effect of field stimulation on cellular repolarization in rabbit myocardium: Implications for reentry induction, *Cir Res*, vol 70, page 710, 1992.)

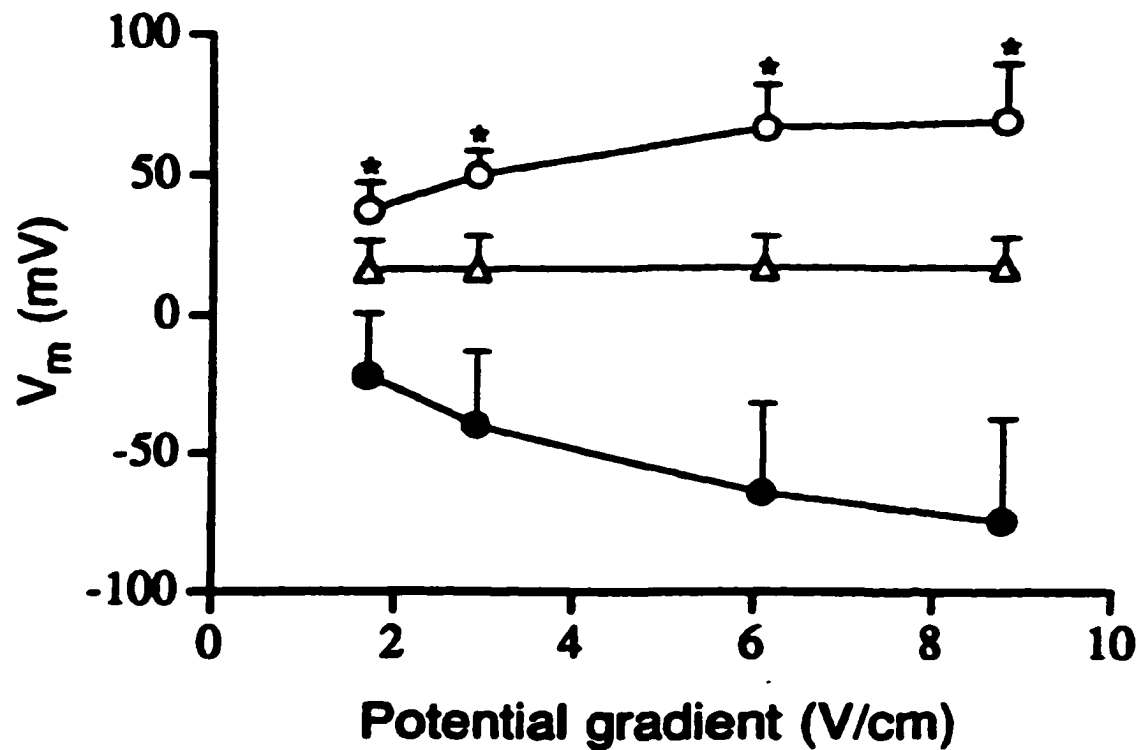


Figure 6. The mean and standard deviation of the peak ΔV_m during shocks delivered during the action potential plateau. Open circles represent ΔV_m during depolarizing shocks; closed circles represent ΔV_m during hyperpolarizing shocks; triangles represent the membrane potential during the plateau just before the shocks were given. (Figure with permission from Zhou X, Rollins DL, Smith WM et al.: Responses of the transmembrane potential of myocardial cells during a shock, J Cardiovasc Electrophysiol, vol 6, page 258, 1995.)

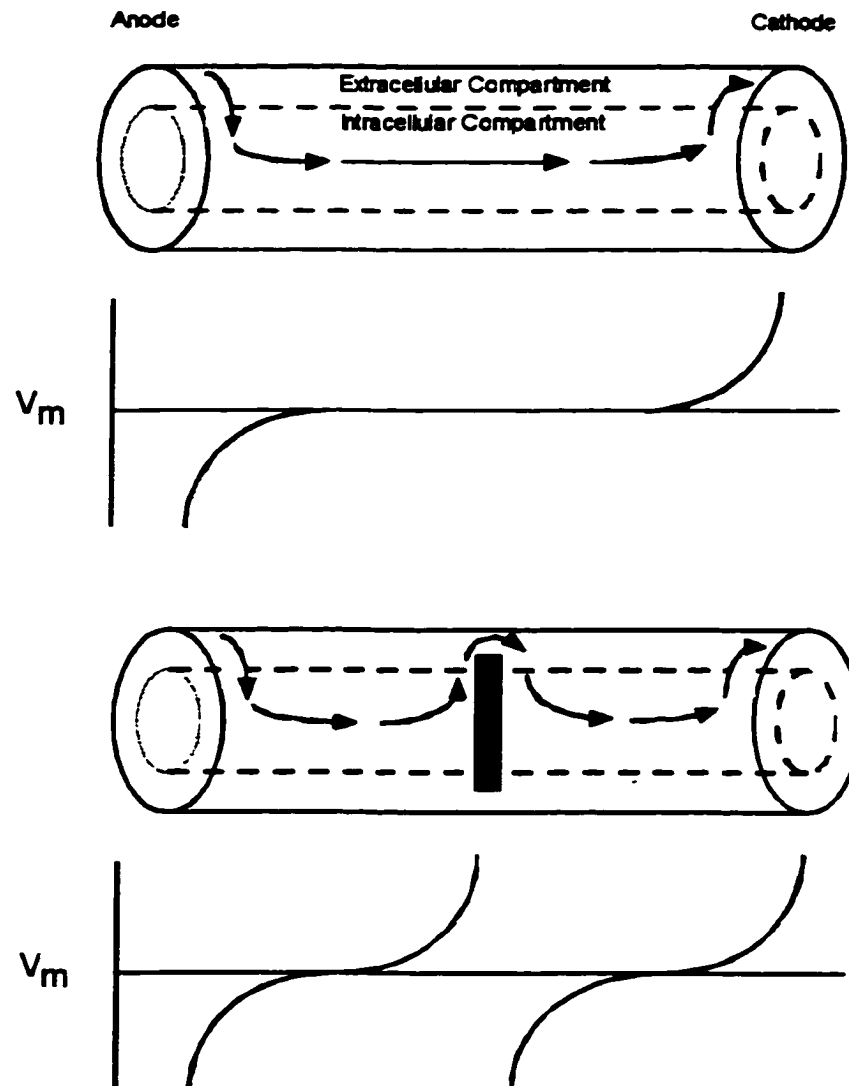


Figure 7. The effect of myocardial discontinuities on current flow. Top, As current (indicated by arrows) crosses between the extracellular compartment and the intracellular compartment near the electrodes, a change in the transmembrane potential is observed. Near the anode, the transmembrane potential (V_m) is hyperpolarized. Near the cathode, current exits the intracellular compartment and depolarizes the transmembrane potential. Bottom, When a discontinuity is present, current is forced from the intracellular to the extracellular compartment and then reenters the cell on the other side of the discontinuity. Virtual electrodes are formed adjacent to the discontinuity generating secondary sources that may then produce local activations. (Figure with permission from White JB, Walcott GP, Pollard AE et al.: Myocardial discontinuities: a substrate for producing virtual electrodes that directly excite the myocardium by shocks, *Circulation*, vol 97, page 1739, 1998.)

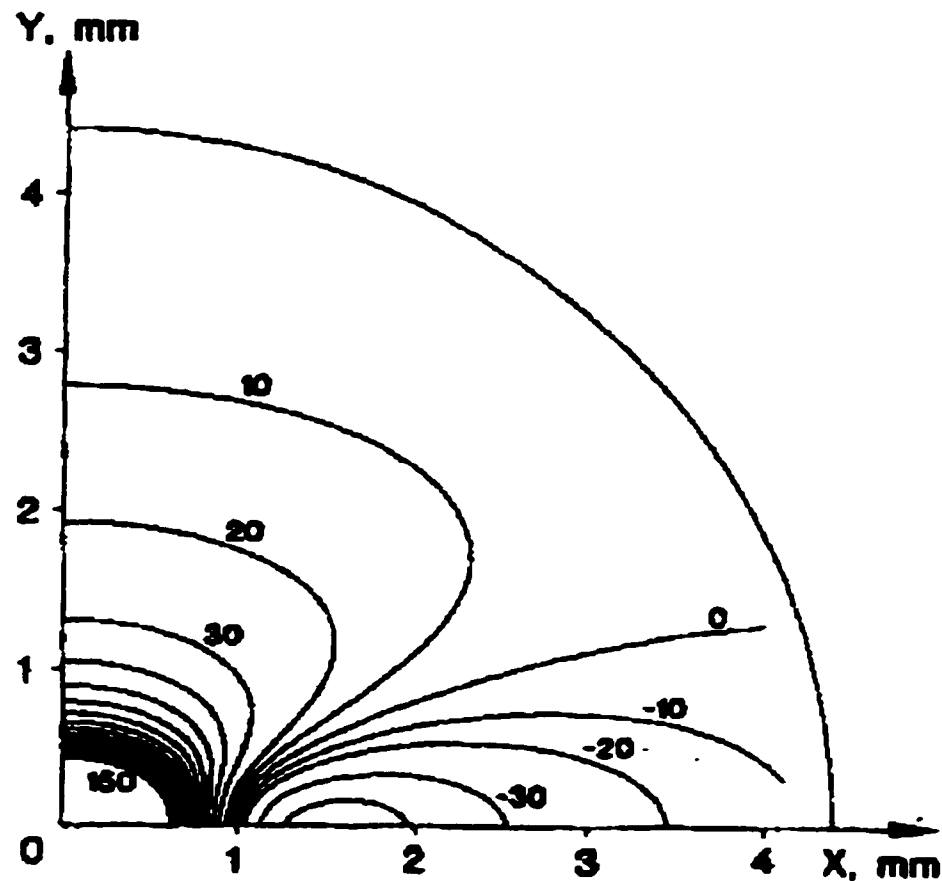


Figure 8. Transmembrane isopotential contours in response to an extracellular cathodal current (4 mA/mm) derived from the bidomain model. Across the fibers (y axis), the transmembrane change decreases with distance. Along the fibers (x axis), a change in polarity occurs approximately 1 mm from the electrode. Mirroring the quadrant across both axes produces a “dog-bone” pattern of polarization. (Figure with permission from Sepulveda NG, Roth BJ, and Wikswo JP: Current injection into a two-dimensional anisotropic bidomain, *Biophys J*, vol 55, page 990, 1989.)

**PREDICTING THE RELATIVE EFFICACY OF SHOCK WAVEFORMS FOR
TRANSTHORACIC DEFIBRILLATION IN DOGS**

by

**JAMES B. WHITE, GREGORY P. WALCOTT , JAMES L. WAYLAND, JR.,
WILLIAM M. SMITH, RAYMOND E. IDEKER.**

Annals of Emergency Medicine 1999;34:309-320

**Copyright
1999**

**by
American College of Emergency Physicians**

Used by permission

Format adapted for dissertation

Abstract

Study objective—Previous work has shown that a passive membrane model using a parallel resistor-capacitor circuit is capable of predicting optimal waveforms for transvenous defibrillation. This study tested the ability of that model to predict optimal waveforms for transthoracic defibrillation.

Methods—This study was divided into 3 parts, each of which determined transthoracic defibrillation thresholds (DFTs) in 6 dogs for several different waveform shapes and durations. For each part, strength-duration relationships were determined from both experimental and model data and then compared with test model predictions. Part 1 DFTs were determined at various durations for 3 different monophasic waveforms--the ascending ramp, descending ramp, and square waveform. Part 2 DFTs were determined for 3 biphasic waveforms. Phase 1 was a 30-ms ascending ramp, and phase 2 was an ascending ramp, a descending ramp, or a square waveform. Part 3 DFTs were determined for 3 biphasic waveforms with very short second-phase durations. Phase 1 was a 30-ms ascending ramp, and phase 2 was a descending ramp.

Results—For part 1, the model was able to predict the relative defibrillation efficacy of the 3 monophasic waveforms ($P<.05$). For parts 2 and 3, the model was able to predict the biphasic waveforms with the lowest DFTs. These predictions were based on the criterion that the model response at the end of the second phase should return to or slightly past the model response value at the beginning of the first phase.

Conclusion—The resistor-capacitor model successfully predicted the relative defibrillation efficacy of several different waveforms delivered transthoracically.

Introduction

A passive membrane model, consisting of a parallel resistor capacitor (RC) circuit, has been used to simulate the response of the myocardium to an electrical stimulus.¹⁻⁶ One of the key determinants of the behavior of this model is the product of its resistance and capacitance, or time constant. The time constant determines the voltage response of the RC circuit as various waveform currents and durations are applied. Implementing physiological values for the time constant into the model is often accomplished by retrospective analysis and fitting of theoretical with experimental data. Although the RC model is a simple representation of the heart, it is beneficial in that it is easy to use and lacks the computationally intensive algorithms of active models.^{7,8}

The first studies to use the RC model applied it to nerve⁹ and later cardiac stimulation.¹ Based on the response of the model generated by square wave pulses, Blair¹ was able to derive a strength-duration relationship in which the strength of the stimulus needed to capture the myocardium decreased as the duration of the stimulus increased, resulting in an exponential curve for electrical stimulation of the heart. Assuming a qualitatively similar relationship between stimulation and defibrillation,¹⁰ Walcott et al.⁶ recently adapted this model to incorporate internal defibrillation. Their model used a time constant based on previously published experimental data and showed that the relative defibrillation efficacy of both monophasic and biphasic waveforms could be predicted.

The main goal of this study was to test the ability of the same RC model to predict the relative defibrillation efficacies of monophasic and biphasic waveforms delivered *transthoracically*. Ascending ramp, descending ramp, and square waveforms were used

because the model predicts notably different defibrillation efficacies for these waveforms. A second objective of this study was to determine the optimal time constant for the model when applied to transthoracic defibrillation and to determine whether it differed from the 2.8 ms reported for internal defibrillation.⁶ Validation of the goals set forth in this study have important implications--robust mathematical models may be useful in determining the most advantageous waveforms for clinical and public access transthoracic defibrillation.

Materials and Methods

This study consisted of 3 similar yet distinct protocols described as parts 1, 2, and 3. For each part, data were obtained from the model and compared with canine experiments. The model and the animal preparation and defibrillation procedures common to all parts are discussed first.

The responses of the membrane model to input waveforms were calculated using a parallel RC circuit emulated by the Pspice software package (MicroSim Corporation, Irvine, CA). For each waveform applied to the RC circuit, a model response is generated consisting of the voltage measured across the circuit that is characteristic of the waveform shape, current, duration, and model time constant. To make predictions and model comparisons, we used a value for the membrane time constant that was reported by Walcott et al.⁶ for transvenous defibrillation, 2.8 ms. The model defibrillation threshold (DFT) was set to equal an arbitrary voltage level. The current needed to reach that same response magnitude was then determined for all waveforms to compare relative defibrillation efficacy.

Figure 1 shows the strength-duration relationships for 3 waveform shapes at 5 durations that can be derived from the model response. The peak current of each waveform that must be delivered for the model response to reach the threshold value for defibrillation varies with duration. Waveforms with shorter durations require higher currents to produce a model response equal in amplitude to that of a lower-current, longer-duration waveform.

After the delivered shock, the model response exponentially decays to zero. When biphasic waveforms are applied to the model, the second phase of the shock forces the model response achieved by the first phase back to its starting value more rapidly than the response would decay with a first phase alone (Figure 2). If the second phase is of sufficient magnitude and duration, the model response will be forced past its starting value. Previous studies have shown that those truncated exponential biphasic waveforms that force the model response during the second phase 100% of the way back to its starting value or slightly past its starting value were found to have the lowest DFTs.^{5,6,11,12} In parts 2 and 3 of the study, we defibrillated with square, ascending ramp, and descending ramp biphasic waveforms to determine whether this finding was also true for transthoracic defibrillation with other shaped waveforms.

This study involving experimental animals was approved by the Institutional Animal Care and Use Committee at the University of Alabama at Birmingham. All dogs were treated and cared for in accordance with the National Institutes of *Health Guide for the Care and Use of Laboratory Animals*. Eighteen mongrel dogs (6 for each of the 3 parts of the study) weighing 19 to 25 kg were anesthetized with an intramuscular bolus of pentobarbital (30 to 35 mg/kg). Anesthesia was subsequently maintained with an intra-

venous dose of 0.05 mg/kg/minute. To maintain muscle relaxation, an initial dose (1.0 mg/kg) of succinylcholine was given and then supplemented (0.3 mg/kg) intravenously every 20 minutes. The dogs were intubated and ventilated with room air and oxygen through a respirator. Body temperature and arterial pressure were monitored continuously and maintained within normal limits. Arterial blood samples were obtained every 30 minutes for determination of pH, blood gas levels, and electrolyte concentrations. Normal saline solution with dextrose was continuously infused and supplemented with electrolytes as needed to maintain normal pH. Limb leads were applied for continuous monitoring of the ECG. A catheter sheath was placed into the right femoral vein and under fluoroscopic guidance, a quadripolar catheter was advanced into the right ventricular apex. The lateral portions of the chest were shaved, and 2 electrode gel-coated 4x9-cm patches (Fast patches, Physio-Control Inc., Redmond, WA) were applied--1 on each side of the sternum, caudal to the shoulder. The chest was then wrapped securely with a cohesive bandage (CO-FLEX, Andover Inc., Salisbury, MA). The patches were connected to the defibrillator such that the left patch received the cathodal current for monophasic and the first phase of biphasic waveforms.

Ventricular fibrillation was induced by 60-Hz alternating current delivered for approximately 1 second through 2 poles of the quadripolar catheter. Ventricular fibrillation was sustained for 15 seconds before attempting defibrillation. Defibrillation waveforms were delivered from a constant-current arbitrary waveform generator.^{13,14} The DFT was defined as the lowest peak current and total energy that achieved defibrillation. The initial peak current for each waveform tested was 8 A in the first animal. For subsequent animals, the initial peak current was the mean DFT for that waveform and duration in all

previous animals. If the first defibrillation shock was successful, the current for that waveform was decreased by 1.0 A, fibrillation was again induced, and an attempt at defibrillation repeated. This procedure continued until a failed shock was achieved. The current was then increased by 0.5 A, and a final defibrillation shock was delivered. If a defibrillation shock was unsuccessful, then the current was increased by 1.0 A. These increases continued until a successful defibrillation occurred, at which point a 0.5-A decrease was made for a final defibrillation attempt. Failed defibrillation shocks were followed by a rescue shock of known effectiveness delivered by an external defibrillator (Lifepak 7Bi, Physio-Control Inc.). During each defibrillation attempt, the applied current and voltage across the heart were sampled at 20 kHz by a waveform analyzer (Model 6100, Data Precision, Inc., Danvers, MA), and signal analysis software within the analyzer was used to obtain the impedance and energy measurements. The output of the waveform analyzer was recorded by a computer workstation (Sparc 5, Sun Microsystems, Inc., Mountain View, CA). A period of at least 4 minutes was allowed to elapse after each fibrillation/defibrillation episode or until hemodynamic stability was restored. The order in which the waveforms were tested for each animal was determined by random selection. After each protocol, the dogs were sacrificed and the hearts were excised, weighed, and preserved. Strength-duration relationships were then constructed for both peak current and total delivered energy.

In part 1 of the study, using the relative currents required to achieve the same model response (Figure 1), strength-duration relationships for peak current were obtained for the monophasic ascending ramp, descending ramp, and square waveforms at 5 durations (5, 10, 15, 20, and 30 ms) with 1 additional duration (2.5 ms) for the square

waveform (Figure 3A). Using an impedance of 50 Ω , the energy required for each waveform to defibrillate, as predicted by the model, was also calculated (Figure 3B).

In each of 6 dogs, a total of 16 defibrillation thresholds was determined, 1 for each duration of the 3 waveforms applied to the model.

To obtain the ideal model time constant for the waveforms tested in the experimental portion, the time constant of the model was altered by multiples of 0.1 ms over a range of 2.5 to 4.5 ms until the strength-duration relationships for the 3 waveforms obtained from the model most closely coincided in a least squares sense with the strength-duration relationships obtained experimentally. Comparisons were made using the peak current for each waveform after the model data were normalized to the DFT of the 30-ms square wave.

In part 2 of the study, 4 waveforms were tested: a 30-ms ascending monophasic ramp and 3 biphasic waveforms with a common first phase and a variable second phase. Each biphasic waveform had a first-phase shape and duration equal to the tested monophasic waveform. The second phase consisted of an ascending ramp, a descending ramp, or a square waveform each with 6 durations (2.5, 5, 7.5, 10, 15, and 30 ms). The effect of the second-phase response on the first-phase response, expressed as the percent change from the maximum response of the first phase, was compared with the peak current DFT determined experimentally.

A total of 19 defibrillation thresholds were determined in each of 6 dogs, 1 for each waveform shape and duration combination. The peak current of the second phase was set equal to the peak current of the first phase.

In part 3 of the study, 3 biphasic waveforms with variable durations for both phases were tested. The first phase was an ascending ramp with durations of 5, 15, or 30 ms. The second phase was a descending ramp with short durations of 0.5, 1, 1.75, 2.5, or 7.5 ms. The effect of the second-phase response on the first-phase response was plotted against the experimentally derived peak current DFT for each waveform.

A total of 15 DFTs was determined in each of 6 dogs for the 3 biphasic waveforms. DFTs were also determined for 3 monophasic waveforms (5, 15, and 30 ms). The peak current of the first phase was set equal to the peak current of the second phase.

The DFTs obtained from the model and from the experiments in part 1 were compared using scatter plots and linear regression analysis. The effect of waveform shape and duration on the DFT was determined from the experimental data using analysis of variance (ANOVA) with repeated measures. When a significant difference was found, post hoc analysis was performed using 1-way ANOVA with the Newman-Keuls test. The optimum time constant for transthoracic predictions was determined by comparing the experimental thresholds with the thresholds derived by the model using a least squares fit. The minimum of the summed square error for each comparison was deemed optimum.

In parts 2 and 3, the DFT for each waveform was compared with the percent change in the first-phase response as a result of the second phase using ANOVA with repeated measures. To examine the model over a wide range of second-phase durations, waveforms from parts 2 and 3 with a first phase, 30-ms ascending ramp were analyzed by fitting the second-phase model response curves to a parabola using a least squares fit. The minimum value of the resulting parabola was then obtained by setting the first

derivative to zero. Differences in the DFT for different waveform shapes and durations were determined using ANOVA with repeated measures and 1-way ANOVA when required. Results from all statistical tests were significant at values of P less than .05.

Results

The strength-duration curves of the model in part 1 of the study predicted that the square waveform should defibrillate at lower peak currents than the ascending waveform, which should defibrillate at lower peak currents than the descending waveform (Figure 3A). As the waveform durations increased for all 3 waveform shapes, the predicted DFT currents decreased. The model predicted that the energy needed for defibrillation should be lower for the ascending waveform than for both the square waveform and the descending waveform (Figure 3B). For durations greater than 5 ms, energy increased with increasing duration for all 3 waveforms. The efficacy of the descending and square waveforms crossed at a duration just less than 10 ms.

The average heart weight of animals in part 1 was 181 ± 53 gm. For each animal, an average of 61 ± 6 shocks were delivered for all DFT determinations. The square waveform defibrillated at significantly lower peak currents than did the ascending and descending waveforms for most durations (Figure 4A). A significant difference was observed between the 5-ms and 30-ms duration for each waveform shape ($P < .05$), indicating a trend of decreasing thresholds with longer durations. For longer durations, the ascending ramp defibrillated at a lower energy than did the descending ramp or square waveform (Figure 4B). DFTs increased with duration, producing significant

differences between the shortest and longest durations within each waveform shape ($P<.05$).

With a time constant equal to 2.8 ms, a strong correlation was observed ($r=0.94$, $P<.01$) between the experimental data and the data obtained from the model for peak current (Figure 5A). The DFT for energy increased with increasing waveform duration for all waveform durations, including the waveform less than 5 ms, and the energy curves for the descending and square waveforms did not cross. A strong relationship was observed for energy ($r=0.88$, $P<.01$) between the 2 data sets (Figure 5B). Comparison of the experimental data with the thresholds obtained by altering the membrane time constant of the model resulted in an optimal time constant value larger (4.0 ms) than that used to make the predictions in each part (Figure 6). The 4.0-ms time constant yielded a summed squared error half that of the 2.8 ms value. However, for a range of time constants from approximately 3.7 ms to 4.1 ms, the model predicted the experimental results with almost equally low error.

In part 2 of the study, with a constant first-phase shape and duration, the second-phase response, expressed as the percent change in the peak first-phase response, increased as the second-phase duration increased for all 3 second phase waveform shapes (Figure 2). For the same second-phase duration, the second-phase response increased as the shape changed from a descending ramp to an ascending ramp and then to a square waveform.

The average heart weight of animals in part 2 of the study was 144 ± 16 gm. For each animal, an average of 61 ± 7 shocks were delivered for all DFT determinations. The peak current required to defibrillate was significantly larger for the longest second-phase

duration compared with the shortest second-phase duration ($P<.05$, Figure 7A). As the second-phase duration increased to 15 and 30 ms, the energy required to defibrillate also increased (Figure 7B). For both peak current and energy, waveform shape did not alter the defibrillation efficacy of the waveforms until the second-phase durations reached the 15-ms or 30-ms duration. The mean peak current and energy required to defibrillate for the monophasic waveform were 6.2 ± 1.2 A and 14.8 ± 0.4 J, respectively.

In Figure 8, the experimentally determined DFTs are plotted against the decrease in the model response during the second phase expressed as a percent of the peak model response during the first phase. The lowest DFTs were observed for those waveforms in which the maximum model response during the second phase was 90% to 180%.

In part 3 of the study, the relative DFTs of the waveforms tested were determined as they were in part 2. The second-phase response became greater with longer second-phase durations. As the duration of the first phase increased, the magnitude of the first phase response also increased.

The average heart weight of animals in part 3 was 149 ± 27 gm. For each animal, an average of 68 ± 5 shocks were delivered for all DFT determinations. As second-phase durations became very short (0.5 to 1.75 ms), the biphasic waveform did not defibrillate at a lower threshold than did the monophasic waveform ($P>.05$, Figure 9A). The defibrillation efficacy of the biphasic waveform improved over the monophasic waveform as the second-phase durations increased to 1.75 ms ($P<.05$). At each second-phase duration, the DFT current for the biphasic waveforms increased as the first-phase duration decreased.

As the first phase of the waveforms increased for a given second-phase duration, the energy required for defibrillation was not significantly different except for second-phase durations of 0 ms (monophasic waveforms) and 0.5 ms (Figure 9B). In addition, the amount of energy required for defibrillation did not significantly decrease compared with the monophasic waveform when adding a second phase to any first-phase duration.

As the magnitude of the second-phase response reached 110% to 140% of the maximum first-phase response, the peak current required for defibrillation decreased (Figure 10).

Biphasic waveforms, with the first phase an ascending ramp of 30-ms duration, were tested in study parts 2 and 3. The second phase consisted of a descending ramp, which ranged from 2.5 to 30 ms in part 2 and from 0 to 7.5 ms in part 3. The parabola fit to these data had a minimum with a second-phase response of 110% (Figure 11). The second phase duration generating this optimal model response is approximately 4 ms.

Discussion

The results of this study indicate that the simple parallel RC model is able to predict the relative transthoracic defibrillation efficacy of the different monophasic and biphasic waveforms that were experimentally tested. Many different waveforms were examined: 19 monophasic and 33 biphasic waveforms. Although the RC model has been developed from and has been applied to internal defibrillation, this study demonstrates that the model also is applicable to transthoracic defibrillation.

In the model, the defibrillation threshold is assumed to correspond to an arbitrary value of the voltage response across the RC circuit. As waveforms of any shape and

duration are applied to the model, those that reach or exceed the arbitrary value are assumed to successfully defibrillate, whereas those that do not are considered unsuccessful. The model also assumes no need for a sustained model response at the threshold level. This is an important consideration when comparing waveforms with different shaped responses. For instance, for ascending ramps that are longer than the time constant, the model response ascends to track the waveform (Figure 1B). For square pulses considerably longer than the time constant, the model response is near the asymptote for a long period as it approaches the threshold (Figure 1A). Thus, the defibrillation threshold energy is lower for the ascending ramp than for the square waveform.

Biphasic waveforms with second-phase durations that return the voltage across the RC network back to or just past its starting value during the second phase have the lowest DFTs. When this condition is achieved, the threshold model response that must be reached during the first phase across the RC network is maximally decreased compared with that required for monophasic or other biphasic waveforms. It is not known if the model response bears any similarity to the change in the transmembrane potential during the defibrillation shock. Nevertheless, the model response appears to be a good predictor of defibrillation efficacy. The defibrillation model by Kroll also predicts an increase in current with a decrease in waveform duration as does our model.¹⁸ The Kroll model, however, uses a hyperbolic strength-duration relationship, whereas our model uses an exponential relationship. The Kroll model also approximates the shape of the monophasic waveform and the first phase of the biphasic waveform with an average current and waveform duration. This fact makes it difficult to include arbitrary waveform shapes in

the model. Both models use the same method for determining the second-phase response for biphasic waveforms.

The model time constant used in this study was 2.8 ms, which is the value that was found by Walcott et al.⁶ to best fit canine results for internal defibrillation. Others have used time constants for internal defibrillation that differ slightly from this value, ranging from 1.3 to 3.5 ms.^{2,5,19} A time constant value of 2.8 ms also provided good results in this study for transthoracic defibrillation. However, a slightly better fit with the experimental results was obtained with a longer time constant, 4.0 ms. These findings indicate that the optimum monophasic and biphasic membrane time constant for transthoracic defibrillation may be slightly longer than that for internal defibrillation. The difference in time constants for internal and external defibrillation may be related to the differences found experimentally in chronaxie values for stimulation near and far from stimulating electrodes. Previous studies have shown a wide range for chronaxie values for both point stimulation and field stimulation, with those for field stimulation being slightly larger.²⁰⁻²⁷ If the RC model for defibrillation is qualitatively similar to stimulation, then our results suggest that the larger time constant value may be a result of differences in the electric field produced between external and internal defibrillation just as is observed between field and point stimulation.

For monophasic waveforms of 3 different shapes but the same duration, the model predicted and the experiments verified that square waves had the lowest peak current requirement for defibrillation, whereas ascending ramps had the lowest energy requirements. These results support earlier studies by Hillsley et al.¹³ for internal defibrillation, who showed that a 16-ms ascending ramp defibrillated at lower energy than

did a 16-ms square waveform. Part 1 of the study also showed, as predicted by the model, that the descending ramp was the least effective waveform for defibrillation. This result confirms earlier work by Schuder et al,²⁸ who hypothesized the detrimental effect of the descending ramp was caused by refrillation by the low voltage at the end of the waveform.

Parts 2 and 3 indicated that defibrillation efficacy was relatively independent of the shape and, within limits, the duration of the second phase of the biphasic waveforms. As shown in part 2 of the study, waveform shape did not appear to affect defibrillation thresholds in terms of energy and peak current until the second-phase duration nearly equaled that of the first phase. Part 3 of the study extended to external defibrillation the results of Hillsley et al¹³ for internal defibrillation that show changing the duration of the first phase of the biphasic waveform has similar effects on defibrillation requirements as the same change for a monophasic waveform. The strength-duration relationships found within each duration for the waveforms in part 3 track the same strength-duration relationship found for the monophasic ascending ramps in part 1. Thus, although debate still exists over which phase of a biphasic waveform is the defibrillating phase,^{5,6,29} these results are consistent with the hypothesis that the first phase of the biphasic waveform is the defibrillating phase, similar in action to that of the monophasic waveform, whereas the second phase performs some additional function that lowers the defibrillation threshold.⁵ Kroll⁵ considers this function that he calls “burping” to be restorative in nature. He characterizes it as a protective mechanism that removes remaining residual charge on the cell membrane created by the first phase. In fact, our data, as well as those of others,

showed that those waveforms for which the second-phase model response returned the model voltage to near its starting level produced the lowest thresholds.^{6,11}

The results of part 3 conflict with earlier studies that compare the defibrillation efficacy of biphasic and monophasic waveforms. Many internal defibrillation studies have shown that a second-phase duration shorter than the first phase lowers the defibrillation threshold compared with the monophasic waveform consisting of just the first phase alone even when the second phase is 1 ms or shorter in duration.^{29-31,32} Part 3 of our study has shown for transthoracic defibrillation that as the second-phase duration becomes very short, 2.5 ms or less, the biphasic waveform no longer defibrillates at lower thresholds than the monophasic waveform. Although some studies have shown that the biphasic waveform is better than the monophasic waveforms when applied externally,^{32,33} others have reported that for transthoracic defibrillation, the biphasic waveform poses no advantage over the monophasic waveform for waveforms with the same total duration.^{16,17} Data from part 3 do indicate that at appropriate durations, the second phase can reduce the defibrillation thresholds to a significant degree when delivered transthoracically.

Although it is tempting to visualize the passive RC circuit as a model that represents the cell membrane, the actual changes in the transmembrane potential caused by a defibrillation shock are much more complex than this simple model. It is known that the cell membrane exhibits rectification properties,³⁴ thereby preventing current from flowing uniformly in both directions across the membrane as it does in the RC model. In addition, the membrane undergoes a host of active processes that are triggered by the shock itself.^{7,8,34} Because of these active processes and rectification, the time constant of

cardiac tissue is dependent on the polarity and the strength of the shock.²⁶ In addition, the time constant of the membrane response during the shock differs from that of the recovery of the membrane after the shock.^{26,35} The passive RC model reproduces none of these findings. Furthermore, the canine model of transthoracic defibrillation we used has the following limitations: (1) the thoracic cavity of the dog is shaped quite differently from that of human beings, and, (2) the animals were healthy, lacking the myocardial disease and dysfunction that may be present in humans. Such conditions, if considered, may require alteration of the parameters used by the model to produce results consistent with those found in this study.

References

1. Blair HA. On the intensity-time relations for stimulation by electric currents. II. *J Gen Physiol.* 1932;15:731-755.
2. Cleland BG. A conceptual basis for defibrillation waveforms. *Pacing Clin Electrophysiol.* 1996;19:1186-1195.
3. Cleland BG. A conceptual basis for pacing waveforms. *Pacing Clin Electrophysiol.* 1996;19:1177-1185.
4. Gold MR, Shorofsky SR. Strength-duration relationship for human transvenous defibrillation. *Circulation.* 1997;96:3517-3520.
5. Kroll MW. A minimal model of the single capacitor biphasic defibrillation waveform. *Pacing Clin Electrophysiol.* 1994;17:1782-1792.
6. Walcott GP, Walker RG, Cates AW, Krassowska W, Smith WM, Ideker RE. Choosing the optimal monophasic and biphasic waveforms for ventricular defibrillation. *J Cardiovasc Electrophysiol.* 1995;6:737-750.
7. Luo C-H, Rudy Y. A dynamic model of the cardiac ventricular action potential. I. Simulations of ionic currents and concentration changes. *Circ Res.* 1994;74:1071-1096.

8. DiFrancesco D, Noble D. A model of cardiac electrical activity incorporating ionic pumps and concentration changes. *Phil Trans R Soc.* 1985;B307:353-398.
9. Lapicque L. L'excitabilite en fonction du temps. In: *L'Excitabilite en Fonction du Temps*. Paris: Libraire J. Gilbert; 1926:371.
10. Irnich W. The fundamental law of electrostimulation and its application to defibrillation. *Pacing Clin Electrophysiol.* 1990;13:1433-1447.
11. Swerdlow CD, Fan W, Brewer JE. Charge-burping theory correctly predicts optimal ratios of phase duration for biphasic defibrillation waveforms. *Circulation.* 1996;94:2278-2284.
12. Yamanouchi Y, Brewer J, Mowrey K, Donohoo A, Steinkogler G, Wilkoff B, Tchou P. The "charge burping" model predicts optimal small capacitor biphasic external defibrillation. *Circulation.* 1997;96:1-60.
13. Hillsley RE, Walker RG, Swanson DK, Rollins DL, Wolf PD, Smith WM, Ideker RE. Is the second phase of a biphasic defibrillation waveform the defibrillating phase? *Pacing Clin Electrophysiol.* 1993;16:1401-1411.
14. Sweeney RJ, Gill RM, Jones JL, Reid PR. Defibrillation using a high-frequency series of monophasic rectangular pulses: observations and model predictions. *J Cardiovasc Electrophysiol.* 1996;7:134-143.
15. Hoffman BF, Suckling EE, Brooks CM. Vulnerability of the dog ventricle and effects of defibrillation. *Circ Res.* 1955;3:147-151.
16. Kerber RE, Bourland JE, Kallok MJ, Hite P, Pritchard B, Charbonnier F, Birkett C, Fox-Eastham K, Kieso RA. Transthoracic defibrillation using sequential and simultaneous dual shock pathways: experimental studies. *Pacing Clin Electrophysiol.* 1990;13:207-217.
17. Scott BD, Kallok MJ, Birkett C, Kieso RA, Kerber RE. Transthoracic defibrillation: Effect of dual-pathway sequential pulse shocks and single-pathway biphasic pulse shocks in a canine model. *Am Heart J.* 1993;125:99-109.
18. Kroll MW. The minimal model of the monophasic defibrillation pulse. *Pacing Clin Electrophysiol.* 1993;16:769-777.
19. Chapman PD, Wetherbee JN, Vetter JW, Troup P, Souza J. Strength-duration curves of fixed pulse width variable tilt truncated exponential waveforms for nonthoracotomy internal defibrillation in dogs. *Pacing Clin Electrophysiol.* 1988;11:1045-1050.

20. Leonelli FM, Kroll MW, Brewer JE. Defibrillation thresholds are lower with smaller storage capacitors. *Pacing Clin Electrophysiol.* 1995;18:1661-1665.
21. Voorhees CR, Voorhees WD, Geddes LA, Bourland JD, Hinds M. The chronaxie for myocardium and motor nerve in the dog with chest-surface electrodes. *IEEE Trans Biomed Eng.* 1992;39:624-627.
22. Schuchert A, Cappato R, Kuck K-H, Meinertz T. Programming of the pacing impulse in pacemakers connected to steroid lead systems. *Pacing Clin Electrophysiol.* 1995;18:318-322.
23. Wessale JL, Boulard JD, Tacker WA, Jr., Geddes LA. Bipolar catheter defibrillation in dogs using trapezoidal waveforms of various tilts. *J Electrophysiol.* 1980;13:359-366.
24. Koning G, Schneider H, Hoelen AJ. Amplitude-duration relation for direct ventricular defibrillation with rectangular current pulses. *Med Biol Eng.* 1975;13:388-395.
25. Shorofsky SR, Foster AH, Gold MR. Effect of waveform tilt on defibrillation thresholds in humans. *J Cardiovasc Electrophysiol.* 1997;8:496-501.
26. Zhou X, Rollins DL, Smith WM, Ideker RE. Responses of the transmembrane potential of myocardial cells during a shock. *J Cardiovasc Electrophysiol.* 1995;6:252-263.
27. Kay GN, Mulholland DH, Epstein AE, Plumb VJ. Effect of pacing rate on the human atrial strength-duration curve. *J Am Coll Cardiol.* 1990;15:1618-1623.
28. Schuder JC, Rahmoeller GA, Stoeckle H. Transthoracic ventricular defibrillation with triangular and trapezoidal waveforms. *Circ Res.* 1966;19:689-694.
29. Jones JL, Jones RE. Threshold reduction with biphasic defibrillator waveforms: Role of excitation channel recovery in a computer model of the ventricular action potential. *J Electrocardiol.* 1990;23:30-35.
30. Chapman PD, Vetter JW, Souza JJ, Wetherbee JN, Troup PJ. Comparison of monophasic with single and dual capacitor biphasic waveforms for nonthoracotomy canine internal defibrillation. *J Am Coll Cardiol.* 1989;14:242-245.
31. Flaker GC, Schuder JC, McDaniel WC, Stoeckle H, Dbeis M. Superiority of biphasic shocks in the defibrillation of dogs by epicardial patches and catheter electrodes. *Am Heart J.* 1989;118:288-291.

32. Gliner BE, Lyster TE, Dillion SM, Bardy GH. Transthoracic defibrillation of swine with monophasic and biphasic waveforms. *Circulation*. 1995;92:1634-1643.
33. Bardy GH, Gliner BE, Kudenchuk PJ, Poole JE, Dolack GL, Jones GK, Anderson J, Troutman C, Johnson G. Truncated biphasic pulses for transthoracic defibrillation. *Circulation*. 1995;91:1768-1774.
34. Cohen IS, Falk RT, Kline RP. Voltage-clamp studies on the canine purkinje strand. *Proc Roy Soc B*. 1982;217:215-236.
35. Knisley SB, Smith WM, Ideker RE. Effect of field stimulation on cellular repolarization in rabbit myocardium: Implications for reentry induction. *Circ Res*. 1992;70:707-715.

Figure 1. The model response to 3 monophasic waveform shapes with a time constant equal to 2.8 ms. For each waveform shape, the peak currents are plotted that are necessary to reach the same model response, thereby providing a strength-duration relationship. The model responses are shown for square (A), ascending ramp (B), and descending ramp (C) waveforms.

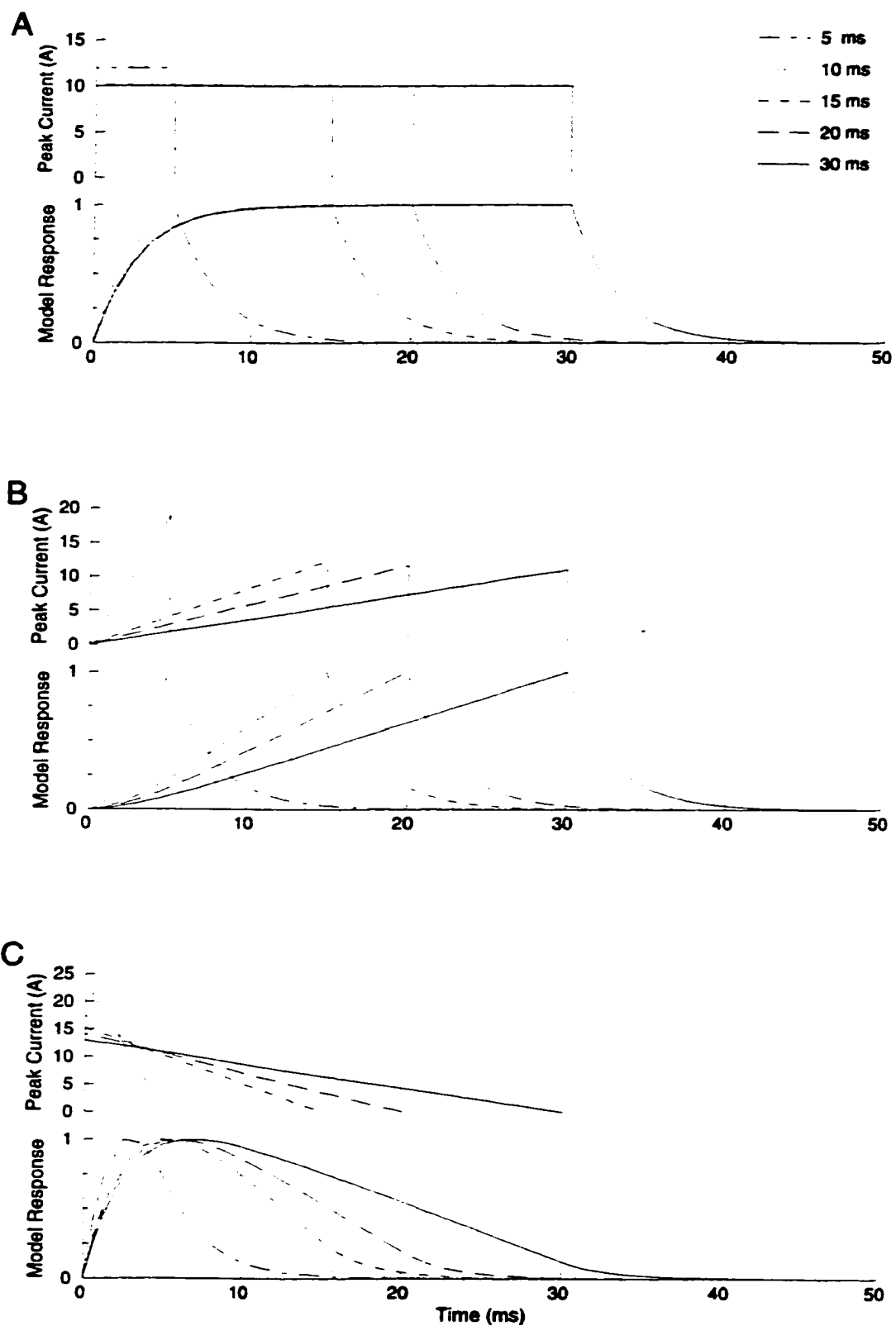


Figure 2. The model responses for 3 biphasic waveforms with the membrane time constant equal to 2.8 ms. For all waveforms, the first phase was an ascending ramp with a duration of 30 ms. The second phase was either a square wave (A), ascending ramp (B), or descending ramp (C) that varied in duration (2.5, 5, 7.5, 10, 15, and 30 ms). The second-phase model response as a percentage of the peak magnitude of the first-phase model response is indicated by the scale on the right side of the model response plots.

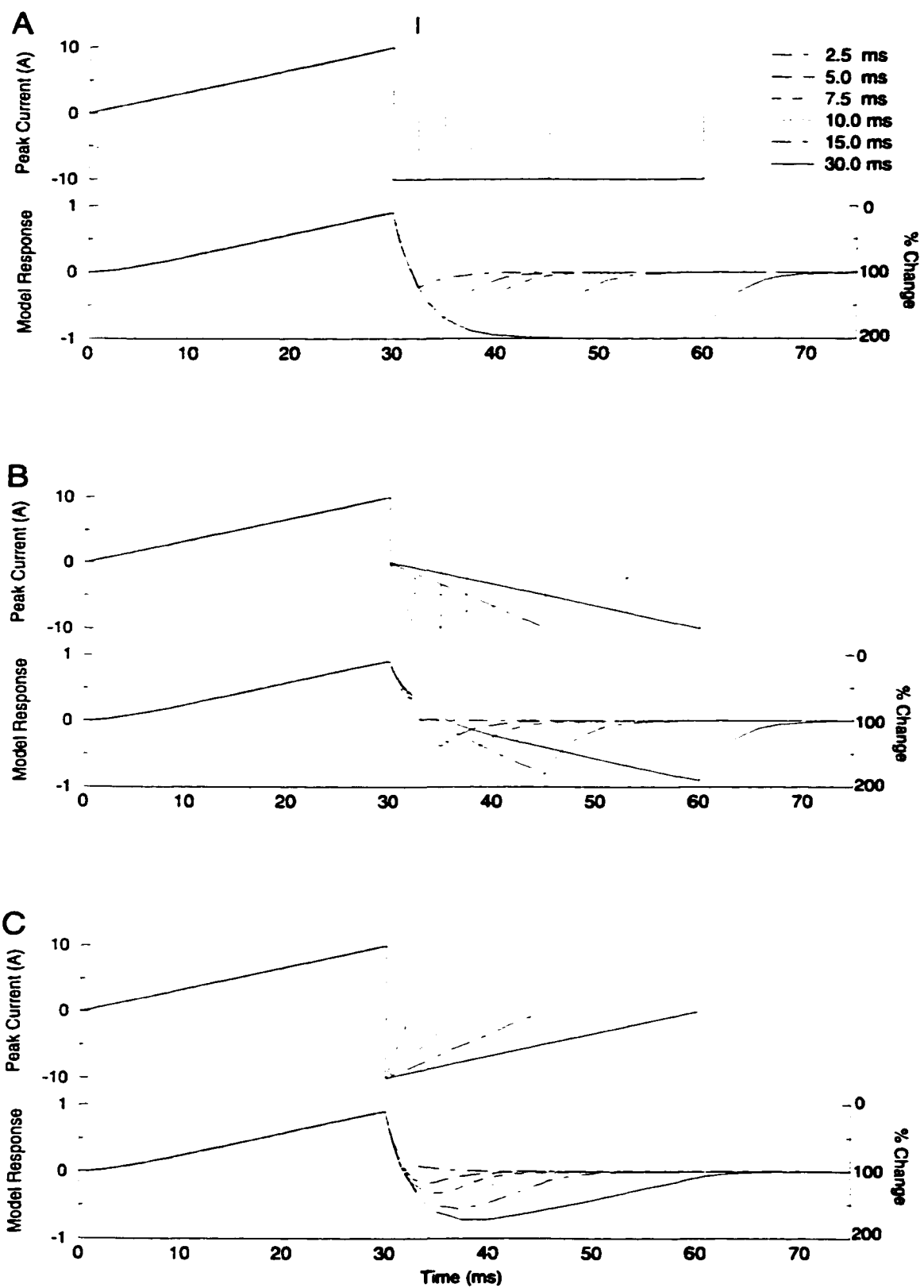


Figure 3. Strength-duration curves for peak current and energy. A, Strength-duration curves predicted by the model for peak current based on data generated as in Figure 1 for ascending ramp, descending ramp, and square waveforms. B, Strength-duration curves predicted by the model for energy.

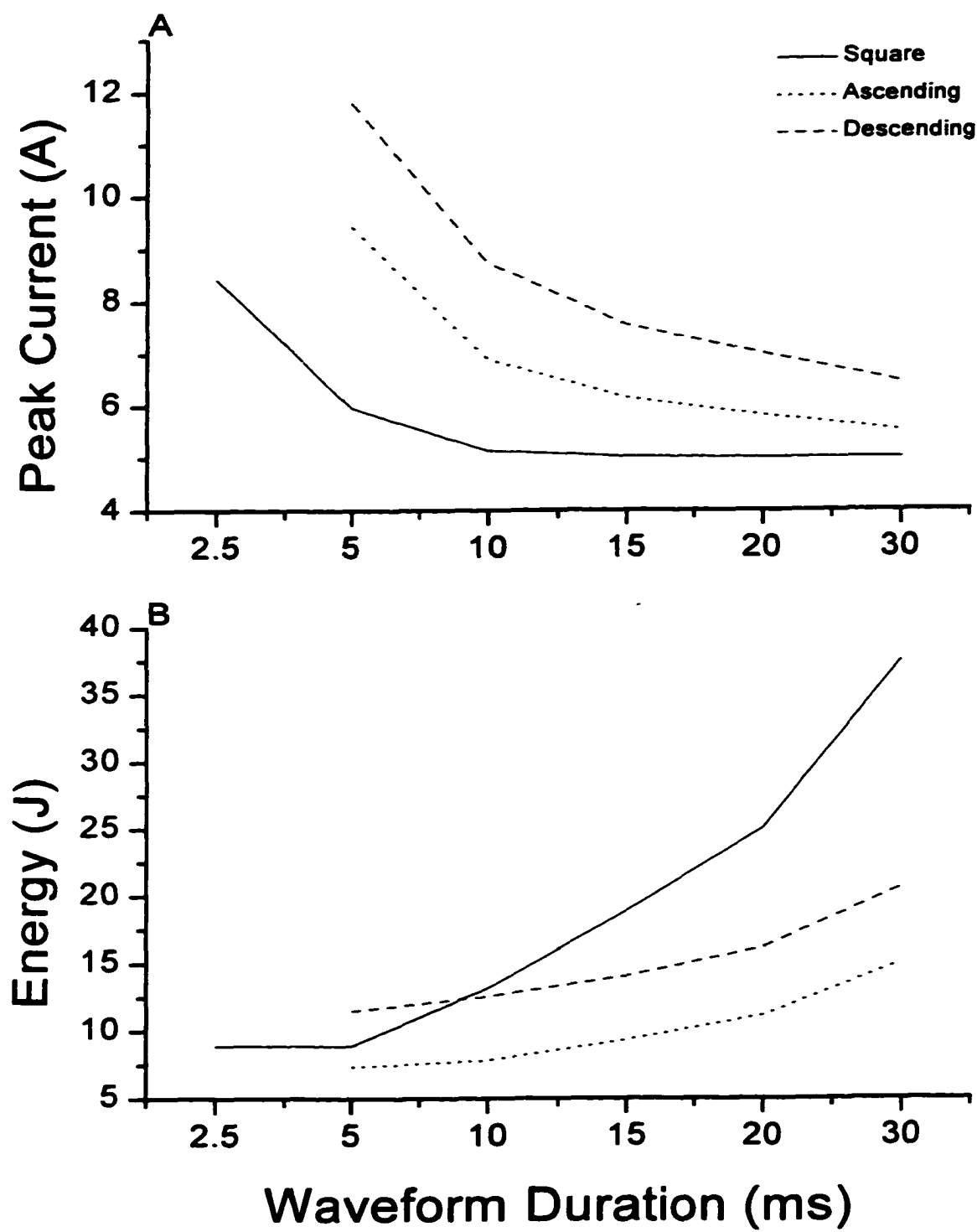


Figure 4. Monophasic waveform strength-duration relationships determined experimentally in part 1 of the study. DFTs as peak current (A) and as energy (B) are plotted against waveform duration. * $P < .05$ versus square waveform within that duration. † $P < .05$ versus ascending ramp within that duration. Vertical bars represent the SD.

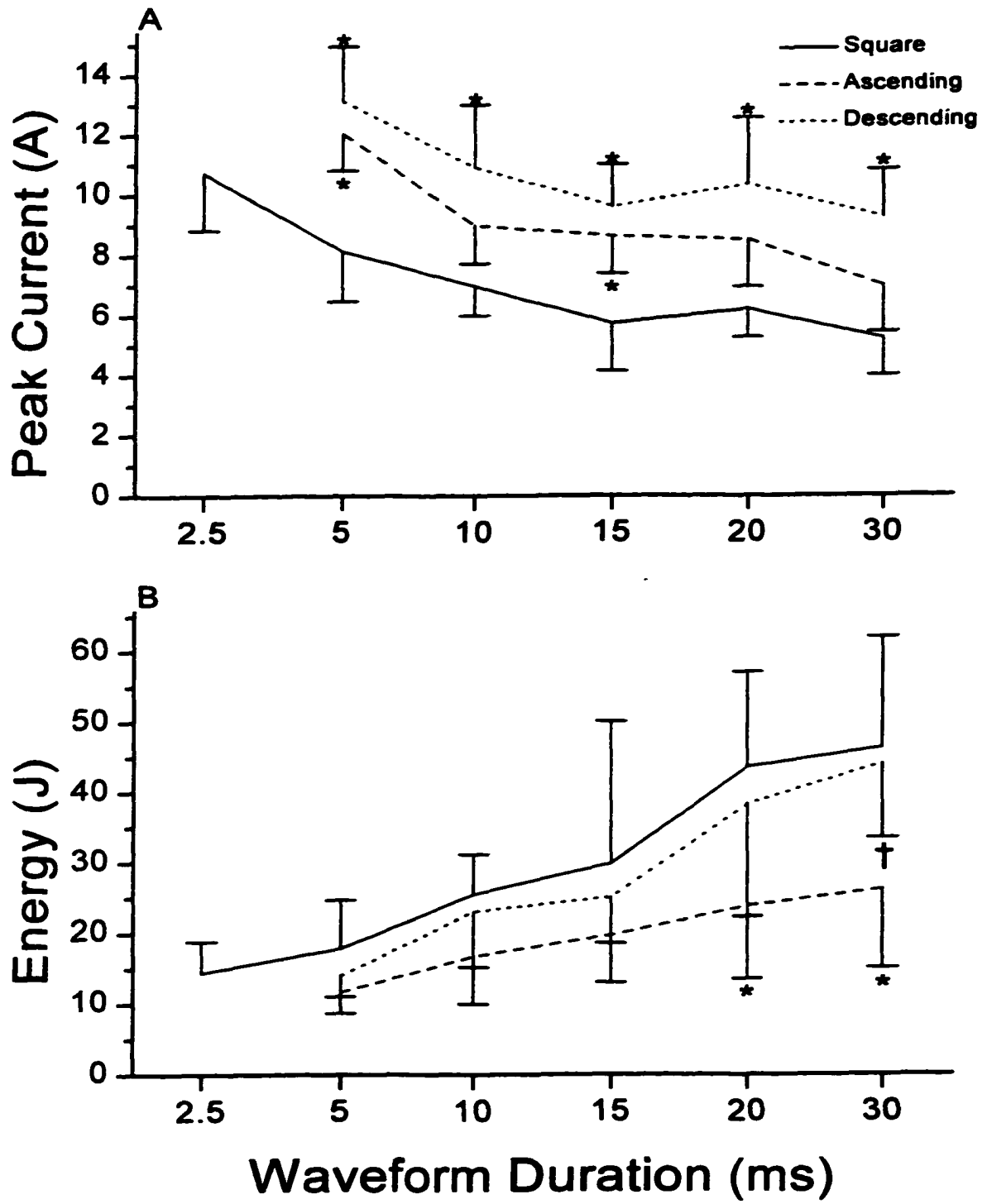


Figure 5. Experimental thresholds plotted against the model thresholds for peak current (A) and energy (B) for the monophasic waveforms in part 1 of the study. Regression lines are shown.

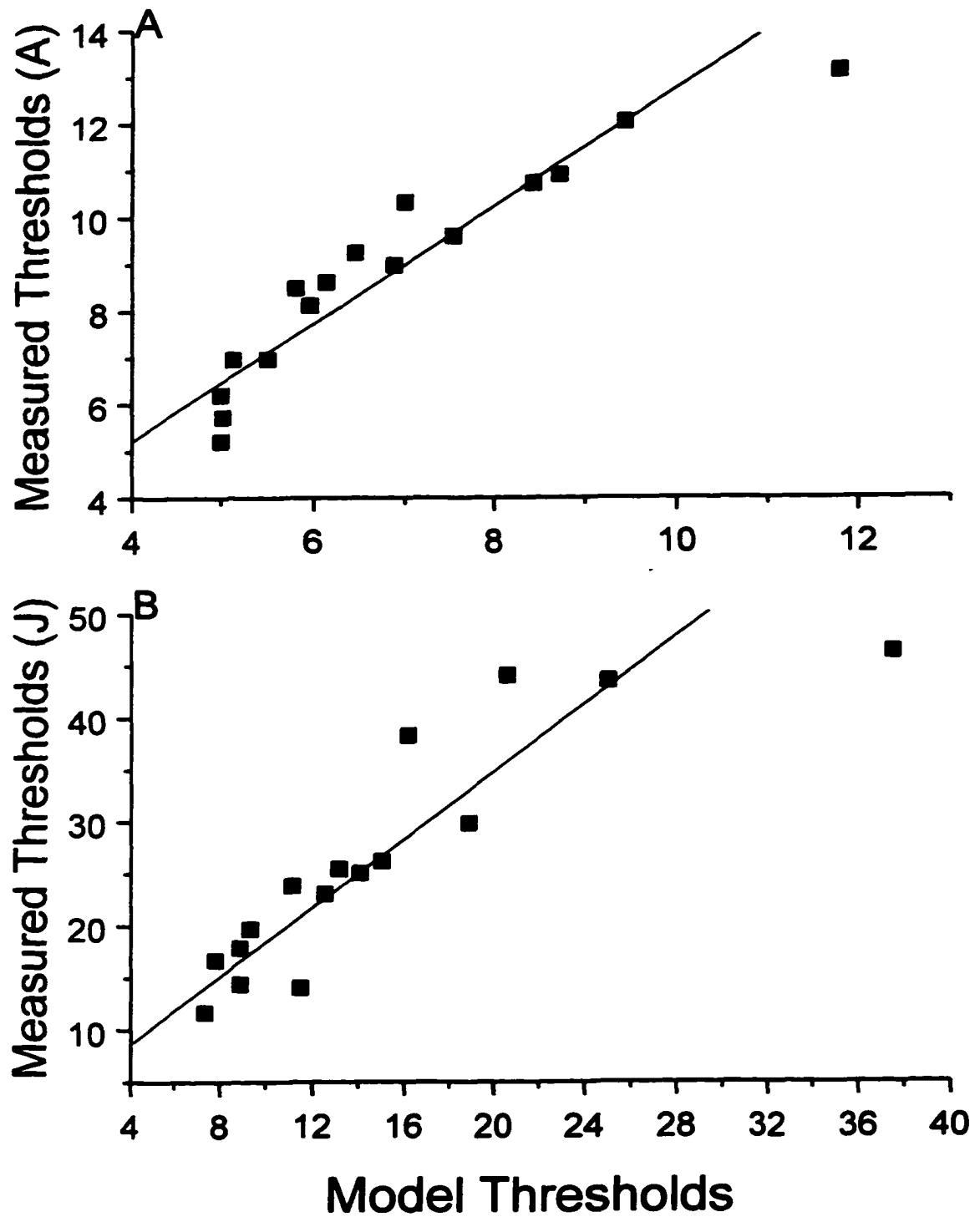


Figure 6. Effect of the membrane time constant on the summed square error of the model data compared with the experimental data.

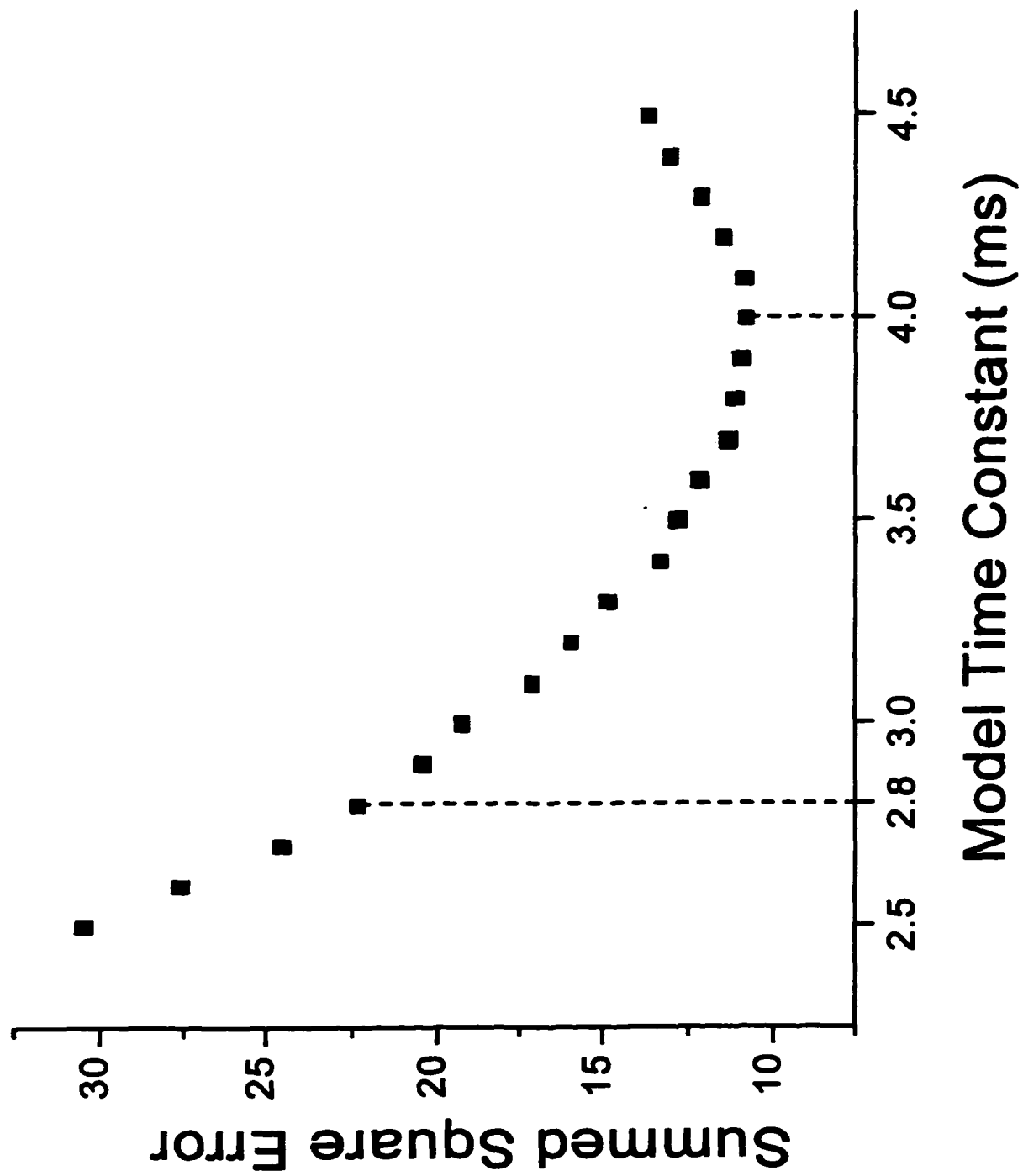


Figure 7. Strength-duration relationships for the biphasic waveforms studied in part 2 of the study. * $P < .05$ versus square waveform within the same duration. † $P < 0.5$ versus ascending waveform within the same duration. Vertical bars represent the SD. for each waveform.

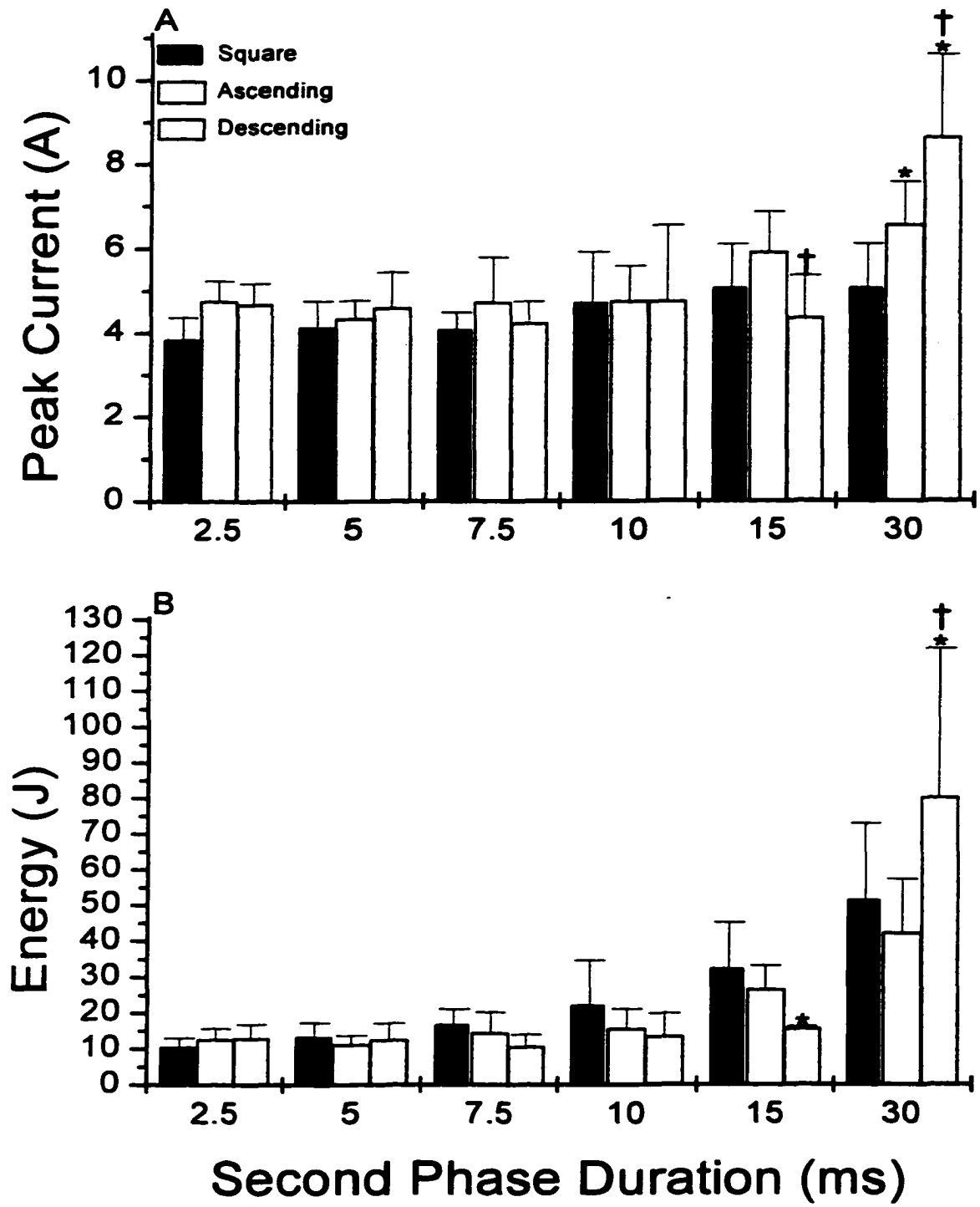


Figure 8. The experimental DFTs in part 2 plotted against the decrease in the model response during the second phase expressed as a percent of the peak model response during the first phase. Points on the graph represent each second-phase duration for each waveform shape shown in Figure 7. The minimum and maximum durations (in milliseconds) are shown for each waveform shape.

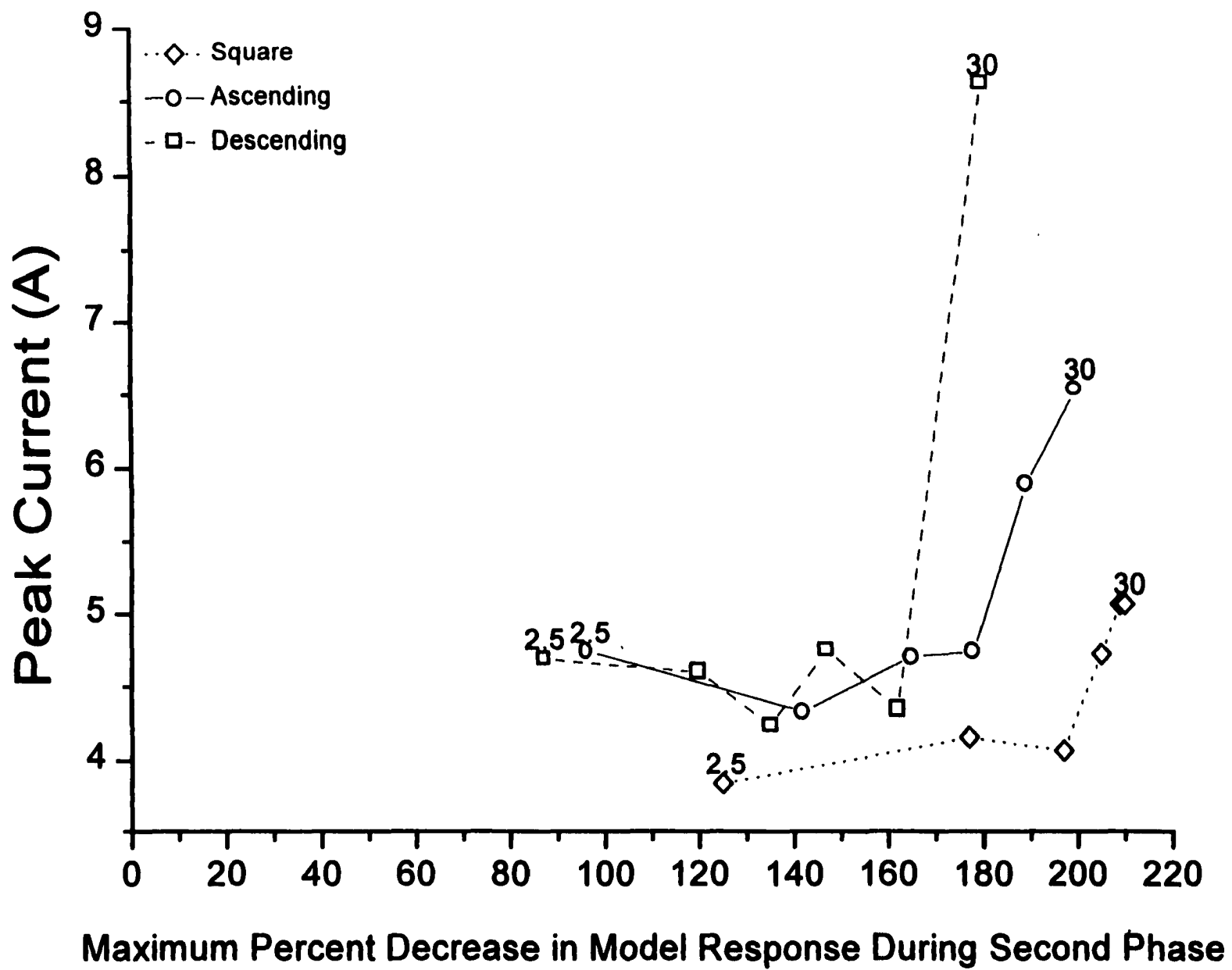


Figure 9. Strength-duration relationships for the biphasic waveforms studied in part 3 of the study. The DFTs are plotted as peak current (A) and total energy (B). * $P < .05$ versus 5-ms waveform within the same duration. Vertical bars represent the SD.

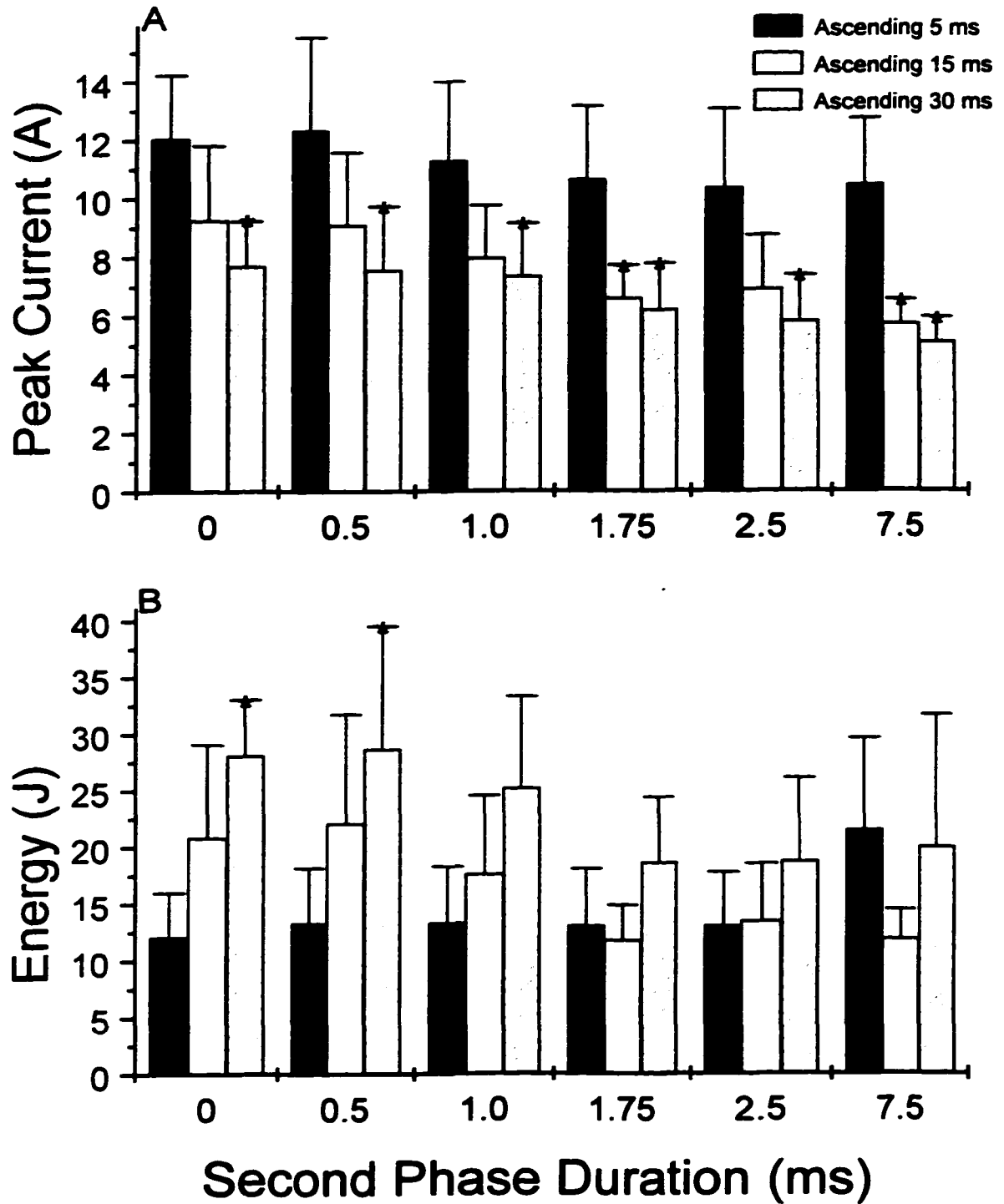


Figure 10. Experimental thresholds obtained in part 3 of the study plotted against the second-phase model response. See Figure 8 for additional description.

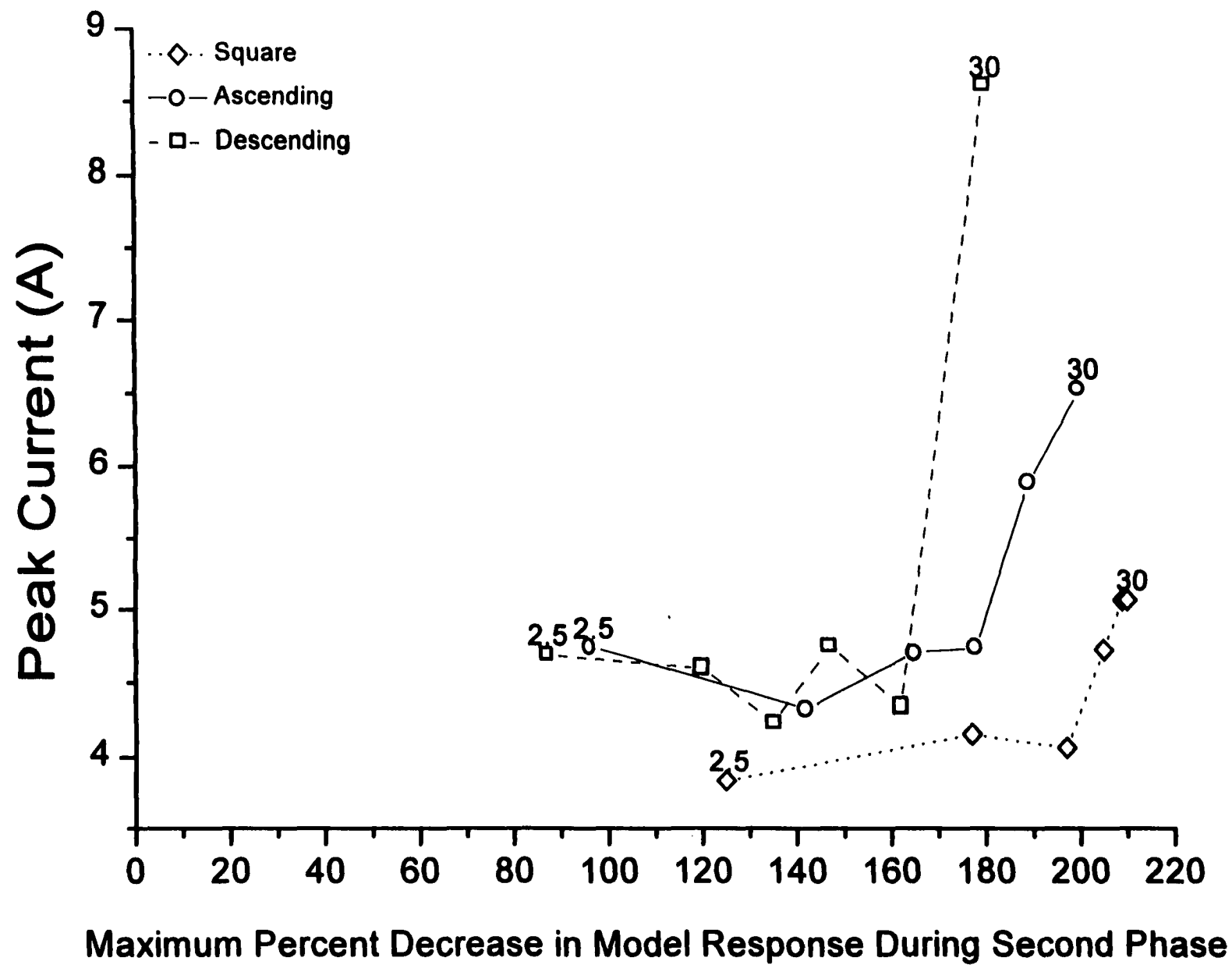
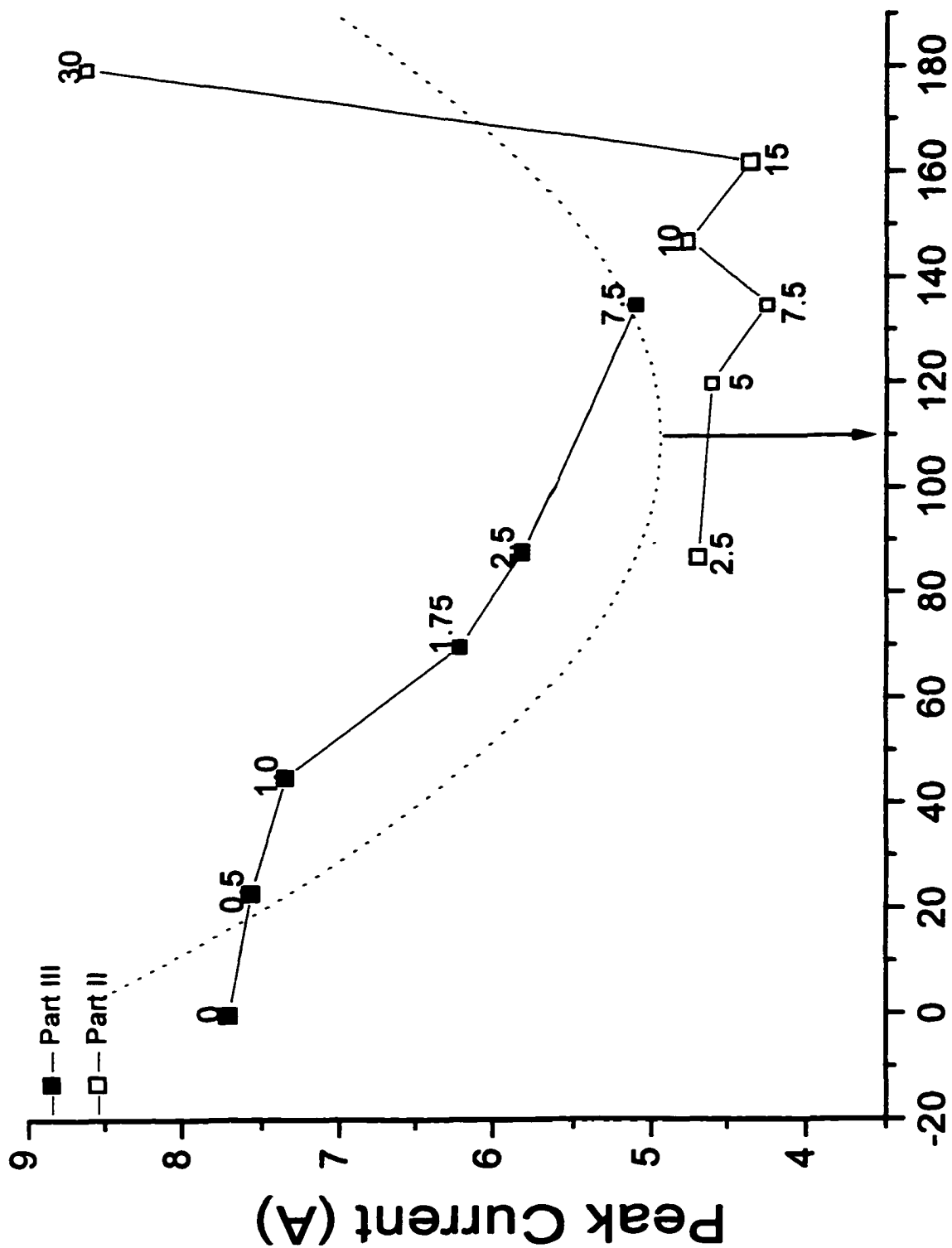


Figure 11. Mean DFTs and second-phase model responses for the biphasic waveforms that had a first phase equal to a 30-ms ascending ramp and a second phase equal to a descending ramp in parts 2 and 3 of the study. Data from part 2 are plotted with open squares. Data from part 3 are plotted with closed squares. Second-phase durations for each waveform are shown above their respective symbols. The parabolic fit and minimum are shown.



Maximum Percent Decrease in Model Response During Second Phase

**MYOCARDIAL DISCONTINUITIES: A SUBSTRATE FOR PRODUCING VIRTUAL
ELECTRODES THAT DIRECTLY EXCITE THE MYOCARDIUM BY SHOCKS**

by

**JAMES B. WHITE, GREGORY P. WALCOTT, ANDREW E. POLLARD,
RAYMOND E. IDEKER**

Circulation 1998;97:1738-1745

**Copyright
1998**

**by
American Heart Association**

Used by Permission

Format adapted for dissertation

Abstract

Background—Theoretical models suggest that an electrical stimulus causes regions of depolarization and hyperpolarization on either side of a myocardial discontinuity. This study determined experimentally whether an artificial discontinuity gives rise to an activation front in response to an electrical stimulus, consistent with the creation of such polarized regions.

Methods and Results—After a thoracotomy in six dogs, a 504-unipolar-electrode plaque was sutured to the right ventricular epicardium to map activations. From a line electrode parallel to one side of the plaque, 10 S_1 stimuli were delivered, followed by S_2 and S_3 stimuli (S_1S_1 , S_1S_2 , S_2S_3 interval = 300 ms). S_1 and S_3 stimuli were 25 mA; 5-ms S_2 stimuli of both polarities were initially 25 mA and increased in 25 mA increments. The plaque was removed, and a transmural incision was made through the ventricular wall in the middle of the mapped region and sutured closed. The plaque was replaced and the stimulation protocol repeated. Before the incision, S_2 stimuli directly activated tissue only near the stimulation site. An activation front arose at the border of the directly activated region and propagated across the plaque. As the S_2 stimulus strength was increased, the size of the directly activated region increased. After the incision, sufficiently large S_2 stimuli caused direct activation of tissue adjacent to the transmural incision as well as at the stimulation site. Activation fronts that arose adjacent to the transmural incision either propagated proximally toward the stimulation site and collided with the activation front originating from the stimulation wire or propagated distally away from the incision. Minimum S_2 stimulus strengths activating areas adjacent

to the incision were only $45\pm 14\%$ (cathode) and $39\pm 18\%$ (anode) of the strengths required to directly activate the same area before the incision was formed ($P<.05$).

Conclusions—Myocardial discontinuities can give rise to activation fronts after a stimulus, suggesting the presence of polarized regions adjacent to the discontinuity.

Introduction

An electrical shock is thought to defibrillate by directly exciting tissue to cause new cardiac action potentials or extension of action potentials.¹⁻⁵ One of several factors that may contribute to the mechanisms by which the shock directly excites myocardium to cause a new action potential in tissue distant from the defibrillation electrodes is discontinuities between myofibers or between bundles of myofibers.^{6,7} These discontinuities can be normal, such as interstitial connective tissue and blood vessels, or abnormal, such as myocardial infarct scars and surgical incisions. By interrupting the closely coupled syncytium of myocytes, these discontinuities interrupt the intracellular space, requiring current that crosses the discontinuity caused by the shock to exit the intracellular space on one side and reenter the intracellular space on the other side of the discontinuity (Figure 1). This transmembrane current should alter the transmembrane potential near the discontinuity, causing depolarization on one side and hyperpolarization on the other. Thus, secondary sources can be created with a virtual cathode in the depolarized region and a virtual anode in the hyperpolarized region.

This study determined whether the magnitude of these secondary sources can be sufficient to directly activate tissue adjacent to the discontinuity. This was done by use of a series of electrical stimuli of increasing strength given before and after a large disconti-

nuity was created by a transmural incision made through the right ventricle of the canine heart. Activation sequence maps were examined to see whether activation fronts arose from either side of the surgical incision, which would indicate that the discontinuity formed by the incision created a virtual electrode.

Methods

Six dogs (18 to 22.5 kg) were anesthetized with pentobarbital (30 mg/kg), intubated and mechanically ventilated using supplemental oxygen, and given maintenance intravenous fluids. The ECG and arterial blood pressure were continuously monitored. Core body temperature, arterial blood gas values, and electrolyte levels were maintained within normal limits. Succinylcholine (0.3 mg/kg) was administered as needed to minimize skeletal muscle stimulation by the shocks. The chest was opened through a right thoracotomy, and a pericardial cradle was created to expose the right ventricle. A plaque containing 504 unipolar epicardial recording electrodes arranged in a 24X21 pattern was sutured onto the right ventricle (Figure 2). The interelectrode distance was 2 mm, resulting in a mapped area of 18.4 cm². The return electrode was sutured to the aortic root. A silver wire 4 cm long was sutured along one side of the plaque (Figure 2) for application of a series of stimuli, called S₁, S₂, and S₃. A titanium mesh electrode sutured on the left ventricle was used as the return electrode for stimulation.

All stimuli were 5-ms, square, constant-current pulses of the same polarity, with the S₁S₁, S₁S₂, and S₂S₃ intervals equal to 300 ms. The S₁ and S₃ stimuli were 25 mA. After 10 S₁ stimuli, the S₂ stimulus initially was 25 mA and then was increased in 25-mA increments until all tissue under the plaque was directly excited as determined by analysis

of results during the study. Cathodal pulses were delivered first, followed by anodal pulses.

After all stimuli were delivered, the plaque was removed, with the sutures left in place. With umbilical tape, the superior and inferior venae cavae were constricted, and a transmural incision averaging 3.6 ± 0.3 cm in length was formed by a cut through the right ventricle in the middle of the mapped area (Figure 2). The incision was sutured closed, and venous inflow was reinstituted. After the animal stabilized, as determined from ECG, blood-pressure, and blood-gas measurements, the plaque was resutured to the same location, and the stimulation protocol as described above was then repeated. In addition to the six experimental animals, two sham-treated animals were also studied. These animals underwent the same protocol as described above minus the creation of the incision.

After the experiment, a lethal dose of KCl was given, and the heart was removed. The region under the plaque was excised, and the tissue was fixed in formalin and sectioned parallel to the epicardial surface at 0.5-mm increments. Fiber orientation was determined from the histological sections. All animals were treated and cared for in accordance with the National Institutes of Health *Guide for the Care and Use of Laboratory Animals*.

Data Acquisition

Simultaneous recordings were made from the plaque with a 528-channel mapping system⁸ with AC-coupled amplifiers with a 0.5-Hz high-pass filter and a 500-Hz low-pass filter. During the S₂ stimulus, the attenuators were switched on, amplifiers were

DC-coupled, and the gain of each channel was decreased. The signals were digitized at 2000 samples per second per channel and stored on a Sun workstation (Sun Microsystems Inc) for analysis during and after the experiment.

Data Analysis

The direction of wave fronts and the presence of collision or block were observed on a computer screen showing animated maps of the first derivative of the electrograms (dV/dt)⁹ determined by a parabola fitted to five data points.¹⁰ Electrodes were displayed as recording an activation when dV/dt was more negative than -0.5 V/s.¹¹ In some cases, activation times were manually assigned to the fastest downslope¹² of the electrograms to construct isochronal maps by use of discrete smooth interpolation.¹³ Electrodes with signals that were saturated or too noisy to allow identification of activations were not analyzed.

For each polarity, the minimum current required to directly activate the areas adjacent to the transmural incision after the incision was compared with the current required to directly activate the same areas before the incision. Also, the current required to directly activate all columns of the mapped region both before and after the incision was determined for each polarity. Direct activation of the mapped area was determined by viewing of animation sequences and by electrogram analysis. Tissue under electrodes that did not record an activation after S_2 stimulation was considered to be directly excited by the stimulus as described previously.^{14,15} To quantify the effect of the incision on the activation sequence, the time interval was determined from the beginning of the S_1 stimulus to activation at electrode 254 in the center of the plaque distal to the incision

(Figure 2). The time interval from the beginning of the S_2 stimulus at the minimum strength required to directly activate tissue adjacent to the incision until the activation time at electrode 254 was also determined. These times were recorded both before and after the incision was created. Activation after the S_3 stimulus was examined to determine whether the large S_2 stimulus altered the activation sequence in response to a 25-mA stimulus. To assess the presence of injury currents as a result of the incision, ST segments were measured in all six animals at electrode 254 and compared at three times: the beginning of the study, immediately after the incision, and the end of the study.

Data are expressed as the mean \pm SD unless otherwise specified. ANOVA with repeated measures and Student's t test for paired samples were used to determine statistical significance. A value of $P \leq 0.05$ was considered significant.

Results

Cathodal Stimuli

Before incision formation. Before the incision, activation after cathodal S_1 stimuli originated near the stimulating electrode and propagated across the recorded area (Figures 3A and 4A). Activation times for the S_3 stimuli were similar to those for the S_1 stimuli. The isochronal activation contours for five out of the six animals were approximately linear and parallel to the stimulating electrode.

Increasing S_2 strength increased the area of tissue directly activated. Figures 3B and 4B show an example for a 75-mA S_2 stimulus that was sufficient only to directly activate a few electrodes in the first two columns of the plaque. At the border of the directly activated area, a wave front arose and propagated across the mapped area. As the S_2 stimulus strength was increased, more tissue was directly activated. For a 250-mA S_2

stimulus (Figures 3C and 4C), almost the entire proximal half of the plaque was directly activated. In Figure 4C, the top seven traces appear to be directly activated by the S₂ stimulus, which corresponds to the direct activation of the first seven columns of electrodes in this region shown in Figure 3C. Eventually, the S₂ stimulus strength was increased enough (400 to 600 mA, Table 1) to directly activate all columns of the mapped region.

Table 1. Minimum Current Required to Activate All Columns of the Mapped Area, mA

Animal	Before Incision		After Incision	
	Cathode	Anode	Cathode	Anode
1	400	400	350	300
2	500	500	350	300
3	600	600	500	500
4	500	500	400	325
5	500	500	475	400
6	600	600	325	225
Average	517	517	400*	342†
SD	75	75	73	96

* $P < .05$ vs cathode, before incision; † $P < .05$ vs anode, before incision.

After incision formation. For cathodal S₁ stimuli after the incision, wave fronts propagated away from the stimulating electrode, blocked near the proximal border of the incision, and wrapped around the ends of the incision to collide on the distal side of the incision (Figures 3D and 4D). The activation patterns after S₃ stimuli were similar to those after S₁ stimuli.

As the S₂ stimulus strength increased, areas of direct activation were observed on both sides of the incision as well as at the stimulation site. Activations originating on the proximal side of the incision propagated toward the stimulating electrode, colliding with

the wave front arising near the stimulating electrode (Figures 3E and 4E). Activations originating on the distal side of the incision propagated distally off the mapped region. The minimum S_2 strength required to directly activate areas adjacent to the incision averaged 104 ± 37 mA (Table 2). This strength differs significantly from the strength required to directly activate the same tissue before the incision (229 ± 49 mA). The area directly activated by a 75-mA S_2 stimulus before the incision (Figure 3B) was smaller than that directly activated after the incision (Figure 3E). Before the incision was made, an S_2 strength of 250 mA was necessary to directly activate the tissue at the site of the incision (Figure 3C). The S_2 strength required to activate all of the mapped region after the incision was also significantly different from that required before the incision (Table 1).

Table 2. Minimum Current Required to Activate Area Adjacent to Transmural Incision, mA

Animal	Before Incision		After Incision		
	Cathode	Anode	Cathode	Anode, P	Anode, D
1	150	75	75	50	100
2	200	150	75	50	225
3	225	75	150	50	125
4	275	175	150	50	250
5	275	150	100	50	175
6	250	150	75	50	100
Average	229	129*	104*	50†‡	163§
SD	49	43	37	0	65

P indicates proximal; D, distal.

* $P < .05$ vs cathode, before incision; † $P < .05$ vs anode, before incision;

‡ $P < .05$ vs cathode, after incision; § $P < .05$ vs anode, P.

Activation times. The time interval from the S_1 stimulus to activation at electrode 254 was significantly shorter before the incision than after (Table 3), consistent

with the incision's creating a barrier that increased the conduction path from the stimulus site to the electrode (Figure 3A versus 3D). At the minimum S_2 stimulus strength that caused activations adjacent to the incision (104 ± 37 mA), the time from the S_2 stimulus to activation at electrode 254 was longer than for this same S_2 stimulus strength before the incision (Table 4), consistent with direct activation at the incision's creating a shorter conduction path (Figure 3B versus 3E).

Table 3. Interval From Beginning of S_1 Stimulus to Activation at Electrode 254, ms

Animal	Before Incision		After Incision	
	Cathode	Anode	Cathode	Anode
1	47	44	56	51
2	54	44	52	60
3	43	35	46	47
4	50	47	72	64
5	51	44	66	56
6	52	45	55	39
Average	50	43*	58*	53†
SD	4	4	10	9

* $P < .05$ vs cathode, before incision; † $P < .05$ vs anode, before incision.

Anodal Stimuli

Before incision formation. As for cathodal S_1 stimuli, activation after anodal S_1 stimuli originated from the proximal portion of the plaque (Figures 5A and 6A). For anodal pulses, however, the line of propagation was approximately parallel with the stimulation wire in only two animals, although this was observed in five animals with cathodal S_1 pulses. The S_3 stimuli activation patterns were again similar to those of S_1 stimuli. As for cathodal S_2 stimuli, increasing anodal S_2 strength increased the area of

tissue directly activated (Figures 5B and 6B). The average anodal S₂ stimulus strength required to activate all columns of the mapped region was 517±75 mA (Table 1).

Table 4. Interval from Beginning of S₂ Stimulus to Activation at Electrode 254, ms

Animal	Before Incision		After Incision	
	Cathode	Anode	Cathode	Anode
1	17	16	11	19
2	26	30	5	36
3	12	26	5	29
4	23	37	13	31
5	33	35	5	49
6	24	21	11	27
Average	23	28	8*	32†
SD	7	8	4	10

* $P < .05$ vs cathode, before incision; † $P < .05$ vs cathode, after incision.

After incision formation. After the incision, wave fronts originated near the anodal S₁ stimulation site, propagated until they blocked at the incision, and then wrapped around the ends of the incision to propagate and collide on the distal side of the incision (Figures 5C and 6C), similar to the activation sequence after cathodal S₁ stimulation.

When the anodal S₂ strength was increased to 50 mA for all animals (Table 2), areas of direct activation were observed adjacent to the incision, as with cathodal S₂ stimulation. Unlike with cathodal S₂ stimuli, however, activation originated only on the proximal side of the incision at this anodal S₂ strength (Figures 5D and 6D). The wave fronts that arose from the proximal side of the incision wrapped around to collide on the distal side of the incision. The anodal S₂ strength that directly activated the area proximal to the incision was significantly smaller than that required to activate the same tissue

before the incision was formed (Table 2). When the S_2 stimulus strength increased to 163 ± 65 mA (Table 2), activation began to originate directly from the tissue on the distal side of the incision. This S_2 stimulus strength was so large that it directly activated all of the tissue proximal to the incision (Figures 5E and 6E).

Activation times. As with the cathodal S_1 stimuli, the time from anodal S_1 stimulation to activation at electrode 254 was shorter before than after the incision (Table 3), consistent with creation of a conduction barrier by the incision. For the minimum anodal S_2 strength that caused direct activation at the incision (50 mA), no significant difference was observed for activation times at electrode 254 before and after the incision (Table 4), consistent with the observation that, at this minimum S_2 stimulus strength, direct activation occurred only on the proximal side of the incision.

Cathodal Stimuli Versus Anodal Stimuli

Before and after the incision, anodal stimuli directly activated tissue just proximal to the incision site at a significantly lower S_2 strength than did cathodal stimuli (Table 2). No significant differences were observed for the two polarities in the stimulus strength required to activate the entire mapped region both before and after the incision (Table 1). Activation times at electrode 254 (Table 3) were significantly shorter for anodal than cathodal S_1 stimuli before the incision, whereas no significant differences for the two polarities were observed after the incision. Conversely, the activation times at electrode 254 were significantly shorter for cathodal than anodal S_2 stimuli after but not before the incision (Table 4).

Visual analysis of the computer animation of activation as well as statistical comparison of the activation times after S_1 and S_2 stimuli in the two sham-treated animals in which no incision was created indicated no significant differences in the activation patterns observed before and after the sham procedure, suggesting that the changes in the other six animals were caused by the incision.

Comparison and statistical analysis of the ST segments measured from electrode 254 before and after the incision indicated a significant change from before (0.58 ± 0.72 mV) to after (6.96 ± 2.68 mV) the incision. As the study progressed, the degree of ST-segment change decreased from 6.96 ± 2.68 mV to 3.82 ± 3.51 mV ($P = .11$).

Fiber Orientation

Fiber orientation for five animals ranged from 48° to 103° with respect to the parallel stimulation wire and incision (Figures 3F and 5F). For the sixth animal, the average fiber angle was 8° , nearly parallel to the stimulation wire and incision. The five hearts with a similar fiber orientation ranged in weight from 155 to 183 g, whereas the sixth heart had a large interatrial defect and weighed 344 g.

Discussion

Our major finding is that surgical incisions can create secondary sources during electrical stimulation. Evidence for this finding is that an electrical stimulus given from an electrode >2 cm away from the incision causes activation fronts to arise and propagate away from the incision at a stimulus strength that does not give rise to activation fronts in this area before the incision. In addition to visual examination of the animation se-

quences and isochronal maps (Figure 3), this finding was verified by quantification of the changes in activation time at a recording electrode near the incision (electrode 254, Figure 2). Before the incision, the time for activation to reach this electrode after a cathodal S_2 stimulus of 104 ± 37 mA was 23 ± 7 ms, whereas after the incision, this electrode recorded activation significantly earlier, 8 ± 4 ms, in response to the same S_2 stimulus (Table 4).

A likely reason that activation arose near the incision was that the incision altered the transmembrane potential response in the adjacent myocardium caused by the S_2 stimulus. Such transmembrane potential changes were observed in a simulation using the bidomain formulation by Street and Plonsey.¹⁶ The surgical incision is thought to interrupt the intracellular space but, because the myocardium is sutured back together, not to interrupt the extracellular space. Because the intracellular space is interrupted, any intracellular current that would normally flow during the S_2 stimulus is forced to exit the intracellular space, cross the incision in the extracellular space, and then reenter the intracellular space on the other side of the incision (Figure 1). As current crosses the cell membrane, it alters the transmembrane potential. In this way, the incision serves as a boundary to current flow, causing depolarization on one side of the incision and hyperpolarization on the other.^{6,7}

Injury potentials caused by the incision may have influenced these findings. To explore this possibility, computer simulations were performed that are presented in the "Appendix." These simulations suggest that changes in the transmembrane potential caused by the incision can lower the stimulus strength required to directly excite tissue at the incision (Figure 7D). Elevation of the resting membrane potential to just below the

threshold for activation of the sodium channels can cause the electrical stimulus to activate the tissue in this region even in the absence of an incision (Figure 7C). However, the alteration to cause this effect is extreme (ie, 17 mmol/L extracellular potassium concentration) and may not be present 30 minutes after the incision is created.

The S_2 stimulus was delivered in diastole, when activation is thought to occur in tissue that is sufficiently depolarized, but not in regions of hyperpolarization.^{17,18} Depolarization should occur on the distal side of the incision when the stimulus electrode is a cathode and on the proximal side of the incision when the stimulus electrode is an anode (Figures 1 and 7). Activation propagated away from both sides of the incision, not just the side that was thought to be depolarized. For a cathodal S_2 stimulus, activation propagated away from both sides of the incision with the smallest S_2 stimulus strength that caused activation to originate near the incision (Figure 3D). For an anodal S_2 stimulus, activation first appeared only at the proximal side of the incision as the S_2 strength was increased (Figure 5D). As the anodal stimulus strength was increased still further, activation fronts also originated from the distal side of the incision (Figure 5E).

The reason for these observations is unclear, but may be related to the "dog bone" phenomenon reported by Wikswo and others,¹⁹⁻²¹ who found that along myofibers only 1 to 2 mm away from an anode, the change in transmembrane potential reversed from hyperpolarization to depolarization. Conversely, a few millimeters along fibers away from a cathode, depolarization changed to hyperpolarization. Similar findings have recently been observed for a wire stimulating electrode as used in our study.²² These changes in transmembrane potential are not seen in the simulation discussed in the "Appendix" because they are one-dimensional. If the same changes occur just outside

the secondary sources formed by the incision, a depolarized region should exist just proximal to the hyperpolarized region on the proximal side of the incision during a cathodal stimulus. Similarly, a depolarized region should exist just distal to the hyperpolarized region on the distal side of the incision during an anodal S_2 stimulus. The areas of depolarization may give rise to the activation fronts seen in these regions after the S_2 stimulus. Because the field strength of the S_2 stimulus decreases with distance away from the electrode, it is probably smaller on the distal side of the incision than on the proximal side. If so, the depolarized region on the distal side of the incision during an anodal S_2 stimulus may be weaker than the depolarized region on the proximal side during a cathodal stimulus. This may explain why a larger S_2 stimulus is necessary to create an activation front on the distal side of the incision for an anodal stimulus than on the proximal side for a cathodal stimulus.

Another possible reason for this poststimulus activation behavior is the injury currents created by the incision (see "Appendix"). Experimentally, injury currents were detected adjacent to the incision in all animals. As the stimulation protocol progressed, the ST-segment changes tended to decrease with time, although they never completely disappeared. This suggests that the tissue surrounding the incision never had ample time to heal and as such may have continually produced an elevation in the transmembrane potential, which in turn may have altered tissue excitability after the incision. A third possible explanation for these findings is that break excitation occurred in areas hyperpolarized during the stimulus. For cathodal stimuli, break excitation may occur in the hyperpolarized region on the proximal side of the incision, resulting in subsequent propagation toward the stimulation wire. For an anodal shock of the same strength,

hyperpolarization distal to the incision may be smaller than on the proximal side of the incision for a cathodal shock as a result of the smaller electrical field on the distal side of the incision, because it is farther from the stimulating electrode than the proximal side. Consequently, a larger stimulus strength would be required to directly activate the distal side of the incision by means of break excitation for anodal stimuli. On the basis of the results generated from the simulations, however, break excitation is not the likely means of stimulation observed in this set of experiments, even in the presence of injury currents (see “Appendix”).

These results have several implications for defibrillation. It is likely that secondary sources are not specific for surgical incisions but rather can form at any site in which the intracellular space is interrupted. Such interruptions occur naturally between bundles of myocardial fibers and where blood vessels and nerves traverse the myocardium. Thus, these results support the findings of Gillis et al⁶ and suggest that secondary sources can be an important mechanism for defibrillation. The magnitude of the secondary source probably depends on many factors, including size of the discontinuity, strength of the shock field, fiber orientation, and degree of anisotropy. This study indicates that when the discontinuity is transmural and several centimeters long, the secondary source can significantly affect the response to a shock. Such an interruption directly activated the tissue on at least one side of the incision with a stimulus strength that was only 39% of that required to directly activate this tissue when the interruption was absent (Table 2). The interruption had a smaller but still significant effect on direct activation by the shock 1 to 2 cm distal to the incision; the mean shock strength needed to directly activate tissue beneath all columns of the plaque was reduced 34% by the incision (Table 1).

Scars caused by infarction, cardiomyopathy, or surgical incisions may also serve as secondary sources. This phenomenon may explain why defibrillation thresholds are typically not increased by infarction,^{23,24} even though current shunting may occur through the scar because its conductivity is higher than that of myocardium.²⁵ Current shunting may be offset by secondary sources at the infarct border.

Surgical or ablation incisions may alter the defibrillation threshold. If the incisions are not transmural and do not extend to a boundary, they may be arrhythmogenic by allowing reentry to form around the anatomic barrier formed by the incision. If they are transmural and reach a boundary, however, they may lower the defibrillation threshold by creating barriers to conduction that decrease the incidence of reentrant pathways immediately after the shock, just as the maze surgical procedure decreases the incidence of spontaneous reentry leading to atrial fibrillation.²⁶ Our study raises the possibility that surgical or ablation incisions also may lower the defibrillation threshold by a second mechanism: creation of secondary sources. These secondary sources may lower the shock strength needed to directly activate tissue, thus lowering the defibrillation threshold.

Appendix

We performed computer simulations to examine the effects of elevated $[K^+]_e$, one factor responsible for injury potentials associated with acute injury near the incision. Electrical activity was modeled by use of a one-dimensional bidomain representation of tissue structure,²⁷

$$(1) \quad I_m = \nabla \cdot (\sigma_i \nabla \phi_i) = -\nabla \cdot (\sigma_e \nabla \phi_e)$$

with σ_i is intracellular conductivity, σ_e is interstitial conductivity, ϕ_i is intracellular potential, ϕ_e is interstitial potential, and I_m is transmembrane current density. I_m was further specified in terms of membrane sources:

$$(2) \quad I_m = A_m (C_m \frac{\partial V_m}{\partial t} + I_{ion})$$

where C_m is specific membrane capacitance, $V_m = (\phi_i - \phi_e)$ is transmembrane potential, I_{ion} is ionic current source density, and A_m is ratio of membrane surface to intracellular volume. Substituting $\phi_i = V_m + \phi_e$ into Equation 1, Equation 2 is rewritten as

$$(3) \quad G_{ix} (\frac{\partial^2 V_m}{\partial x^2} + \frac{\partial^2 \phi_e}{\partial x^2}) + G_{iy} (\frac{\partial^2 V_m}{\partial y^2} + \frac{\partial^2 \phi_e}{\partial y^2}) = C_m \frac{\partial V_m}{\partial t} + I_{ion}$$

where $G_{ix} = (g_{il} / A_m)$ is a coupling coefficient expressed in terms of the specific intracellular conductivity along the fiber axis (g_{il}) and $G_{iy} = (g_{it} / A_m)$ is expressed in terms of the specific intracellular conductivity across the fiber axis (g_{it}). In solving Equation 3, we assumed sealed end boundary conditions at the edges of the tissue and the interstitium. The model was 10 cm long and 50 μm wide, resulting in 2002 nodes (Table 5). We determined the interstitial potential distributions from the transmembrane potential distribution using a rewritten form of Equation 2,

$$(4) \quad (G_{ix} + G_{ex}) \frac{\partial^2 \phi_e}{\partial x^2} + (G_{iy} + G_{ey}) \frac{\partial^2 \phi_e}{\partial y^2} = -G_{ix} \frac{\partial^2 V_m}{\partial x^2} - G_{iy} \frac{\partial^2 V_m}{\partial y^2}$$

where $G_{ex} = (g_{el} / A_m)$ is a coupling coefficient expressed in terms of the specific interstitial conductivity along the fiber axis (g_{el}) and $G_{ey} = (g_{et} / A_m)$ is expressed in terms of the specific interstitial conductivity across the fiber axis (g_{et}).

The numerical solution scheme was similar to that reported previously.²⁸ Ordinary differential equations defining the gating variables for the individual ionic currents

of I_{ion} in Equation 2 were integrated numerically in time by an analytic method with Luo-Rudy membrane equations at all tissue nodes.^{29,30} Equations 3 and 4 were discretized in space with a five-point finite-difference stencil. Discretization in time used a semi-implicit averaging scheme analogous to the Crank-Nicholson method in one space dimension. Because the matrix for the linear system was sparse, efficient solutions for V_m were achieved with a preconditioned conjugate gradient scheme (DITSOL_PCG from the Digital Equipment Corp Digital Extended Math Library, dxml). A 5-ms monophasic “shock” was applied by modification of the difference equations for nodes on the left and right edges of the model to fix the interstitial potentials on each edge. Calculations were then continued for 5 ms after the shock. The resulting sparse linear system for ϕ_e was solved with the same preconditioned conjugate gradient method as in solutions for V_m .

Table 5. Modeling Parameters

Specific membrane capacitance	C_m	1.0 $\mu\text{F}/\text{cm}^2$
Membrane surface to intracellular volume ratio	A_m	500 cm^{-1}
Spatial integration step size	dx	100 μm
Spatial integration step size	dy	25 μm
Temporal integration step size	dt_{min}	4.0 μs
Number of nodes in x direction	N_x	1001
Number of nodes in y direction	N_y	2
Longitudinal intracellular coupling coefficient	G_{ix}	0.001 mS
Transverse intracellular coupling coefficient	G_{iy}	0.0001 mS
Longitudinal interstitial coupling coefficient	G_{ex}	0.001 mS
Transverse interstitial coupling coefficient	G_{ey}	0.0005 mS

To represent configurations similar to the experiments, we performed simulations using models that included (1) no incision and nominal $[\text{K}^+]_e$ (5.4 mmol/L, resting membrane potential $[\text{RMP}] = -82.3$ mV); (2) an incision, represented as a complete

interruption in intracellular coupling between adjacent nodes located 2.5 cm from the left edge, combined with nominal $[K^+]_e$; (3) no incision and elevated $[K^+]_e$ at nodes 2 and 3 cm from the left edge; and (4) an incision combined with elevated $[K^+]_e$. In each simulation, the cathode was located on the left edge of the model and the anode on the right edge. In models 1 and 2, shock strengths were increased until the diastolic threshold for stimulation (DTS) current was found. In models 3 and 4, $[K^+]_e$ current was increased until a shock of strength 0.96XDTS initiated a depolarization wave front from the elevated $[K^+]_e$ region.

No Incision, Nominal $[K^+]_e$

At the end of the stimulus, depolarization occurred at the cathode at DTS and 0.96XDTS (Figure 7A). At 10 ms, an action potential arose from the site of depolarization for the DTS stimulus and propagated toward the anode (Figure 7, right). Because the 0.96XDTS stimulus did not reach threshold, no action potential occurred.

Incision, Nominal $[K^+]_e$

With the incision, an area of depolarization occurred with both stimulus strengths at the cathode (Figure 7A). For both stimulus strengths, areas of hyperpolarization and depolarization occurred adjacent to the proximal and distal sides of the incision, respectively (Figure 7B, left). At 10 ms after the stimulus (Figure 7B, right), a depolarization wave front arose at the stimulation site for the DTS stimulus. A wave front also arose from the distal side of the incision where depolarization was created by the stimulus. No wave front arose at either site after the 0.96XDTS stimulus.

No Incision, Elevated $[K^+]_e$

In the absence of an incision when extracellular potassium was increased to 16 and 17 mmol/L, resting membrane potential was elevated to -55.1 and -53.6 mV, respectively (Figure 7C, left). At 10 ms after the stimulus, the 0.96XDTS stimulus elicited an action potential at a potassium concentration of 17 mmol/L but not 16 mmol/L. This action potential propagated in both directions away from the site of elevated potassium but not from the cathodal end of the tissue, because the stimulus was slightly less than the DTS (Figure 7C, right).

Incision, Elevated $[K^+]_e$

With the incision present, 5 ms following the onset of the 0.96XDTS stimulus, an area of depolarization occurred at the cathode for both concentrations of potassium (Figure 7B). At the incision, hyperpolarization and depolarization were observed on the proximal and distal sides of the incision, respectively (Figure 7D, left). The degree of polarization was slightly larger for 7 mmol/L $[K^+]_e$ (RMP= -75.8 mV) than for 6 mmol/L $[K^+]_e$ (RMP= -79.6 mV). At 10 ms after the onset of the 0.96XDTS stimulus, a wave front arose on the distal side of the incision for 7 mmol/L but not 6 mmol/L potassium concentration (Figure 7D, right).

Acknowledgements

This study was supported by a National Institutes of Health research grant (HL-42760), a special opportunity award from the Whitaker Foundation, a grant-in-aid of

research from Sigma Xi, a National Science Foundation/National Young Investigator Award (BES-9457212), and a grant from the National Institutes of Health (R29-HL-54024). The authors wish to thank Dr William M. Smith and Catherine M. Sreenan for their statistical analyses and helpful editorial comments. We are also grateful to Sharon M. Melnick and Anthony L. Sims for their expert technical assistance.

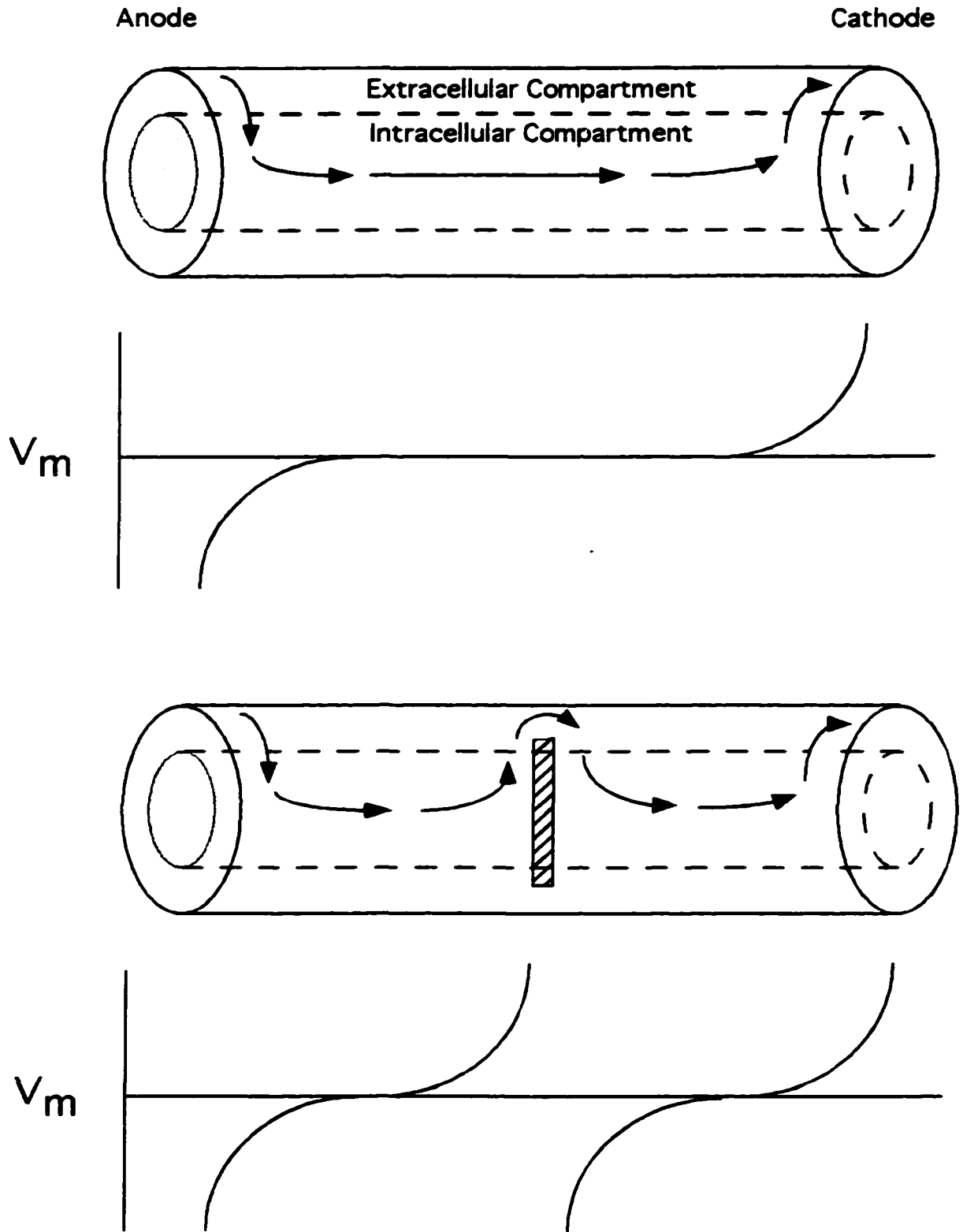
References

1. Chen P-S, Shibata N, Dixon EG, Martin RO, Ideker RE. Comparison of the defibrillation threshold and the upper limit of ventricular vulnerability. *Circulation*. 1986;73:1022-1028.
2. Jones JL, Tovar OH. The mechanism of defibrillation and cardioversion. *Proc IEEE*. 1996;84:392-403.
3. Knisley SB, Smith WM, Ideker RE. Effect of field stimulation on cellular repolarization in rabbit myocardium: Implications for reentry induction. *Circ Res*. 1992;70:707-715.
4. Sweeney RJ, Gill RM, Steinberg MI, Reid PR. Ventricular refractory period extension caused by defibrillation shocks. *Circulation*. 1990;82:965-972.
5. Zhou X, Knisley SB, Wolf PD, Rollins DL, Smith WM, Ideker RE. Prolongation of repolarization time by electric field stimulation with monophasic and biphasic shocks in open chest dogs. *Circ Res*. 1991;68:1761-1767.
6. Gillis AM, Fast VG, Rohr S, Kléber AG. Spatial changes in transmembrane potential during extracellular electrical shocks in cultured monolayers of neonatal rat ventricular myocytes. *Circ Res*. 1996;79:676-690.
7. Krassowska W, Frazier DW, Pilkington TC, Ideker RE. Potential distribution in three-dimensional periodic myocardium-- Part II: Application to extracellular stimulation. *IEEE Trans Biomed Eng*. 1990;37:267-284.
8. Wolf PD, Rollins DL, Blitchington TF, Ideker RE, Smith WM. Design for a 512 channel cardiac mapping system. In: Mikulecky DC, Clarke AM, eds. *Biomedical Engineering: Opening New Doors. Proceedings of the Fall 1990 Annual Meeting of the Biomedical Engineering Society*. New York: New York University Press; 1990:5-13.

9. Laxer C, Ideker RE, Smith WM, Wolf PD, Simpson EV. A graphical display system for animating mapped cardiac potentials. In: *Proceedings of the 3rd IEEE Symposium on Computer-Based Medical Systems*. Los Alamitos, Calif:IEEE Computer Society Press; 1990:197-204.
10. Cabo C, Wharton JM, Wolf PD, Ideker RE, Smith WM. Activation in unipolar cardiac electrograms: A frequency analysis. *IEEE Trans Biomed Eng*. 1990;37:500-508.
11. Bollacker KD, Simpson EV, Hillsley RE, Blanchard SM, Gerstle RJ, Walcott GP, Callihan RC, King MC, Smith WM, Ideker RE. An automated technique for identification and analysis of activation fronts in a two-dimensional electrogram array. *Comput Biomed Res*. 1994;27:229-244.
12. Spach MS, Barr RC, Serwer GA, Kootsey JM, Johnson EA. Extracellular potentials related to intracellular action potentials in dog Purkinje system. *Circ Res*. 1972;30:505-519.
13. Simpson EV, Ideker RE, Kavanagh KM, Alferness CA, Melnick SB, Smith WM. Discrete smooth interpolation as an aid to visualizing electrical variables in the heart wall. In: Murray A, Arzbaecher R, eds. *Proceedings. Computers in Cardiology*. Los Alamitos, Calif.: IEEE Computer Society Press; 1991:409-412.
14. Daubert JP, Frazier DW, Wolf PD, Franz MR, Smith WM, Ideker RE. Response of relatively refractory canine myocardium to monophasic and biphasic shocks. *Circulation*. 1991;84:2522-2538.
15. Colavita PG, Wolf PD, Smith WM, Bartram FR, Hardage M, Ideker RE. Determination of effects of internal countershock by direct cardiac recordings during normal rhythm. *Am J Physiol*. 1986;250:H736-H740.
16. Street AM, Plonsey R. Activation fronts elicited remote to the pacing site due to the presence of scar tissue. In: *IEEE Engineering in Medicine & Biology: 17th Annual Conference*. Piscataway, NJ: IEEE-EMB; 1995:1-2.
17. Roth BJ. A mathematical model of make and break electrical stimulation of cardiac tissue by a unipolar anode or cathode. *IEEE Trans Biomed Eng*. 1995;42:1174-1184.
18. Dekker E. Direct current make and break thresholds for pacemaker electrodes on the canine ventricle. *Circ Res*. 1970;27:811-823.
19. Wikswo JP Jr, Lin S-F, Abbas RA. Virtual electrodes in cardiac tissue: A common mechanism for anodal and cathodal stimulation. *Biophys J*. 1995;69:2195-2210.

20. Tung L, Borderies J-R. Analysis of electric field stimulation of single cardiac muscle cells. *Biophys J*. 1992;63:371-386.
21. Knisley SB, Hill B, Ideker RE. Virtual electrode effects in myocardial fibers. *Biophys J*. 1994;66:719-728.
22. Knisley SB, Baynham TC. Line stimulation parallel to myofibers enhances regional uniformity of transmembrane voltage changes in rabbit hearts. *Circ Res*. 1997;81:229-241.
23. Wharton JM, Richard VJ, Murry CE, Jr., Dixon EG, Reimer KA, Meador J, Smith WM, Ideker RE. Electrophysiological effects of monophasic and biphasic stimuli in normal and infarcted dogs. *Pacing Clin Electrophysiol*. 1990;13:1158-1172.
24. Chang MS, Inoue H, Kallok MJ, Zipes DP. Double and triple sequential shocks reduce ventricular defibrillation threshold in dogs with and without myocardial infarction. *J Am Coll Cardiol*. 1986;8:1393-1405.
25. Fallert MA, Mirotznik MS, Downing SW, Savage EB, Foster KR, Josephson ME, Bogen DK. Myocardial electrical impedance mapping of ischemic sheep hearts and healing aneurysms. *Circulation*. 1993;87:199-207.
26. Cox JL. The surgical treatment of atrial fibrillation: IV. surgical technique. *J Thorac Cardiovasc Surg*. 1991;101:584-592.
27. Roth BJ. Action potential propagation in a thick strand of cardiac muscle. *Circ Res*. 1991;68:162-173.
28. Pollard AE, Hooke N, Henriquez CS. Cardiac propagation simulation. *Crit Rev Biomed Eng*. 1992;20:171-210.
29. Luo C-H, Rudy Y. A dynamic model of the cardiac ventricular action potential; I: simulations of ionic currents and concentration changes. *Circ Res*. 1994;74:1071-1096.
30. Zeng J, Laurita KR, Rosenbaum DS, Rudy Y. Two components of the delayed rectifier K⁺ current in ventricular myocytes of the guinea pig type: Theoretical formulation and their role in repolarization. *Circ Res*. 1995;77:140-152.

Figure 1. Effect of an intracellular discontinuity on current flow. Top, As current (indicated by the arrows) crosses from extracellular compartment to intracellular, a change in transmembrane potential is observed. Near an extracellular anode, transmembrane potential (V_m) is hyperpolarized as shown below. Near cathode, current exits intracellular compartment and depolarizes transmembrane potential. Bottom, When an intracellular discontinuity is present (hatched region), current is forced from intracellular to extracellular compartment and reenters cell on other side of discontinuity. On side of discontinuity close to anode, a virtual cathode is formed as current leaves cell while a virtual anode is formed on opposite side of discontinuity as current reenters cell.



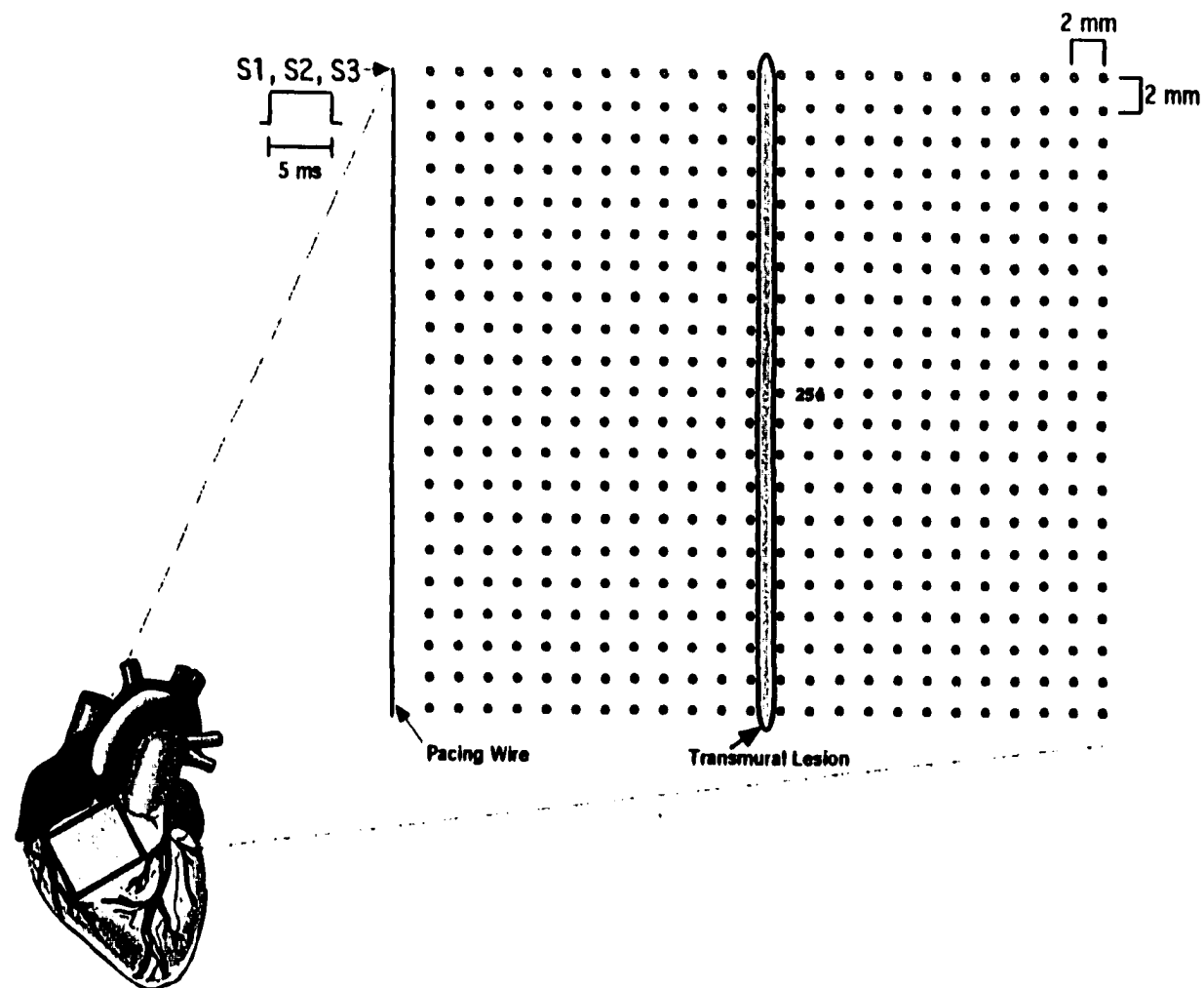


Figure 2. Mapped area and incision on right ventricle. Each small circle represents a recording site on mapping plaque. Location of electrode 254 is indicated.

Figure 3. Isochronal activation maps after cathodal stimuli for one animal. Isochrones are drawn at 5-ms intervals timed from onset of S_1 or S_2 stimulus. Arrows represent direction of activation. Darkened regions represent areas directly activated by the stimulus. Black vertical bars represent approximate location of transmural incision. A, S_1 stimulus delivered before incision; B, 75-mA S_2 stimulus delivered before incision; C, 250-mA S_2 stimulus delivered before incision; D, S_1 stimulus delivered after incision; E, 75-mA S_2 stimulus delivered after incision; F, orientation of long axis of myocardial fibers. *Most proximal electrode in row 6, from which the recordings are shown in Figure 4.

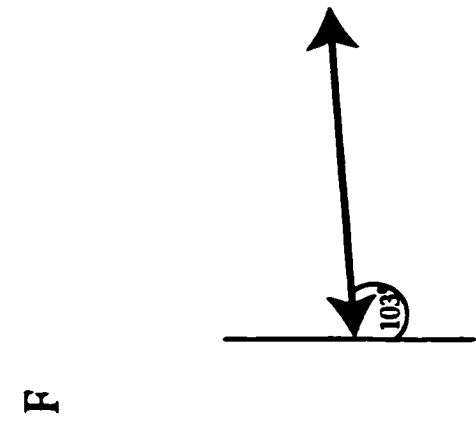
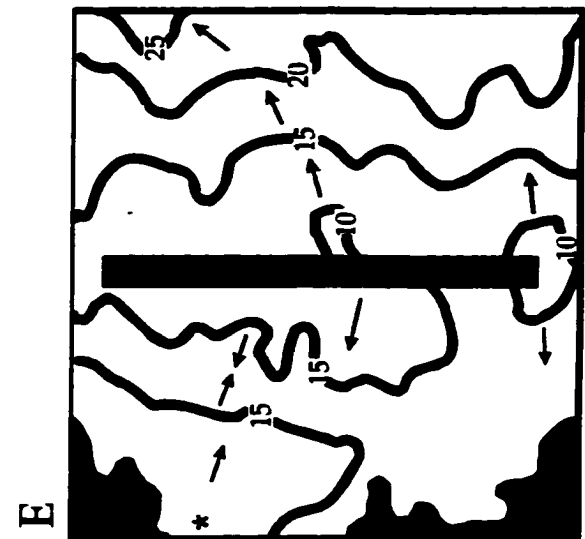
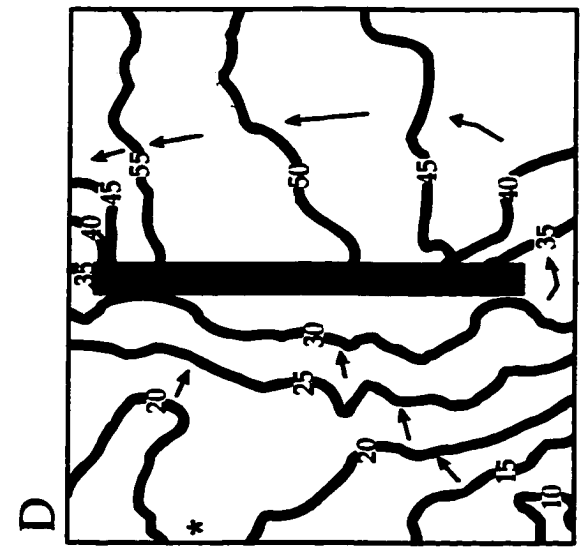
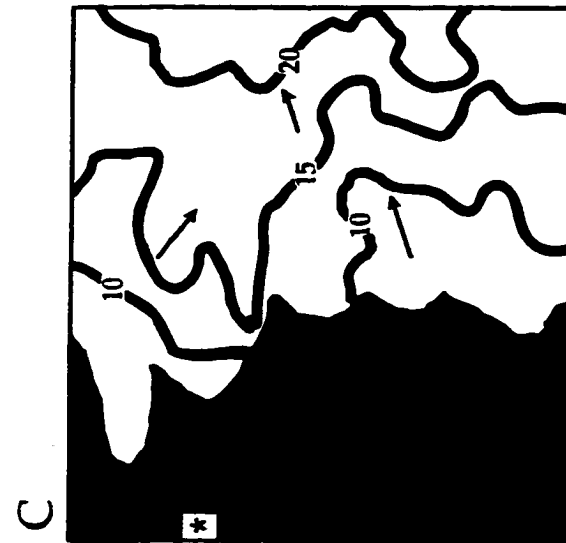
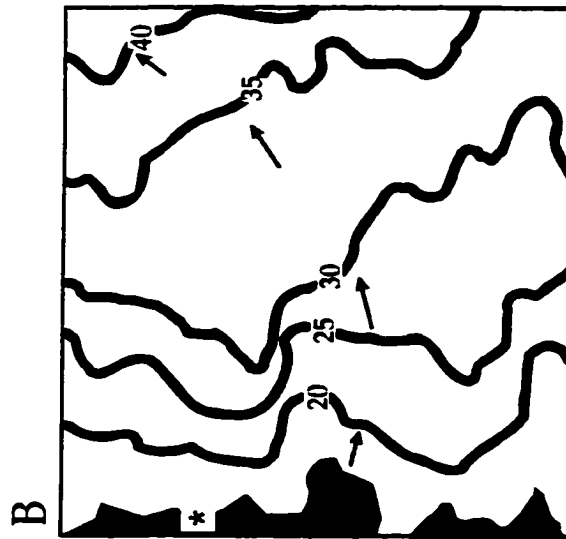
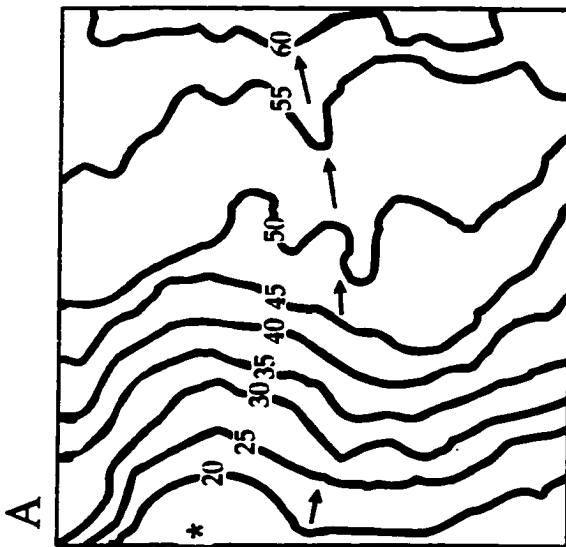


Figure 4. Electrograms recorded from row 6 of electrodes during activation sequences in Figure 3. Electrode most proximal to stimulating electrode is at top and most distal electrode of row is at bottom of each panel. Vertical daggers represent activation times; arrows, direction of propagation. Each electrogram tracing begins with the 5-ms stimulus. A, S_1 stimulus delivered before incision; B, 75-mA S_2 stimulus delivered before incision; C, 250-mA S_2 stimulus delivered before incision; D, S_1 stimulus delivered after incision; E, 75-mA S_2 stimulus delivered after incision.

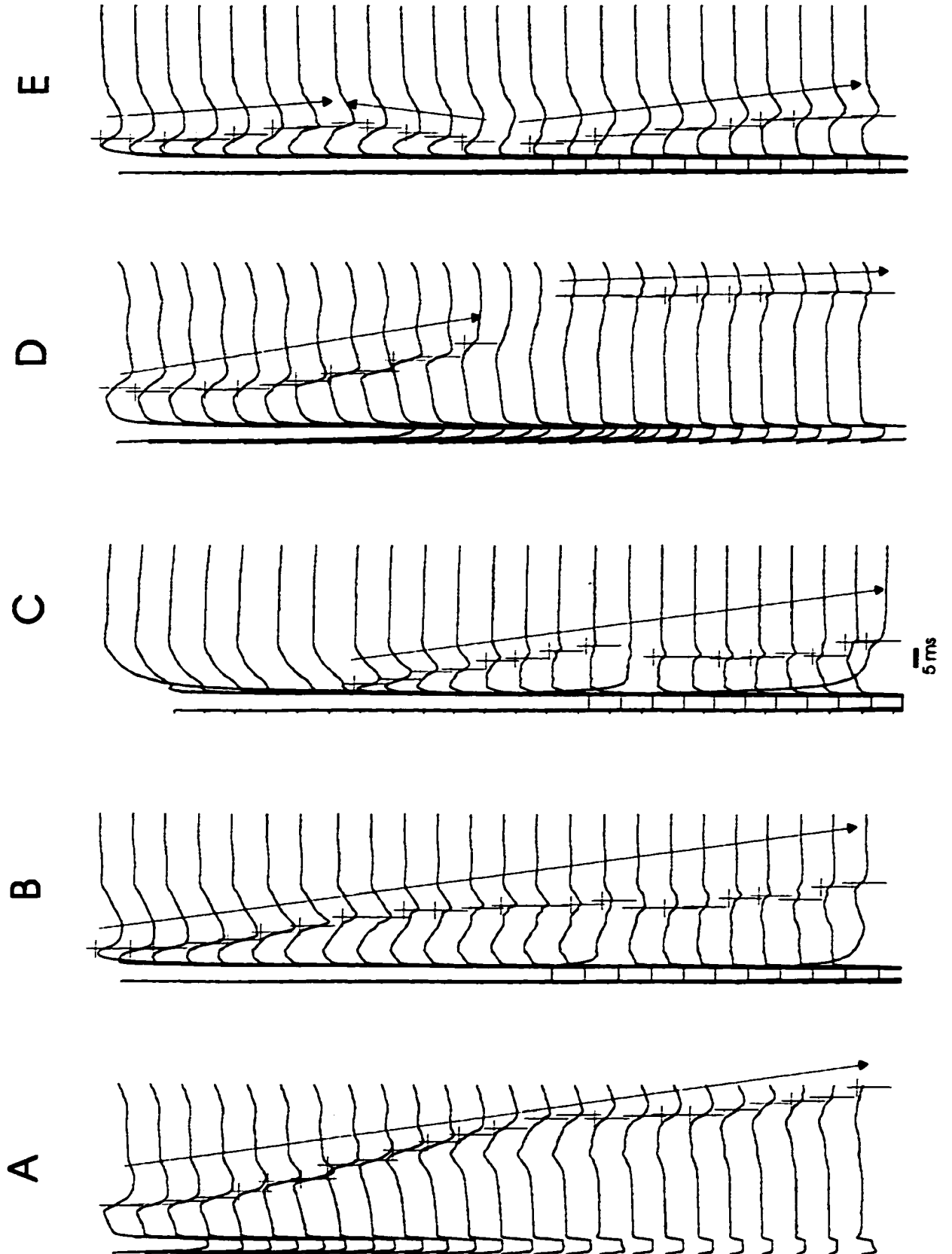
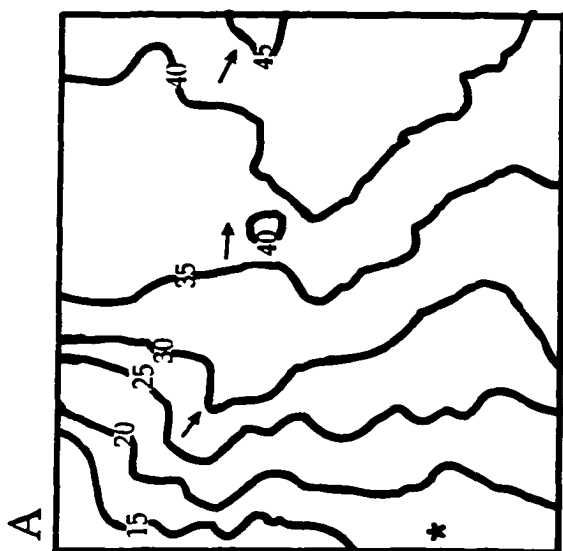
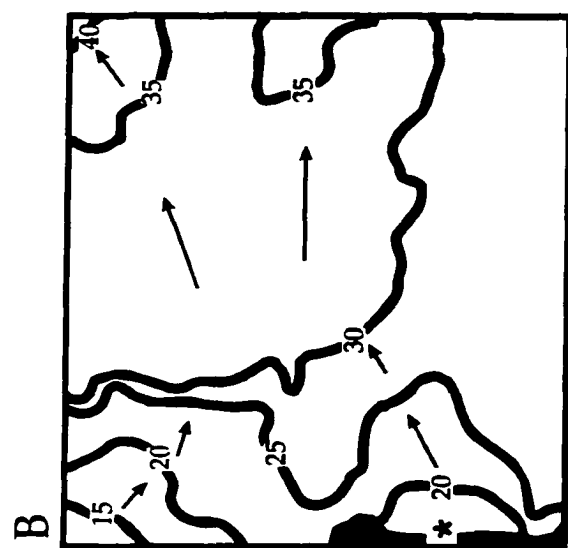
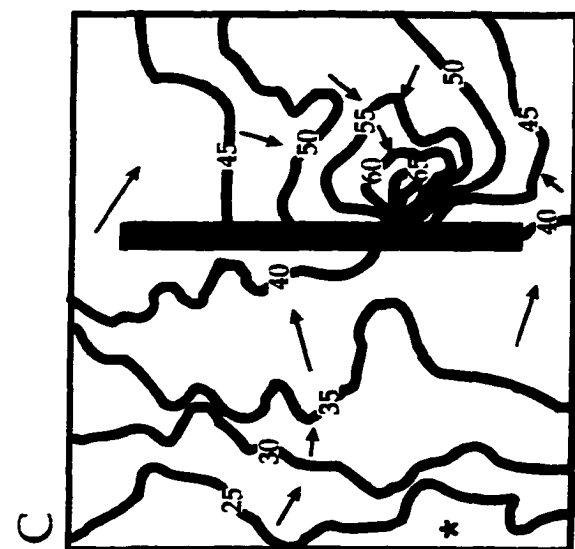


Figure 5. Isochronal activation maps after anodal stimuli for one animal. Isochrones are drawn at 5-ms intervals timed from onset of S_1 or S_2 stimulus. Arrows represent direction of activation. Darkened regions represent areas directly activated. Black vertical lines represent approximate location of transmural incision. A, S_1 stimulus delivered before incision; B, 75-mA S_2 stimulus delivered before incision; C, S_1 stimulus delivered after incision; D, 75-mA S_2 stimulus delivered after incision; E, 250-mA stimulus delivered after incision; F, orientation of long axis of myocardial fibers.



F

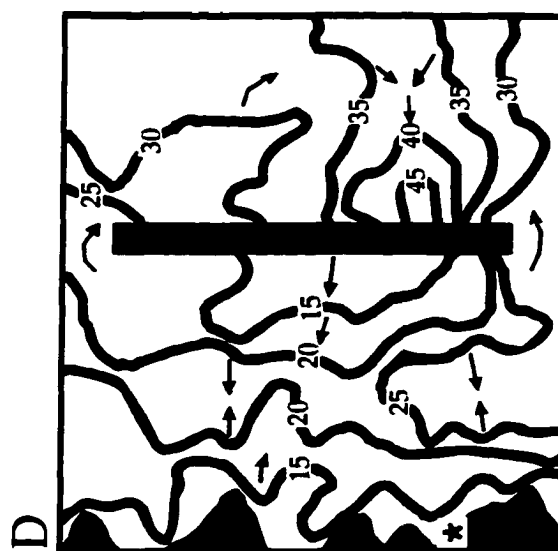
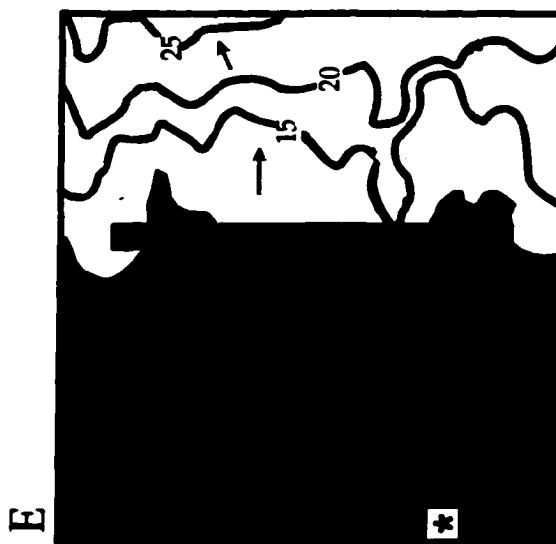
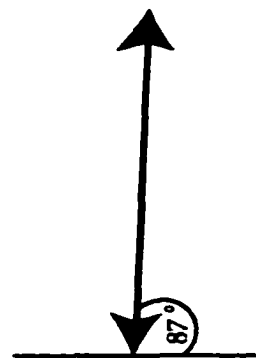
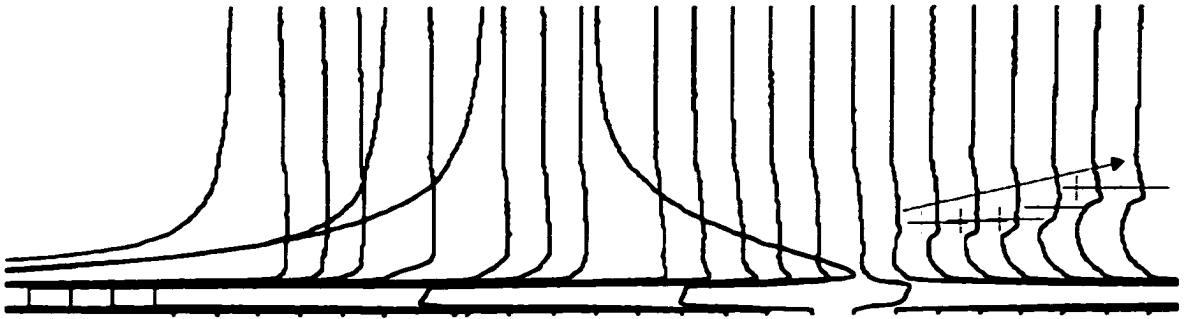
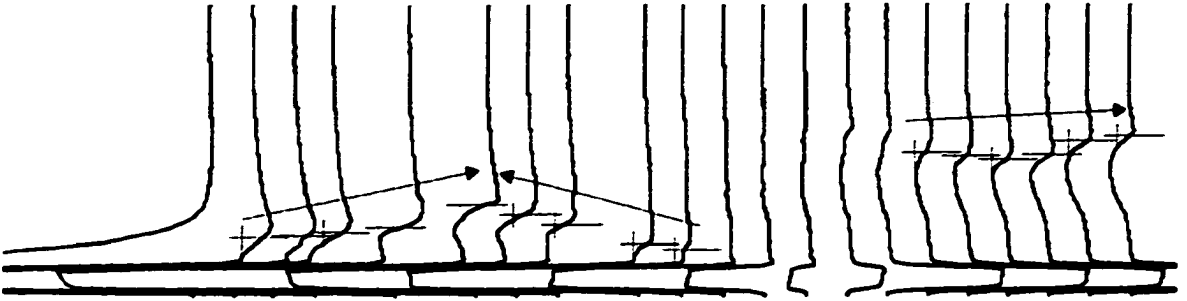


Figure 6. Electrograms recorded from row 15 of electrodes during activation sequences in Figure 5. Electrode most proximal to stimulating electrode is at top and most distal electrode is at bottom of each panel. Vertical daggers represent activation times. Arrows represent direction of propagation. Each electrogram tracing begins with the 5-ms stimulus. A, S₁ stimulus delivered before incision; B, 75-mA S₂ stimulus delivered before incision; C, S₁ stimulus delivered after incision; D, 75-mA S₂ stimulus delivered after incision; E, 250-mA S₂ stimulus delivered after incision.

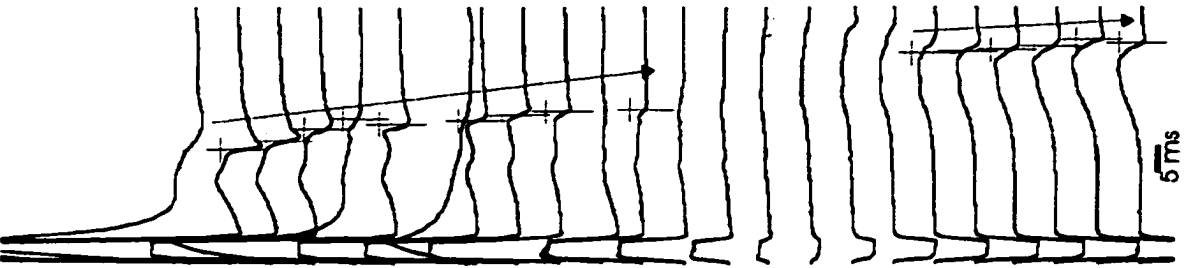
E



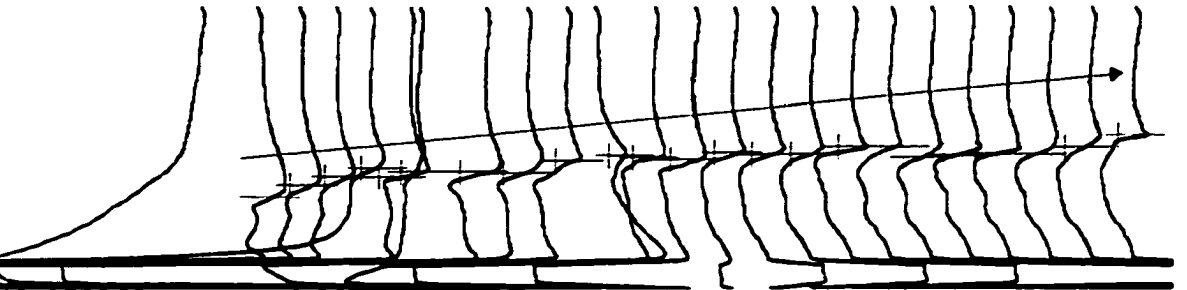
D



C



B



A

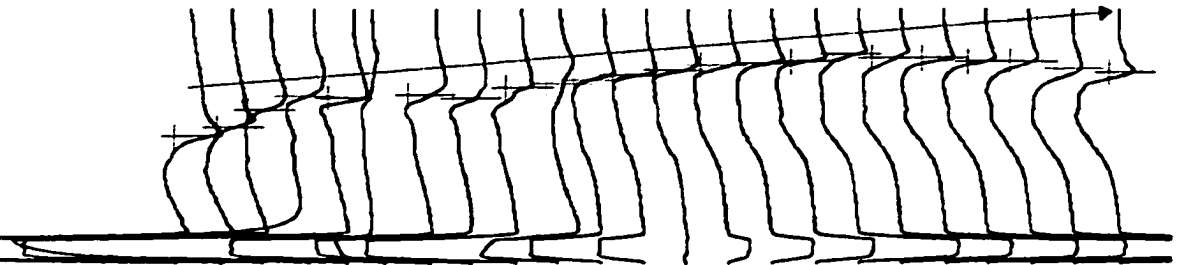
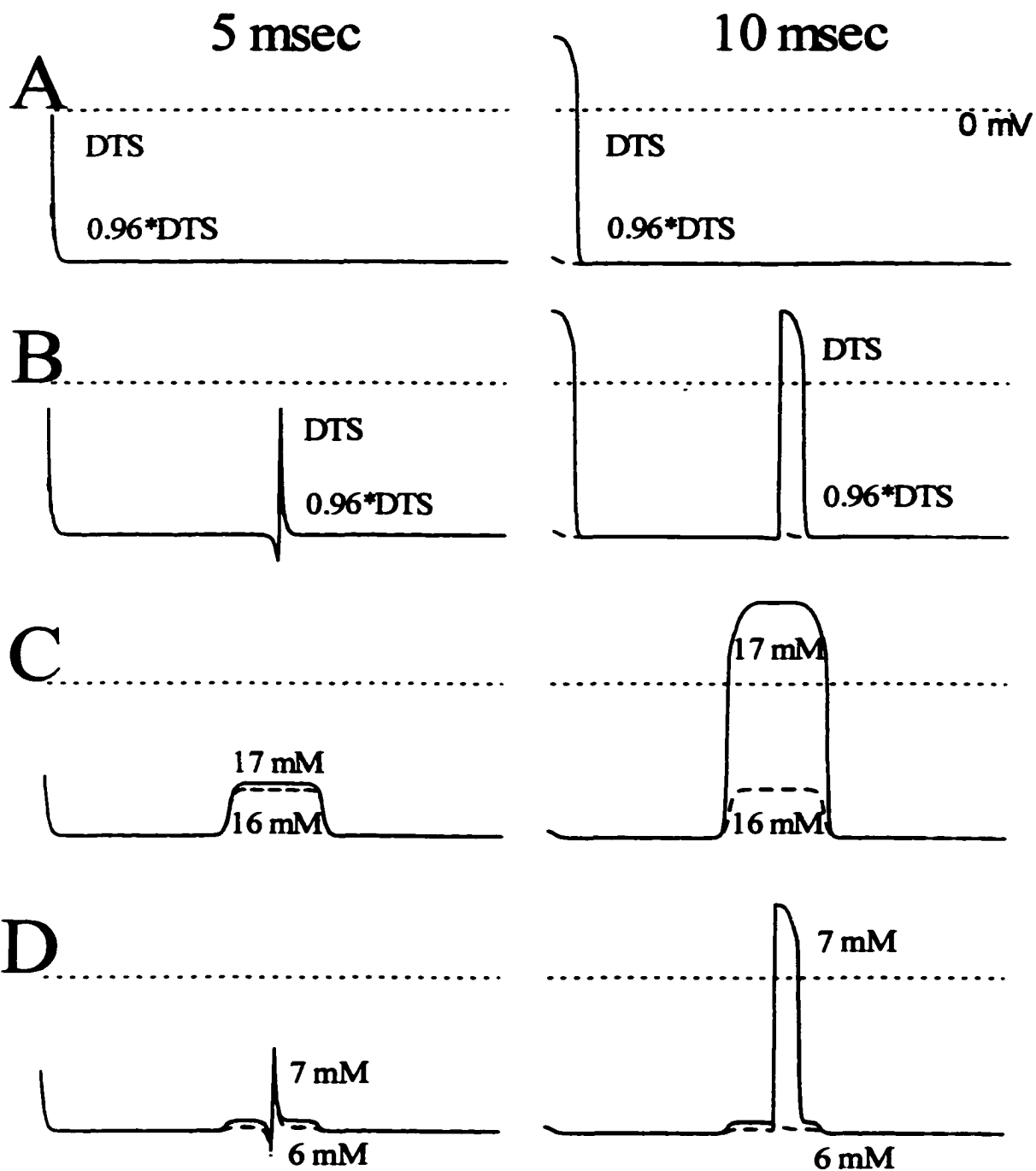
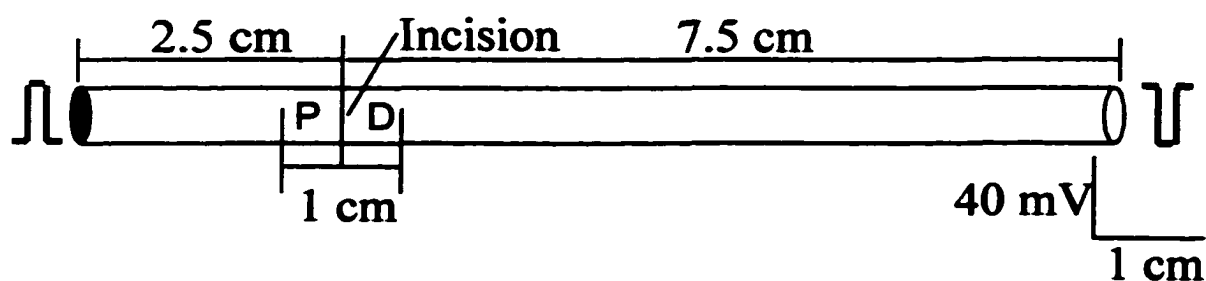


Figure 7. Results from bidomain simulations. Top, Fiber represents bidomain tissue structure 10 cm long. Field stimulation is at fiber's ends. Incision is 2.5 cm from left end. For some simulations, $[K^+]_e$ was altered in a 1-cm area around incision. Bottom, Four panels representing model results for each scenario described in "Appendix." For each panel, two times are shown: 5-ms (left) and 10 ms (right) after onset of stimulation. A, Changes in transmembrane potential (V_m) in absence of incision and with normal $[K^+]_e$; B, changes in V_m in presence of incision and with normal $[K^+]_e$; C, changes in V_m in absence of incision but elevated $[K^+]_e$; D, changes in V_m in presence of both incision and elevated $[K^+]_e$. P indicates proximal; D, distal. Dotted lines represent 0 mV. A and B, Solid line represents change in V_m at diastolic threshold for stimulation (DTS) and dashed line represents change in V_m at 96% DTS. C and D, Lines represent changes in V_m at different potassium concentrations with a 96% DTS stimulus.



**REDUCTION IN ATRIAL DEFIBRILLATION THRESHOLD BY A SINGLE LINEAR
ABLATION LESION**

by

**JAMES B. WHITE , PARWIS C. FOTUHI, RAMON W. PEDOTO,
NIPON CHATTIPAKORN, JACK M. ROGERS,
RAYMOND E. IDEKER**

In preparation for Circulation

Abstract

Background—The purpose of this work was to investigate a hybrid approach to reduce the atrial defibrillation threshold (ADFT) by determining the effect of a single linear radiofrequency ablation (RFA) lesion on both the ADFT and activation patterns during atrial fibrillation (AF).

Methods—A left thoracotomy or median sternotomy was performed on 18 sheep (45–57 kgs). Coil defibrillation electrodes were placed in an SVC/RV configuration. AF was induced by burst pacing and maintained with acetyl β -methylcholine (2–42 μ L/min). Five sequential ADFTs were obtained before and after animals received a linear RFA lesion in the left atrium (LAL, $n=6$), right atrium (RAL, $n=6$), or as a control, neither atrium ($n=6$). In animals receiving a LAL, a 504-unipolar-electrode plaque was sutured to the LA. For animals receiving a RAL, two 504-electrode plaques were placed—one on the LA and one on the RA. From each plaque, activations were recorded before and after ADFT shocks, and organizational characteristics of activations were analyzed using algorithms that track individual wavefronts.

Results—In sham-treated controls, the ADFT did not change during the study. In contrast, LAL reduced the ADFT energy 29%, from 4.5 ± 2.3 to 3.2 ± 2.0 J ($P < 0.05$). RAL animals reduced the ADFT energy 25%, from 2.0 ± 0.9 to 1.5 ± 0.7 J ($P < 0.05$). Quantitative analysis of wavefronts showed that AF was substantially more organized after RFA than before RFA for both the RAL- and LAL-treated animals.

Conclusions—A single RFA lesion in either the RA or LA reduces the ADFT in this sheep model. This decrease is associated with an increase in fibrillatory organization.

Introduction

The internal atrial defibrillator (IAD) has become a viable treatment alternative for a subpopulation of patients suffering from paroxysmal atrial fibrillation (AF).^{1,2} One limiting factor associated with IAD use is the pain caused by the electric shock. Consequently, investigators have sought to reduce the atrial defibrillation threshold (ADFT) to bring shock strengths within tolerable levels. These studies have demonstrated that although a number of electrode configurations and waveform durations are capable of successfully terminating AF,³⁻⁶ none have an ADFT that falls below the threshold of pain considered acceptable to patients.^{7,8}

A potential therapy for further reduction of the ADFT is the incorporation of ablation lesions. Limited experiments and simulations have suggested that AF inducibility and thresholds for cardioversion are reduced when multiple lesions are created in the atrial walls using radiofrequency ablation (RFA).^{9,10} An increase in fibrillatory organization has been suggested as the reason for the observed reductions, although other studies have also suggested interruptions in the myocardium may lower thresholds for defibrillation via a redistribution of current.^{11,12}

One goal of this study was to examine the effect of a single linear lesion on the ADFT when placed in an area of the left atrium (LA) in which the first recorded activa-

tion appears after a shock near the ADFT from electrodes in the RV and SVC/RA junction. This is the atrial region where the shock potential gradient field is thought to be weakest.¹³ A second goal was to determine the effect on the ADFT of a single linear lesion placed in the right atrium (RA) near the SVC/RA defibrillating electrode where the potential gradient is greater.¹⁴ A third goal was to determine whether changes in AF activation patterns caused by the linear lesion were confined to the region around the lesion or were global. A fourth goal was to determine whether a single linear lesion alters the ADFT by changing the organization of AF or by creating secondary sources at the site of the lesion.¹²

Materials and Methods

This study involving experimental animals was approved by the Institutional Animal Care and Use Committee at the University of Alabama at Birmingham Medical Center. It complies with Section 6 of the Animal Welfare Act, 1989, and adheres to the guiding principles outlined in the *Guide for the Care and Use of Animals*, National Institutes of Health publication No. 85-23.

Animal Preparation

A total of 18 adult sheep (45-57 kg) of both sexes were studied. This study was performed in 3 consecutive parts with 6 animals in each part. The first part was a control study in which animals were sham-treated. In the second part, a single linear RFA lesion was placed on the anterior LA, and epicardial mapping of the anterior LA was performed

(Figure 1A). In the third part, a single linear RFA lesion was placed on the anterior RA, and epicardial mapping was performed simultaneously on the anterior LA and RA (Figure 1B). The methods used for all parts are described together with differences noted when applicable.

After initial sedation of the sheep with a 1-to-1 mixture of tiletamine and zolazepam (Telazol, Elkins-Sinn, Inc.) 3 mg/kg intramuscularly, a peripheral intravenous line was established in a hind leg. Induction for intubation was achieved by pentobarbital as a 20- to 30-mg/kg slow IV bolus. Once adequate anesthesia was induced, the animal was endotracheally intubated and placed on a pressure-cycled ventilator with a tidal volume ranging from 800 to 1200 mL cycled at a rate of 8 to 12 breaths per minute. After initial administration of 4% isoflurane, the concentration was decreased to 2% to 3.5% to maintain a surgical plane of anesthesia as determined by monitoring of eye reflexes, deep pain response, blood pressure, and heart rate. The animals were placed in a dorsally recumbent position for fluoroscopic guidance of catheter placement (described below). The sham-treated animals and the animals with LA lesions (LAL) were then placed on their left side for a left thoracotomy for full exposure of the LA; the sheep receiving RA lesions (RAL) were kept on their backs, and a median sternotomy was performed for exposure of both atria.

The heart was suspended in a pericardial cradle. Surface ECG lead II and femoral arterial blood pressure were continuously displayed on a physiological monitor (78534C, Hewlett-Packard Ltd.). Maintenance intravenous fluids were continuously infused. Electrolytes, oxygen delivery, and ventilator settings were adjusted to maintain normal physiological levels as indicated by blood sampling every 30 to 60 minutes. Neuromus-

cular blockade was achieved with succinylcholine (1 mg/kg IV) followed by supplemental doses (0.5 mg/kg) as needed, depending on muscular tone. At the end of each study, euthanasia was induced with an intravenous bolus of potassium chloride. The heart was removed, weighed, and placed in formalin.

Animal Instrumentation

One 8F sheath was placed percutaneously in the right femoral vein. Under fluoroscopic guidance, a quadripolar catheter (Mansfield EP) was inserted via the right femoral vein into the RA appendage. Two of the poles were used for burst pacing and effective refractory period (ERP) determination. The other 2 poles were used for recording the atrial electrogram. A catheter containing 2 coil defibrillation electrodes (Endotak, Guidant Corp, St. Paul, MN) was inserted into the left jugular vein and advanced so that the distal coil rested in the RV apex and the proximal coil sat just above the SVC/RA juncture. A recording between an electrode at the distal tip and the distal coil of the defibrillation catheter was used for ventricular sensing and R-wave shock synchronization. When ventricular sensing was inconsistent using the distal tip, a chloridized Ag/Ag wire was sutured to the ventricular epicardium. A 6F pig-tail catheter was superficially placed at the posterior-lateral epicardial wall of the RA and sutured to the chest wall. The pig-tail catheter was then connected to a microinfuser (55-2226, Harvard Apparatus) for superfusion of acetyl β -methylcholine. A 6F sheath was percutaneously placed in a femoral artery for continuous blood pressure monitoring.

AF Induction and Defibrillation

AF was induced by a burst of 30 rapid atrial stimuli with a 2-ms, 6-mA pulse at a cycle length of 30 to 90 ms delivered from the distal pair of electrodes on the quadripole catheter. Before proceeding with the defibrillation protocol, sustained AF was required, defined as at least 10 minutes of AF with a cycle length < 150 ms and an irregularly irregular ventricular activation rate. Upon the initial burst, if AF was not induced and maintained, acetyl β -methylcholine ($10^{-1.7}$ to $10^{-1.4}$ M) was infused at a rate of 2 μ L/min. After 10 minutes of infusion, AF induction was again attempted. If sustained AF was not induced, the delivery of acetyl β -methylcholine was increased in 2- to 5- μ L/min increments until sustainable AF was achieved. After 10 minutes of AF, the animal was cardioverted, the rate of acetyl β -methylcholine delivery was increased by 10 μ L/min to provide a margin of safety for AF maintenance, and the defibrillation protocol was initiated.

For each fibrillation-defibrillation episode, AF was induced and allowed to continue for 2 minutes before shock delivery. Defibrillation shocks were generated by a Ventritex HVS-02 (Sunnyvale, CA) defibrillator. The waveform was a 3/1 ms truncated biphasic exponential waveform with the rising edge of the second phase equal to the falling edge of the first phase. The RV electrode was the cathode for the first phase of the shock. Each ADFT was determined using an up-down reversal technique with an initial peak voltage of 200 V. If the initial shock failed, the next and subsequent shocks were increased by 40 V until a shock succeeded, after which the voltage was decreased by 20 V and another shock was given. If the initial shock succeeded, the next and subsequent

shocks were decreased by 40 V until a shock failed. The next shock after the failure was increased by 20 V. The ADFT was defined as the lowest voltage that achieved defibrillation. All test shocks failing to defibrillate were followed by a rescue shock. Following rescue shocks or successful defibrillation attempts, 1 minute was allowed to elapse before AF was again induced. After each shock, the delivered voltage, current, energy, and impedance were recorded for each phase of the biphasic waveform. The ADFT was obtained in this manner 4 additional times for a total of 5 ADFTs. After the fifth ADFT was obtained, the ablation protocol was started. After completing the ablation protocol, the fibrillation-defibrillation protocol was repeated so that a total of 5 ADFTs were obtained both before and after the ablation protocol.

Effective Refractory Periods

In order to assess changes to tissue refractoriness during the study, ERPs were measured. The ERP was determined for the sham-treated and experimental animals at 3 different times—at the onset of the experiment before acetyl β -methylcholine infusion, after the determination of the first set of 5 ADFTs, and after the determination of the second set of 5 ADFTs. With the distal 2 electrodes of the quadripole catheter, ERPs were determined using a train of 10 S1 stimuli followed by an S2 stimulus with an S1-S2 interval of 400 ms. The S1-S1 interval was 500 ms and the stimulus strength for both the S1 and S2 was twice diastolic threshold. The S1-S2 interval was decremented in steps of 10 ms. Once capture was no longer obtained, stimulus trains were repeated incrementing the S1-S2 interval in 2-ms steps starting from the shortest S1-S2 interval that did not

capture from the previous step-down protocol. The ERP was defined as the longest S1-S2 interval that did not result in capture.

Ablation Protocol

After the first set of 5 ADFTs was acquired, the mapping plaque was removed from the atrium to receive the lesion, leaving the sutures in place for future relocation of the plaque. An RFA generator (Model 800T EPT-1000, EPT Technologies, Sunnyvale, CA) and a 7F Peanut ablation catheter (EPT) were used to create a single, multi-segmented, linear drag-lesion on the atrial epicardium (Figure 1). For each segment of the linear burn, 50 watts of power were used for 1 minute. Total ablation time for each animal ranged from 8 to 12 minutes. The linear lesion was created from the superior to inferior aspect of the anterior atrium. Segments of the line that did not appear blackened by the procedure were reablated for an additional minute. Saline was continuously dripped over the site of ablation to prevent popping and extreme temperatures. Upon completion of the linear lesion, the mapping plaque was resutured to the epicardium in the same location as before and the fibrillation-defibrillation protocol was repeated. For the sham-treated animals, a mapping plaque was not used and extracellular potentials were not recorded. The ablation protocol, however, was performed using a power output of 0 watts. Following the last of the initial 5 ADFT determinations, approximately 1.5 hours elapsed before the fibrillation-defibrillation protocol was repeated.

Data Acquisition

For animals receiving LAL, unipolar electrograms were recorded with a 528-channel mapping system and a 504-electrode plaque arranged in a 24 x 21-grid array (Figure 1A). For the animals receiving RAL, two 504-electrode plaques were sutured to the atria, 1 each to the LA and RA (Figure 1B). Each plaque was connected to a 528-channel mapping system with both mapping systems synchronized to record simultaneously from 1056 channels. Each recording electrode was a chloridized Ag/Ag wire. The plaques had an interelectrode spacing of 1.5 mm. Each signal was bandpass filtered between 0.5 and 500 Hz and sampled at a frequency of 2 kHz. Approximately 0.5 seconds of data before each defibrillation shock and 2 seconds of data after each shock were transferred to a computer workstation for analysis. The data before and after each defibrillation shock were used for later analysis only if that shock contributed to ADFT determination.

Quantitative Analysis of Atrial Activations

The first derivative of each recorded electrogram was determined, and an activation was considered to be present beneath an electrode when $dV/dt \leq 0.5$ V/s. The organization of atrial activations during AF was quantified before and after RFA by using a series of parameters based on a decomposition of the recorded activations into constitutive wavefronts. This analysis has been described in detail elsewhere.¹⁵⁻¹⁷ Analysis was performed on 500-ms epochs of AF recorded before and after RFA. The electrodes that did not record activations after RFA, because the tissue beneath them was ablated, were

removed from both datasets before and after RFA. The parameters analyzed and compared were number of wavefronts, multiplicity, break-through fraction, block fraction, area swept out, and activation rate. In brief, the number of wavefronts is the total number of wavefronts recorded during the 500-ms epoch. Multiplicity is a parameter that measures the number of different wavefront pathways; it is a descriptor of spatiotemporal complexity. The lower the multiplicity, the lower the number of different clusters of activation sequences. Break-through fraction refers to the fraction of wavefronts that appear in the mapped region (1) without arising from a wavefront that splits into 2 or more wavefronts (fractionation), (2) without arising from wavefronts that unite to form one wavefront (collision), or (3) without propagating in from an edge of the mapped region. Block fraction refers to the fraction of wavefronts that block. Block occurs when a wavefront terminates without fractionating, colliding with other wavefronts, or propagating out of the mapped region. The mean area swept out by a wavefront is the number of electrodes that recorded activation from that wavefront multiplied by the area of the grid represented by each electrode (2.25 mm² for 1.5-mm spacing). The activation rate is defined as the mean number of activation fronts that pass each epicardial site per second.

Postshock activation patterns were also qualitatively compared to determine the number of different patterns present before and after the ablation procedure. These activation patterns were grouped into one of four categories (Figure 2): type A, defined as the resumption of normal sinus rhythm without any preceding ectopic wavefronts; focal/breakthrough, defined as a wavefront originating from within the mapped region that expanded centrifugally from a single point of origin; unidirectional wavefront, categorized as a wavefront originating within the mapped region, but not propagating

away from its origin in all directions; and external wavefront, defined as a wavefront that propagated in from outside of the mapped region.

Lesion Analysis

The length and width of the grossly visible lesion in each animal were measured with a metric ruler after the study, and an average and standard deviation were calculated for each atrium. The epicardial and endocardial surfaces of each atrium were grossly inspected to assess the extent of the lesion transmurally and longitudinally across the surface. After RFA, each atrium was stimulated perpendicular to the long axis of the lesion to determine whether the lesion blocked passing wavefronts. If propagation was observed through parts of the ablated area, the plaque was removed and RFA was repeated.

Statistical Analysis

The ADFTs determined before and after the sham treatment and RF treatment were averaged for each animal and their mean values were compared by using the t-test for paired samples. The organizational changes in atrial activation and the postshock activation times (interval between the end of the shock and the first recorded activation) were compared by using the t-test for unpaired samples. Logistic regression analysis was used to determine the impact of postshock interval and shock strength on shock outcome. The ERPs were compared by using ANOVA for repeated measures and, when necessary,

the Student-Neuman Keuls test. Numerical differences were considered significant if $P \leq 0.05$.

Results

Atrial Defibrillation Thresholds

For the sham-treated animals, statistical comparison of the ADFTs in terms of leading-edge voltage, leading-edge current, and total energy did not yield significant differences between the 2 measurements (Table 1). For animals with LAL, the leading-edge voltage, leading-edge current, and total energy required to defibrillate decreased after RFA ($P < 0.05$). For animals with RAL, the leading-edge voltage, leading-edge current, and total energy required to defibrillate also decreased after RFA ($P < 0.05$).

Table 1. ADFT Comparisons for Animals Before and After RF Application

		Defibrillation Thresholds		P	Percent Change
		Before Lesion	After Lesion		
<i>SHAM</i>	Leading Edge Voltage	318 ± 127	315 ± 95	NS	-1
	Leading Edge Current	7.6 ± 3.4	8.0 ± 2.5	NS	+5
	Total Energy	6.2 ± 5.1	5.8 ± 3.3	NS	-6
<i>LAL</i>	Leading Edge Voltage	283 ± 65	230 ± 66	< 0.05	-19
	Leading Edge Current	7.1 ± 2.2	6.3 ± 2.4	< 0.05	-11
	Total Energy	4.5 ± 2.3	3.2 ± 2.0	< 0.05	-29
<i>RAL</i>	Leading Edge Voltage	208 ± 46	173 ± 38	< 0.05	-17
	Leading Edge Current	4.0 ± 0.9	3.6 ± 1.0	< 0.05	-10
	Total Energy	2.0 ± 0.9	1.5 ± 0.7	< 0.05	-25

Preshock Activity—Left Atrial Lesion

A total of 98 500-ms epochs of AF before RFA and 105 500-ms epochs of AF after RFA were analyzed with the quantitative wavefront algorithms described in Materials and Methods. The LA activation patterns during AF were significantly different before and after RFA (Table 2). A significant decrease was observed in the number of wavefronts, multiplicity, break-through fraction, block fraction, and activation rate after RFA ($P<0.05$). The mean area swept out by the wavefronts increased after RFA ($P<0.05$).

Activation patterns during normal sinus rhythm were similar from animal to animal. Wavefronts first appeared in the mapped region at the superior-lateral aspect of the LA and propagated inferiorly (Figure 3A). Sinus rhythm patterns after RFA propagated in a similar pattern but were blocked at the site of the lesion (Figure 3B). Pre-shock activations during AF recorded before RFA (Figure 3C) formed numerous wavefronts and complex activation patterns concordant with results from the numerical wavefront analysis shown in Table 2. Maps of activations recorded after RFA (Figure 3D) exhibited more organized AF with fewer wavefronts and fewer collisions and fractionations among activation patterns.

Table 2. Quantification of AF on Left Atrium Before and After LA Lesion

	Before Lesion	After Lesion	P
Number of Wavefronts	21.0 ± 8.8	10.8 ± 9.1	< 0.05
Multiplicity	3.8 ± 1.6	2.3 ± 0.7	< 0.05
Break-Through Fraction	0.31 ± 0.2	0.23 ± 0.2	< 0.05
Block Fraction	0.33 ± 0.2	0.34 ± 0.2	NS
Area Swept Out (mm ²)	156.2 ± 65.3	186.5 ± 76.1	< 0.05
Activation Rate (sec ⁻¹)	4.6 ± 1.2	3.2 ± 2.2	< 0.05

Preshock Activity—Right Atrial Lesion

A total of 91 500-ms epochs of AF before RFA and 80 500-ms epochs of AF after RFA were analyzed on both atria using the quantitative wavefront algorithms described in the Methods.

Left atrium. Normal sinus rhythm recordings produced patterns in the LA, consistent with the LA recordings from the previous set of animals (Figure 4A). Recordings from the LA before and after RFA in the RA did not show significant changes in most quantitative descriptors of AF activation patterns (Table 3).

Table 3. Quantification of AF on Left Atrium Before and After RA Lesion

	Before Lesion	After Lesion	P
Number of Wavefronts	18.6 ± 13.2	15.7 ± 11.8	NS
Multiplicity	4.0 ± 2.8	3.5 ± 2.5	NS
Break-Through Fraction	0.40 ± 0.2	0.45 ± 0.2	<0.05
Block Fraction	0.44 ± 0.2	0.48 ± 0.2	NS
Area Swept Out (mm ²)	170.3 ± 108.7	173.0 ± 118.6	NS
Activation Rate (sec ⁻¹)	4.8 ± 2.8	4.6 ± 3.0	NS

Right atrium. The normal sinus rhythm pattern for the RA was also repeatable from animal to animal and always entered the mapped region from the superior-medial aspect of the RA (Figure 4A). As in the previous set of animals with LAL, the lesion created in the RA produced block. The atrial activation patterns on the RA showed significant differences before and after RFA (Table 4). A significant decrease was observed in the number of wavefronts, multiplicity, break-through fraction, block fraction, area swept out, and activation rate after RFA ($P<0.05$).

Left vs right atrium. For all animals during AF, the activation patterns of the LA appeared more complicated than the patterns recorded in the RA (Figure 4C). Significant differences were observed between the atria for all wavefront activation parameters except area swept out after RFA (Table 4).

Table 4. Quantification of AF on Right Atrium Before and After RA Lesion (vs LA, Table 3)

	Before Lesion	After Lesion	P
Number of Wavefronts	9.8 ± 7.4 (< 0.05)	4.0 ± 3.2 (< 0.05)	< 0.05
Multiplicity	2.5 ± 1.0 (< 0.05)	1.5 ± 0.9 (< 0.05)	< 0.05
Break-Through Fraction	0.42 ± 0.3 (NS)	0.46 ± 0.3 (NS)	NS
Block Fraction	0.53 ± 0.3 (< 0.05)	0.63 ± 0.4 (< 0.05)	< 0.05
Area Swept Out (mm ²)	221.0 ± 120.7 (< 0.05)	169.1 ± 157.5 (NS)	< 0.05
Activation Rate (sec ⁻¹)	3.2 ± 3.0 (< 0.05)	1.2 ± 1.0 (< 0.05)	< 0.05

Postshock Activity—Left Atrial Lesion

For 84% of the shocks, earliest activation after failed defibrillation shocks that were delivered before RFA originated within the mapped region in a focal activation pattern (Table 5). The remaining earliest activations were either external or unidirectional. Successful shocks before RFA were most often followed by type A successes (83%), but occasionally exhibited focal/breakthrough activity, and external and unidirectional wavefronts (Table 5). The time from the end of the shock to the first recorded activation was significantly shorter for failed than for successful shocks ($P < 0.05$, Table 6).

Table 5. Postshock Activations Following Successful and Failed ADFT Shocks (%)

		Successful Shocks		Failed Shocks	
		Before	After	Before	After
<i>LA-LAL</i>	Type A	83	62	-	-
	Focal/Breakthrough	13	32	84	69
	External	2	4	14	28
	Unidirectional	2	2	2	3
<i>LA-RAL</i>	Type A	83	84	-	-
	Focal/Breakthrough	15	8	58	56
	External	1	5	31	12
	Unidirectional	1	3	11	32
<i>RA-RAL</i>	Type A	83	81	-	-
	Focal/Breakthrough	0	0	3	4
	External	17	19	97	80
	Unidirectional	0	0	0	16

Failed defibrillation shocks delivered after RFA produced early sites that were focal for 69% of shocks (Table 5). The remaining earliest recorded activations were primarily external, with some unidirectional wavefronts. The successful shocks were predominately type A (62%) occasionally preceded by breakthrough/focal, external, and unidirectional activations (Table 5). After RFA, the time from the end of the shock to the first recorded activation was significantly shorter for failed shocks than for successful shocks (Table 6).

For successful shocks, the interval from the end of the shock to the first activation was shorter after RFA than before RFA ($P<0.05$, Table 6). For failed shocks, this interval was longer after RFA than before RFA ($P<0.05$).

Table 6. Earliest Postshock Activation Times on Left Atrium Before and After LA Lesion

	Success	Failure	P
Before Lesion	724 ± 314	46 ± 32	< 0.05
After Lesion	564 ± 377	59 ± 35	< 0.05
<i>P</i>	< 0.05	< 0.05	

A comparison of failed and successful shocks at the same shock strength indicated a significant difference in the postshock interval. Successful shocks predominantly occurred at larger postshock intervals than did failed shocks (Figure 5). Furthermore, logistic regression analysis indicated that both shock strength and postshock interval were robust predictors of shock outcome ($P < 0.05$).

Postshock Activity—Right Atrial Lesion

Left atrium. For 58% of the shocks, earliest activation after failed defibrillation shocks that were delivered before RFA originated within the mapped region in a focal activation pattern (Table 5). The remaining earliest activations were either external or unidirectional. Successful shocks before RFA were most often type A successes (83%). The time from the end of the shock to the first recorded activation was significantly shorter for failed than for successful shocks ($P < 0.05$, Table 7).

Failed defibrillation shocks delivered after RFA produced early sites that were focal for 56% of shocks (Table 5). Earliest recorded activations for the remaining shocks were either external or unidirectional. The successful shocks were predominately type A (84%), at times preceded by focal, external, or unidirectional wavefronts (Table 5). After

RFA, the time from the end of the shock to the first recorded activation was significantly shorter for failed than for successful shocks ($P<0.05$, Table 7).

Table 7. Earliest Postshock Activation Times on Left Atrium Before and After RA Lesion

	Success	Failure	P
Before Lesion	729 ± 357	73 ± 59	< 0.05
After Lesion	700 ± 301	73 ± 51	< 0.05
<i>P</i>	NS	NS	

The lesion did not influence the postshock activation times for successful or failed shocks when comparing these interval before and after RFA (Table 7). However, postshock interval and shock strength were found to be significant predictors of defibrillation outcome ($P<0.05$).

Right atrium. For 3% of the shocks, earliest activation after failed defibrillation shocks that were delivered before RFA originated within the mapped region in a focal activation pattern (Table 5). The remaining earliest activations were external. Successful shocks before RFA were usually type A successes (83%), occasionally preceded by external activations. The time from the end of the shock to the first recorded activation was significantly shorter for failed than for successful shocks ($P<0.05$, Table 8).

Table 8. Earliest Postshock Activation Times on Right Atrium Before and After RA Lesion (vs LA, Table 7)

	Success	Failure	P
Before Lesion	718 ± 321 (< 0.05)	135 ± 26 (< 0.05)	< 0.05
After Lesion	675 ± 278 (NS)	147 ± 50 (< 0.05)	< 0.05
<i>P</i>	NS	< 0.05	

Failed defibrillation shocks delivered after RFA produced early sites that were focal for only 4% of shocks (Table 5). Most of the remaining earliest recorded activations were external (80%), with the remainder unidirectional. The successful shocks were predominately type A (81%), with the remainder external. After RFA, the time from the end of the shock to the first recorded activation was significantly shorter for failed than for successful shocks ($P < 0.05$, Table 8).

For failed shocks, the postshock interval was shorter before RFA than after RFA ($P < 0.05$). The postshock interval for successful shocks was not different for shocks delivered before or after RFA (Table 8). As shown for the LA, the postshock interval and shocks strength were positive indicators of shock outcome ($P < 0.05$).

Left vs right atrium. Postshock activation times were compared between the LA and RA for successful and failed shocks before and after RFA. The activation times were significantly different for all shocks delivered before RFA and for failed shocks delivered after RFA (Table 8).

Effective Refractory Periods

The ERPs measured at the 3 intervals described were consistent with autonomic alteration for both the sham-treated, LAL-treated, and RAL-treated animals (Figure 6). The ERP was markedly reduced after treatment with acetyl β -methylcholine.

Lesion Analysis

The lesions created on the LA in all 6 animals measured 43 ± 5 mm in length and 12 ± 2 mm in width. The lesions created on the RA in all 6 animals measured 25 ± 10 mm in length and 7 ± 2 mm in width. The epicardial and endocardial surfaces of each atrial lesion were blackened and continuous by gross examination.

Discussion

We investigated the effect of a single linear RFA lesion on the ADFT in sheep. Epicardial electrograms were recorded from the surface of the atria around the site of the lesion before and after RFA in order to assess atrial activation patterns just before and after a defibrillation shock. The important findings in this paper are (1) a single linear RA or LA lesion created by RFA reduces the ADFT; (2) the AF activity in the LA is more complex than the AF recorded in the RA before and after RFA; (3) changes in the organization of AF associated with an RFA lesion in the RA are local to that atrium; and (4) the type and timing of the first post-shock activation is different when comparing activations recorded before and after RFA and when comparing the RA and LA.

Atrial Defibrillation Thresholds

A single linear lesion in either the RA or LA reduced the ADFT energy by 25-29%. The ADFTs in sham-treated control animals did not change significantly over a 1.5-hour interval, indicating that the RFA lesion was responsible for the decreased ADFT in the study animals.

The few studies of the combination of RFA and atrial defibrillation have produced mixed results.^{9,10,18} Mongeon et al¹⁹ recently demonstrated that a single RFA lesion placed intercavally in chronically paced dogs reduced the ADFT energy by 47%. Kalman et al⁹ tested ADFTs in chronically paced dogs before and after performing the equivalent of the Maze procedure by RFA. Using 4 lesions, Kalman et al were able to reduce the ADFT by as much as 50% in energy. They have since performed similar studies using computer models that have produced comparable outcomes.¹⁰ Conversely, a recent study¹⁸ in humans with structurally normal hearts and recurrent AF undergoing a quasi-Maze procedure with 3 lesions in only the RA did not find a significant ADFT reduction following RFA. The reason for the disparity in these results is unclear but may be due to differences in the species, the model of AF (acute vs chronic), or the shocking electrode configuration.

It is likely that the atria, like the ventricles, require a certain critical mass of tissue to sustain fibrillation.²⁰ It is feasible that creating a lesion in the atria reduces the effective tissue mass, thereby promoting defibrillation. Early studies in ventricular fibrillation have shown that removing portions of the myocardium eventually reduces the substrate needed to maintain the arrhythmia.²¹ It is conceivable that a lesion in the atria, while not

completely eliminating AF, causes the activations sustaining AF to become less complex and more susceptible to cardioversion. Our quantitative analysis of AF before and after creating an RFA lesion provides evidence for this hypothesis. The reduction in AF complexity observed after creating the lesion may be due to a concomitant reduction in the atrial mass required to sustain more complicated wavefront patterns.

One mechanism by which a shock is thought to defibrillate is by a redistribution of transmembrane current at the boundaries of discontinuities in the myocardium creating secondary sources.²² The discontinuous nature of the heart can be due to structural inhomogeneities such as gap junctions and collagenous septa. Recent studies have shown that these discontinuities can also be created artificially, significantly altering the spatial distribution of shock-induced activations.^{11,12} Activations can be induced several centimeters from a shock electrode after the creation of an interruption in the myocardium of this region. Theoretically, an ablation lesion placed in a region of the atria that is the site of defibrillation failure may enhance the effect of the shock by producing activations in this area at the time of the shock. As such, a strategically placed lesion would reduce the ADFT by broadening the area of the atria affected by the shock. Although our data do not reflect postshock activation patterns consistent with this theory (as discussed below), it is conceivable that both reduction in effective tissue mass and secondary source effects contribute to the decrease in the ADFT.

Activation Patterns of AF

Using algorithms to quantify AF activation patterns, we showed that the level of AF organization increased in the LA or RA after each was subjected to RFA. The number of wavefronts, the activation rate, and the incidence of block and break-through markedly decreased after RFA on the atrium undergoing ablation. However, this effect may be strongest in the region near the lesion because organization of activation during AF was not increased in the LA after ablation in the RA.

Sih et al²³ measured the wavelet density, wavelet size, and complexity of activation patterns before and after creating up to 5 lesions in both the LA and RA. Discordant with our results, they report that the wavefront size, wavefront density, and the complexity of the AF did not change after the lesions were introduced. Since their recording plaques were not in contact with ablated areas of the atrium, their results may indicate that changes in activation patterns may be greatest near the RFA lesion.

Activation patterns in the LA during AF were more complex than in the RA. The number of wavefronts, wavefront interactions, and activation rate were considerably greater in the LA. These data support other studies that have shown that the LA possesses a dominant activation frequency, producing a driving force for the RA.^{23,24} The activation differences did not disappear after RFA; in fact, they were accentuated except for the area swept out by each wavefront.

Postshock Activations

One of the goals of this study was to create a lesion in the area of the atria associated with early postshock activity in an attempt to lower the defibrillation threshold by redirecting current to produce secondary sources.²² This early activity area occurs in a region exposed to a low shock potential gradient and is often located distant from the defibrillation electrodes.¹⁴ We created a lesion in such a region in the LA on the basis of an earlier defibrillation study that reported earliest sites of postshock activation in the lateral portion of the LA after shocks delivered between SVC and RV electrodes.¹³ The fact that greater than 85% of all failed defibrillation shocks produced either foci or nonfocal activations in this area shortly after the shock indicated that we created the RFA lesion in the desired region.¹³ Of the postshock activation patterns recorded in the LA, over 50% were focal. The role, if any, that ablation lesions play in producing these foci is unclear. Previous studies showing the beneficial effect of myocardial discontinuities have demonstrated the presence of activations adjacent to the discontinuity occurring during or soon after the shock. Most of the postshock foci in this study originated at sites away from the lesion at postshock intervals much larger than would have been expected if produced by the shock directly. The observation of secondary sources at the lesion site is complicated by the dispersion of tissue refractoriness at the time of the shock. It is feasible that secondary sources are created but do not result in propagating activations because of refractory tissue adjacent to the lesion, particularly if the window of excitability is decreased in the presence of methylcholine. Furthermore, placing a lesion in the right atrium, an area associated with large shock potential gradients, also reduces the

atrial defibrillation threshold. This change in threshold is inconsistent with reductions produced via a secondary source mechanism within a low-gradient area of the atria.

Limitations

The main limitations of this study involve the use of an acute model of AF. The hearts studied were healthy and normal and were therefore unlikely to possess some of the atrial structural and electrophysiological alterations that may be present in chronic models of AF. Furthermore, our use of acetyl β -methylcholine to sustain AF is known to cause a shortening of the action potential, leading to ease of inducibility.²⁵ Although changes in action potential characteristics have been shown to occur as AF evolves into a chronic state,²⁶ we are not certain that our model induced by autonomic alteration parallels those changes observed in chronic AF. In addition, the acetyl β -methylcholine was only superfused on the RA, possibly altering the dynamics of the wavefronts on the RA as compared to the LA. Since the ERPs were determined only on the RA, it is difficult to determine what effect, if any, acetyl β -methylcholine produced on the action potential characteristics of the LA. Another limitation is that the ADFTs determined from the sham treatment animals were done without a mapping plaque sutured to the atria; therefore, it is difficult to exclude the mapping plaque as a factor that altered the ADFTs.

To provide a better understanding of the mechanisms involved in lowering the ADFT, further studies are required. Our recording technique identified only activation times. Optical techniques would permit analysis of the spatial distribution of the transmembrane potential before and after RFA. We did not record intramurally to investigate

the source of the foci present before and after ADFT shocks. And finally, future work should examine the changes in activation patterns of both atria after RFA of the LA.

References

1. Lau CP, Tse HF, Lee K. Initial clinical experience of a human implantable atrial defibrillator. *Pacing Clin Electrophysiol*. 1997;20:220-225.
2. Levy S, Ricard P, Lau C. Multicenter low energy transvenous atrial defibrillation (XAD) trial. *J Am Coll Cardiol*. 1997;29:750-755.
3. Alt E, Schmitt C, Ammer R, Coenen M, Fotuhi P, Karch M, Blasini R. Initial experience with intracardiac atrial defibrillation in patients with chronic atrial fibrillation. *Pacing Clin Electrophysiol*. 1994;17:1067-1078.
4. Cooper RA, Plumb VJ, Epstein AE, Kay GN, Ideker RE. Marked reduction in internal atrial defibrillation thresholds with dual-current pathways and sequential shocks in humans. *Circulation*. 1998;97:2527-2535.
5. Murgatroyd FD, Slade AKB, Sopher SM, Rowland E, Ward DE, Camm AJ. Efficacy and tolerability of transvenous low energy cardioversion of paroxysmal atrial fibrillation in humans. *J Am Coll Cardiol*. 1996;25:1347-1353.
6. Cooper RAS, Johnson EE, Wharton M. Internal atrial defibrillation in humans. Improved efficacy of biphasic waveforms and the importance of phase duration. *Circulation*. 1997;95:1487-1496.
7. Jung J, Heisel A, Fires R, Köllner V. Tolerability of internal low-energy shock strengths currently needed for endocardial atrial cardioversion. *Am J Cardiol*. 1997;80.
8. Lok NS, Lau CP, Tse HF, Ayers GM. Clinical shock tolerability and effect of different right atrial electrode locations on efficacy of low energy human transvenous atrial defibrillation using an implantable lead system. *J Am Coll Cardiol*. 1997;30:1324-1330.
9. Kalman JM, Olgin JE, Karch MR, Steiner PR, Stillson C, Chin MC, Lesh MD. Effect of right atrial linear lesions on atrial defibrillation threshold. Implications for "hybrid therapy." *Pacing Clin Electrophysiol*. 1996;19:625.

10. Ellis WS, SippensGroenewegen A, Lesh MD. The effect of linear lesions on atrial defibrillation threshold and spontaneous termination—a computer modeling study. *Pacing Clin Electrophysiol.* 1997;20:1145.
11. Gillis AM, Fast VG, Rohr S, Kleber AG. Spatial changes in transmembrane potential during extracellular electrical shocks in cultured monolayers of neonatal rat ventricular myocytes. *Circ Res.* 1996;79:676-690.
12. White JB, Walcott GP, Pollard AE, Ideker RE. Myocardial discontinuities: A substrate for producing virtual electrodes to increase directly excited areas of the myocardium by shocks. *Circulation.* 1998;97:1738-1745.
13. Cooper RAS, KenKnight BH. The role of waveforms and lead configurations for internal atrial cardioversion. *Herzschr Elektrophys.* 1998;9:1-7.
14. Wharton JM, Wolf PD, Smith WM, Chen P-S, Frazier DW, Yabe S, Danieleley N, Ideker RE. Cardiac potential and potential gradient fields generated by single, combined, and sequential shocks during ventricular defibrillation. *Circulation.* 1992;85:1510-1523.
15. Huang J, Rogers JM, KenKnight BH, Rollins DL, Smith WM, Ideker RE. Evolution of the organization of epicardial activation patterns during ventricular fibrillation. *J Cardiovasc Electrophysiol.* 1998;9:1291-1304.
16. Rogers JM, Usui M, KenKnight BH, Ideker RE, Smith WM. A quantitative framework for analyzing epicardial activation patterns during ventricular fibrillation. *Ann Biomed Eng.* 1997;25:749-760.
17. Rogers J, Usui M, KenKnight B, Ideker R, Smith W. Recurrent wavefront morphologies: a method for quantifying the complexity of epicardial activation patterns. *Ann Biomed Eng.* 1997;25:761-768.
18. Chaudhry GM, Satti SD, Arshad T, Pacetti PE, Marchese TF, Patton S, Haffajee CI. Can extensive right atrial ablation in atrial fibrillation patients decrease atrial defibrillation thresholds? *J Am Coll Cardiol.* 1999;33:158A.
19. Mongeon LR, Warman EN, Mehra R. One right atrial linear ablation lesion decreases atrial defibrillation thresholds in a canine model of sustained atrial fibrillation. *Pacing Clin Electrophysiol.* 1999;22:755.
20. West TC, Landa JF. Minimal mass required for induction of a sustained arrhythmia in isolated atrial segments. *Am J Physiol.* 1962;202:232-236.

21. Damiano RJ Jr, Asano T, Smith PK, Ideker RE, Cox JL. Critical mass and the surgical treatment of ventricular fibrillation: The effect of right ventricular isolation on ventricular fibrillation thresholds. *J Am Coll Cardiol*. 1984;3:587.
22. Plonsey R, Barr RC. Inclusion of junction elements in a linear cardiac model through secondary sources: Application to defibrillation. *Med Biol Eng Comput*. 1986;24:137-144.
23. Sih HJ, Berbari EJ, Zipes DP. Epicardial maps of atrial fibrillation after linear ablation lesions. *J Cardiovasc Electrophysiol*. 1997;8:1046-1054.
24. Skanes AC, Mandapati R, Berenfeld C, Davidenko JM, Jalife J. Spatiotemporal Periodicity During Atrial Fibrillation in the Isolated Sheep Heart. *Circulation*. 1998;98:1236-1248.
25. Ikeda T, Wu T-J, Uchida T, Hough D, Fishbein MC, Mandel WJ, Chen P-S, Karagueuzian HS. Meandering and unstable reentrant wave fronts induced by acetylcholine in isolated canine right atrium. *Am J Physiol*. 1997;273:H356-H370.
26. Allessie MA. Atrial electrophysiologic remodeling: another vicious circle? *J Cardiovasc Electrophysiol*. 1998;9:1378-1393.

Figure 1. A depiction of the location of the recording plaques with respect to the atria. A, The experimental design for LAL-treated animals. B, The experimental design for RAL-treated animals. Each plaque was sutured to cover the anterior surface of each atrium. The orientations of the mapping plaques as shown in all freeze-frame maps are drawn below each panel (L=lateral, I=inferior, M=medial, S=superior).

Figure 2. Activation maps illustrating the 4 types of postshock activation patterns. A, Type A. B, Focal/Breakthrough. C, Unidirectional. D, External. The time in ms is shown above each frame. Each black-filled square indicates the criterion for activation that was met at the electrode site represented by that square sometime between the time of this frame and the next frame. Time 0 is the onset of the shock.

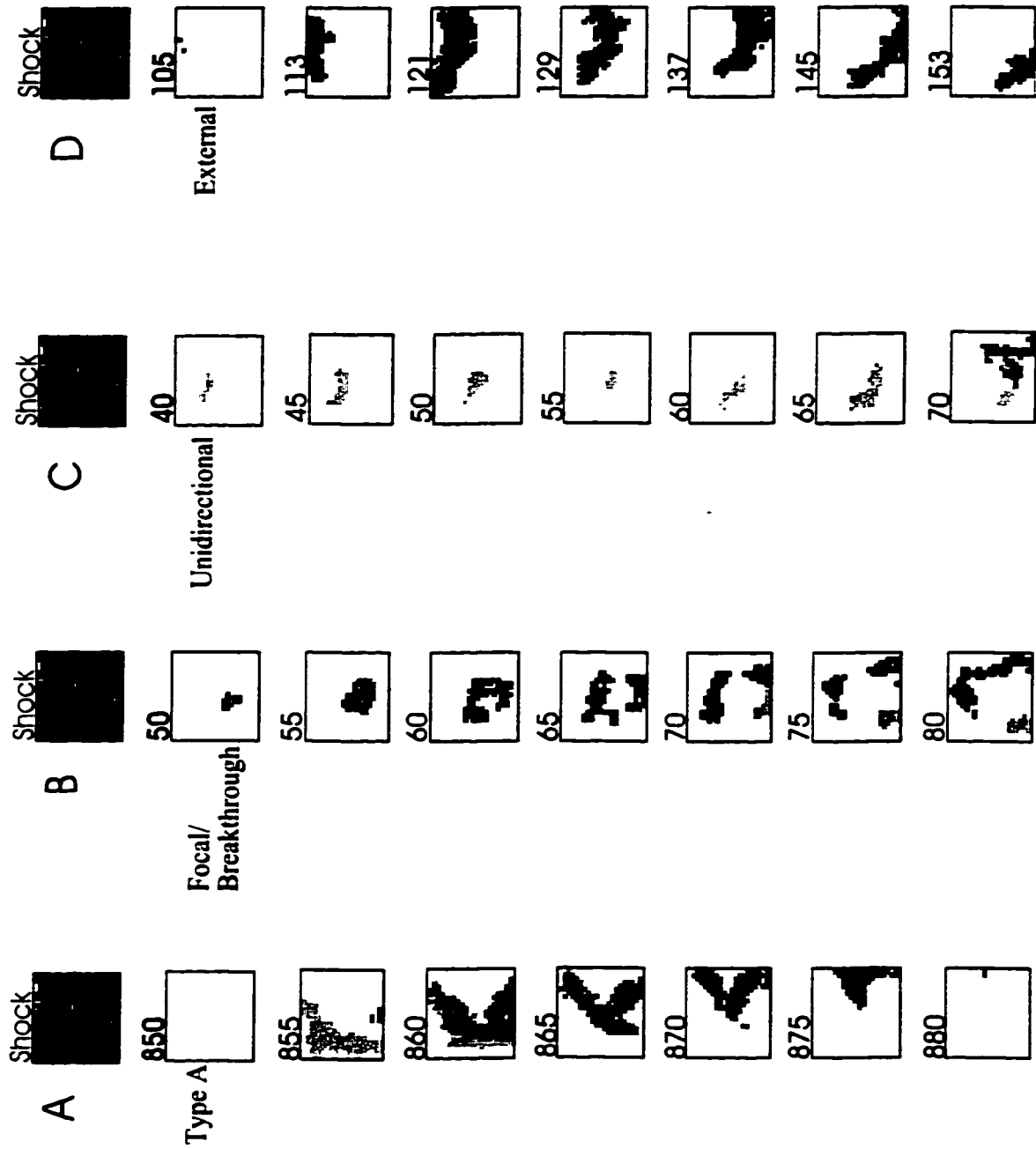


Figure 3. Activation maps of epicardial wavefronts recorded from the LA before and after a linear lesion was created in the LA. Time 0 is an arbitrary value. The black horizontal line in panels B, C and D represents the location of the linear lesion for that animal. Each color represents an individual wavefront. A, Sinus rhythm before RFA. B, Sinus rhythm after RFA. C, AF before RFA. The lesion is drawn for comparison to D. D, AF after RFA. The number of wavefronts and wavefront interactions are more numerous before than after RFA.



Figure 4. Activation maps of epicardial wavefronts recorded from both the LA and RA before and after RFA in the RA. For each time interval, the activation patterns of the RA are shown on the left and the activation patterns of the LA are shown on the right. Time 0 is an arbitrary value. A, Sinus rhythm before RFA in the RA. B, Sinus rhythm after RFA in the RA. C, AF before RFA. The number of wavefronts and number of complex interactions is greater on the LA than on the RA. Arrows indicate direction of propagation.

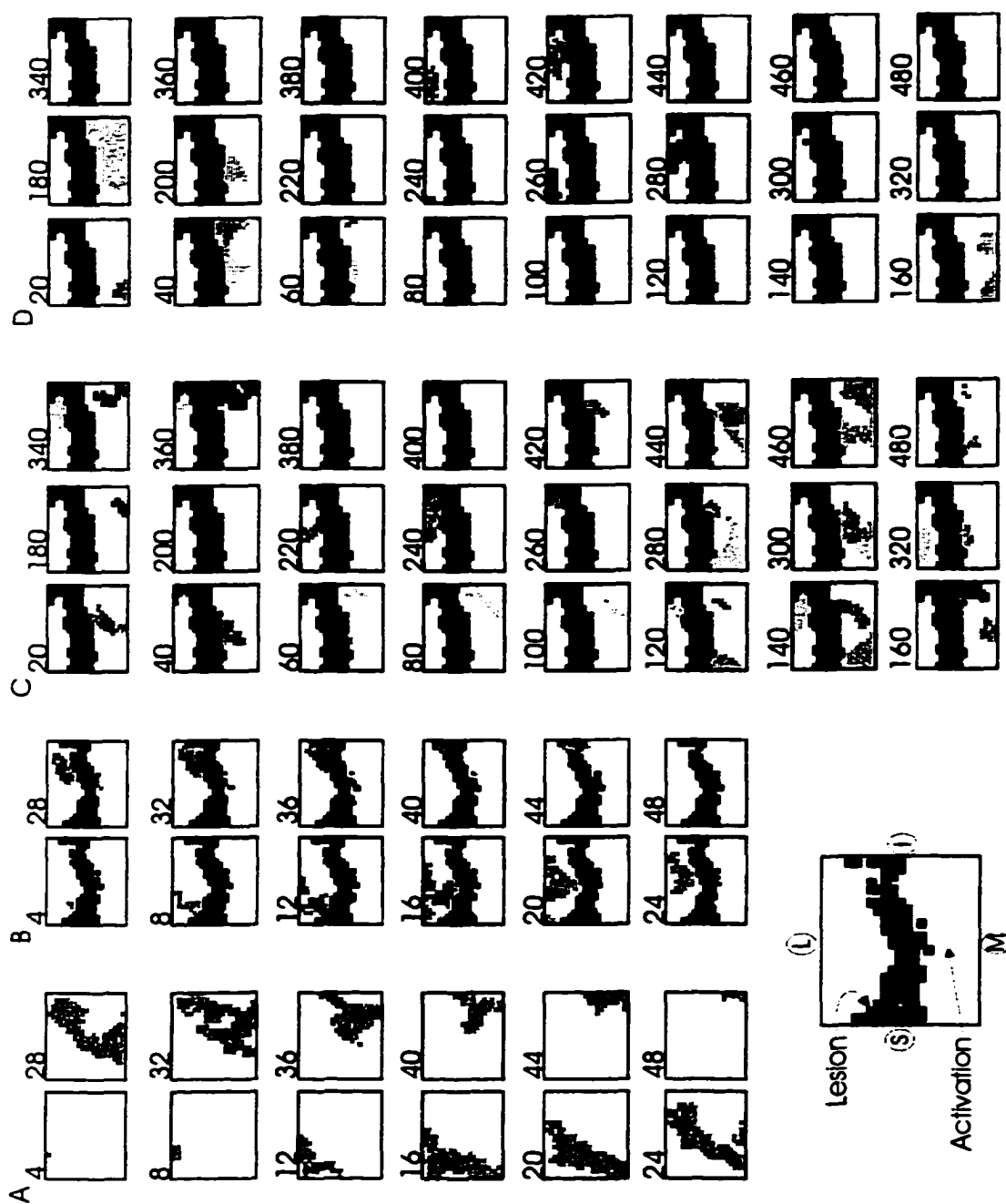


Figure 5. A scatter plot indicating the relationships between postshock interval, shock strength, and shock outcome for shocks delivered before RFA of the LA. Logistic regression analysis indicated that both postshock interval and shock strength were significant predictors of shock outcome ($P<0.05$).

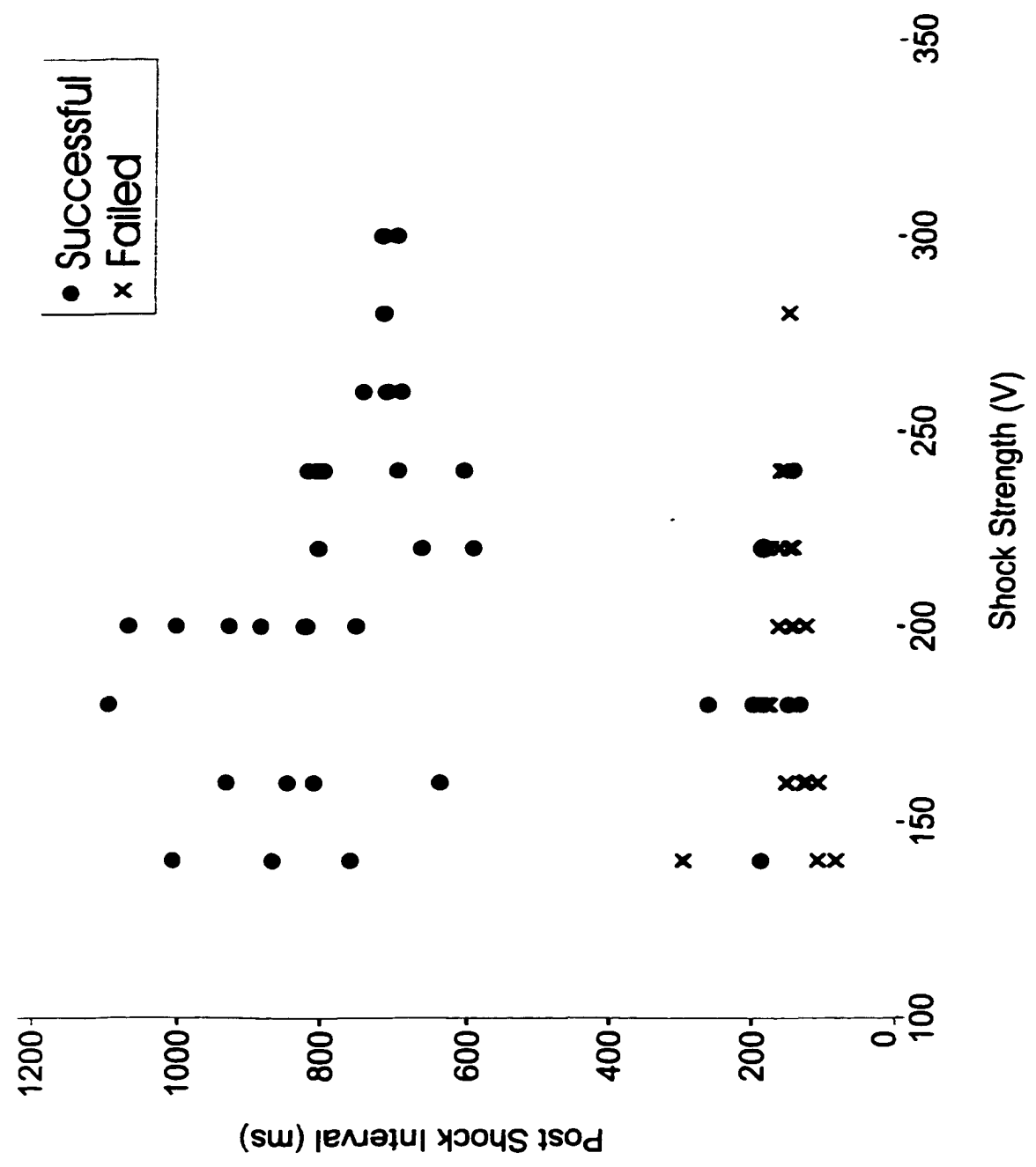
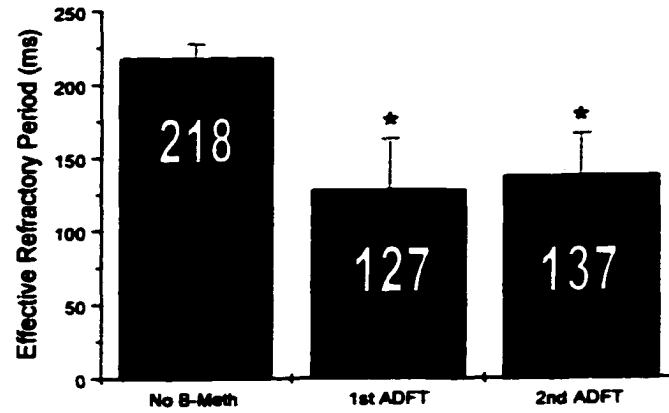
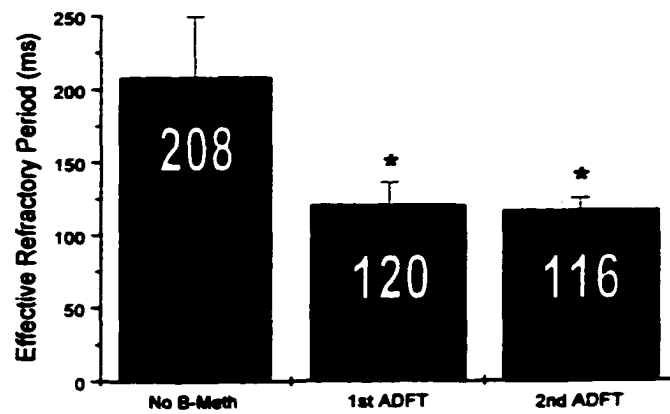
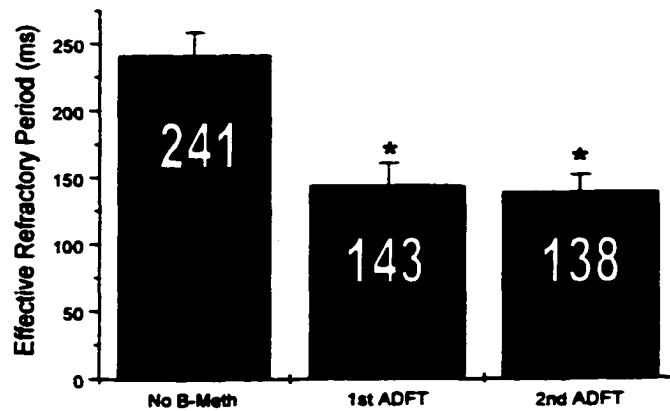


Figure 6. ERPs recorded before acetyl β -methylcholine is administered (No B-Meth), after the first set of ADFTs are acquired (1st ADFT) before RFA, and following the second set of ADFTs (2nd ADFT) after RFA. $\ast=P<0.05$ vs No B-Meth. A, Sham-treated animals. B, LAL-treated animals. C, RAL-treated animals. ERPs recorded before acetyl β -methylcholine is administered (No B-Meth), after the first set of ADFTs are acquired (1st ADFT) before RFA, and following the second set of ADFTs (2nd ADFT) after RFA. $\ast=P<0.05$ vs No B-Meth.

A**B****C**

SUMMARY AND FUTURE RESEARCH

The protocols presented in this dissertation were created to provide a clearer understanding of the characteristics of defibrillation that affect shock outcome. There are variables that determine the effectiveness of the delivered shock waveform, and there are factors that contribute to the mechanism in which the shock waveform alters the underlying tissue. Previous experiments examined the impact of shock waveform characteristics on defibrillation shocks delivered internally.²⁴ These experiments utilized a parallel resistor-capacitor model to simulate the heart's passive response to waveforms with different time constants and phase durations. Our findings indicate that this same model is equally robust in predicting the relative efficacies of different waveforms delivered transthoracically. Our experimental and model design employed several monophasic and biphasic waveforms of varying duration. The model showed that for monophasic waveforms, the maximum model response produced by each waveform was the critical factor in determining defibrillation success. For biphasic waveforms, we demonstrated that the model response of the second phase relative to the model response of the first phase was key in determining defibrillation success.

To determine how shocks such as those delivered in the previous protocol produce changes in activation patterns, a series of shocks were applied across the myocardium with and without a large discontinuity. A large discontinuity, as predicted by the secondary source hypothesis for defibrillation,⁸² should redistribute current at the time of the shock, producing activations at the site of the lesion. The major finding of this study

substantiates this hypothesis. Our results showed that shocks of both polarity are capable of producing secondary sources at the site of the discontinuity. The presence of the discontinuity induced a change in the spatial distribution of activations at the time of the shock. More tissue was activated when the lesion was present than when it was absent. Therefore, it is likely that myocardial discontinuities, pathological and physiological, contribute to changes in activation patterns at the time of the shock.

The presence of discontinuities in the myocardium may be beneficial if they lower the defibrillation threshold. Discontinuities placed in regions of the heart that are responsible for failed shocks may enhance the shock, producing a successful outcome. This notion was investigated in the final study. Using radiofrequency ablation, lesions were placed in the right atrium and left atrium to determine their effect on the shock. The major finding in this study is that atrial lesions reduce the atrial defibrillation threshold. Epicardial mapping and wavefront activation analysis showed that the level of organization of AF after RF ablation was greater than that before RF ablation. Furthermore, the activation patterns of the left atrium before and after RF ablation were more complex than those activation patterns observed on the right atrium. The analysis of postshock data showed that the type and frequency of earliest postshock activations changed after RF ablation. The data from this study suggest that changes in the atrial defibrillation threshold as a result of the lesion were likely due to an increase in the organization of atrial fibrillation. The contribution of secondary sources to the decrease in the atrial defibrillation threshold could not be conclusively established. Therefore, further work is needed to determine what role, if any, secondary sources, as demonstrated in the second study, play in the reduction of defibrillation thresholds as tested in the final study.

Limitations

All of the experiments performed in this dissertation used animal models, either dog or sheep. Therefore, our results and the conclusions drawn from our results must be interpreted carefully when relating to humans. Both the dog and sheep heart are structurally different from human hearts, are considerably smaller than human hearts, and possess conduction systems that are unique to each species.

In addition, the animals in our studies were healthy. Their hearts lacked the underlying disease present in human hearts prone to electrophysiological study. As a consequence, interpretation must be done cautiously. The parameters in our model may require adjustment if used in diseased hearts. The secondary sources observed in the second study may be altered by disease—a diseased heart may create a larger substrate for secondary sources. And finally, atrial fibrillation changes in nature as it evolves from an acute to a chronic state. Electrophysiologic changes occur, such as a shortening of the action potential and the refractory period, that favor both the induction and maintenance of AF; consequently, defibrillation thresholds and activation patterns are likely to change as the remodeling occurs.⁸³

There are also inherent limitations in the recording technique used in the last two protocols. Electrical mapping is limited in that only the extracellular potential is recorded. As such, our recordings are often complicated by stimulus artifact and electrode saturation following shocks. These limitations prevent us from analyzing several milliseconds of data immediately after a defibrillation shock. Therefore, non-propagating activations may have been present but not recorded at the time of the shock at the site of the discontinuities.

Research Implications

The first study presented demonstrated the ability of a simple model to predict the relative efficacy of defibrillation thresholds in dogs. Models such as this may be able to serve as an initial discriminator in choosing defibrillation waveforms for future clinical devices that allow for waveform selection. It is also beneficial in the research sector, potentially reducing the demand for animal experimentation. Perhaps its greatest asset is that the model is simple to use and can be applied to both internal and external defibrillation.

The second study showed that artificial lesions created in the myocardium can lead to activations at the site of the lesion at the time of the shock. The lesion in this study was created by making an incision in the ventricular wall. Therefore, these results may have implications for patients who have had cardiac surgery and ICD/pacemaker implantation. The results of our study have indicated that lesions, under the appropriate conditions, may produce activations as a result of shocks delivered from ICDs or pacemakers. At this time, the clinical impact of such a finding for patients is unclear.

As a result of many device manufacturers and clinicians wishing to lower the thresholds for defibrillation, the concept of hybrid therapies has become popular. The last of the studies presented has shown that radiofrequency ablation in conjunction with internal defibrillation aids in lowering the atrial defibrillation threshold. However, the likelihood of cardiologists creating lesions in the atria for the sole purpose of lowering the atrial defibrillation threshold seems possible but unlikely unless this technique can be improved to create greater reductions in defibrillation thresholds.

Future Research

It is unlikely that the perfect waveform for defibrillation has been discovered. The likelihood, however, of the perfect waveform revolutionizing defibrillation appears remote, but as models evolve into more realistic representations of the heart, waveform technology will likely improve as a result. The existing passive and active models have begun to merge and include more ion channels and cardiac kinetics.⁸⁴ The future of this field will likely involve the modification of mathematical models to include the latest experimental results.

We were able to show that a transmural lesion in the ventricle is capable of forming secondary current sources. Our lesion, however, was created in the same place and oriented with respect to the shocking electrodes the same way for all animals. Bidomain and secondary source studies have shown that there are numerous variables that affect the distribution of the activation patterns after a shock—among them are the field orientation with respect to fiber curvature, the fiber orientation, and the dimensions of the discontinuity.⁸⁵ All of these variables should be tested experimentally to determine their effect on secondary sources.

Our ability to assess secondary sources was based on the detection of activations adjacent to the myocardial discontinuities. With electrical mapping, the observation of direct activation is not possible, nor is the change in polarity associated with shocks. Optical mapping, however, provides information on direct activation as well as the polarity changes associated with the activation. Future studies should include optical mapping in order to determine the mechanism by which activations occur at discontinui-

ties. In particular, bidomain induced activations not easily explained by mere depolarization are of particular interest.

The atrial defibrillation study discussed in this dissertation is based on an acute model of AF. The same protocol should be applied to a chronic model of AF. Furthermore, ablation lesions should be placed in multiple locations, and defibrillation should be performed using multiple electrode configurations.

REFERENCES

1. Engelstein ED, Zipes DP. Sudden cardiac death. In: Alexander RW, Schlant RC, Fuster V, eds. *The Heart, Arteries and Veins*. New York: McGraw-Hill; 1998:1081-1112.
2. Myerburg RJ, Castellanos A. Cardiac arrest and sudden death. In: Braunwald E, ed. *Heart Disease: A Textbook of Cardiovascular Medicine*. Philadelphia: W.B. Saunders; 1997:742-779.
3. Reddy KS, Yusuf S. Emerging epidemic of cardiovascular disease in developing countries. *Circulation*. 1998;97:596-601.
4. Moss AJ, Hill WJ, Cannom DS, Daubert JP, Higgins SL, Klein H, Levine JH, Saksena S, Waldo AL, Wilbur D, Brown MW, Heo M, Multicenter Automatic Defibrillator Implantation Trial Investigators. Improved survival with an implanted defibrillator in patients with coronary disease at high risk for ventricular arrhythmia. *N Engl J Med*. 1996;335:1933-1940.
5. AVID Investigators. The antiarrhythmics versus implantable defibrillators (AVID) investigators: a comparison of antiarrhythmic drug therapy with implantable defibrillators in patients resuscitated from near fatal ventricular arrhythmias. *N Engl J Med*. 1997;337:1576-1583.
6. Kay GN, Mulholland DH, Epstein AE, Plumb VJ. Effect of pacing rate on the human atrial strength-duration curve. *J Am Coll Cardiol*. 1990;15:1618-1623.
7. Ideker RE, Wolf PD, Alferness CA, Krassowska W, Smith WM. Current concepts for selecting the location, size, and shape of defibrillation electrodes. *Pacing Clin Electrophys*. 1991;14:227-240.
8. Beck CS, Pritchard WH, Feil HS. Ventricular fibrillation of long duration abolished by electric shock. *Am J Med*. 1947;135:985-986.
9. Zoll PM, Linenthal AJ, Norman LR, Paul MH, Gibson W. Treatment of unexpected cardiac arrest by external electrical stimulation of the heart. *N Engl J Med*. 1956;254:541-546.
10. Lown B, Newman J, Amarasingham R, Berkovitz BV. Comparison of alternating current with direct current electroshock across the closed chest. *Am J Cardiol*. 1962;10:223-233.

11. Pelèska B. Optimal parameters of electrical impulses for defibrillation by condenser discharges. *Circ Res.* 1966;18:10-17.
12. Gurvich NL, Markarychev VA. Defibrillation of the heart with biphasic electrical impulses. *Kardiologiya.* 1967;7:109-112.
13. Walcott GP, Melnick SB, Chapman FW, Smith WM, Ideker RE. Comparison of damped sinusoidal and truncated exponential waveforms for external defibrillation. *J Am Coll Cardiol.* 1996;27:237A.
14. Geddes LA, Tacker WA Jr. Engineering and physiological considerations of direct capacitor-discharge ventricular defibrillation. *Med Biol Eng.* 1971;9:185-199.
15. Schuder JC, Stoeckle H, West JA, Keskar PY. Transthoracic ventricular defibrillation in the dog with truncated and untruncated exponential stimuli. *IEEE Trans Biomed Eng.* 1971;18:410-415.
16. Hoorweg JL. Electrical stimulation of the nerve. *Arch. f. d. ges. Physiol.* 1892;52:87-109.
17. Weiss G. A comparison of multiple waveforms used for cellular excitation. *Arch. Ital. de Biol.* 1901;35:413-446.
18. Lapicque L. Experimental definition of excitation. *Comptes Rendus Acad. Sci., Paris.* 1909;67:280-283.
19. Koning G, Schneider H, Hoelen AJ. Amplitude-duration relation for direct ventricular defibrillation with rectangular current pulses. *Med Biol Eng.* 1975;13:388-395.
20. Geddes LA, Tacker WA Jr., McFarlane J, Bourland J. Strength-duration curves for ventricular defibrillation in dogs. *Circ Res.* 1970;27:551-560.
21. Bourland JD, Tacker WA Jr., Geddes LA. Strength-duration curves for trapezoidal waveforms of various tilts for transthoracic defibrillation in animals. *Med Instrum.* 1978;12:38-41.
22. Feese SA, Tang ASL, Kavanagh KM, Rollins DL, Smith WM, Wolf PD, Ideker RE. Strength-duration and probability of success curves for defibrillation with biphasic waveforms. *Circulation.* 1990;82:2128-2141.
23. Kroll MW. A minimal model of the monophasic defibrillation pulse. *Pacing Clin Electrophysiol.* 1993;16:769-777.

24. Walcott GP, Walker RG, Cates AW, Krassowska W, Smith WM, Ideker RE. Choosing the optimal monophasic and biphasic waveforms for ventricular defibrillation. *J Cardiovasc Electrophysiol*. 1995;6:737-750.
25. Dixon EG, Tang ASL, Wolf PD, Meador JT, Fine MJ, Calfee RV, Ideker RE. Improved defibrillation thresholds with large contoured epicardial electrodes and biphasic waveforms. *Circulation*. 1987;76:1176-1184.
26. Tang ASL, Yabe S, Wharton JM, Dolker M, Smith WM, Ideker RE. Ventricular defibrillation using biphasic waveforms: The importance of phasic duration. *J Am Coll Cardiol*. 1989;13:207-214.
27. Swartz JF, Fletcher RD, Karasik PE. Optimization of biphasic waveforms for human nonthoracotomy defibrillation. *Circulation*. 1993;88:2646-2654.
28. Jones JL, Jones RE. Threshold reduction with biphasic defibrillator waveforms: Role of excitation channel recovery in computer model of the ventricular action potential. *J Electrocardiol*. 1991;23:30-35.
29. Chapman PD, Vetter JW, Souza JJ, Wetherbee JN, Troup PJ. Comparison of monophasic with single and dual capacitor biphasic waveforms for nonthoracotomy canine internal defibrillation. *J Am Coll Cardiol*. 1989;14:242-245.
30. Zipes DP, Fischer J, King RM, Nicoll A, Jolly WW. Termination of ventricular fibrillation in dogs by depolarizing a critical amount of myocardium. *Am J Cardiol*. 1975;36:37-44.
31. Chen P-S, Shibata N, Dixon EG, Martin RO, Ideker RE. Comparison of the defibrillation threshold and the upper limit of ventricular vulnerability. *Circulation*. 1986;73:1022-1028.
32. Kroll MW. A minimal model of the single capacitor biphasic defibrillation waveform. *Pacing Clin Electrophysiol*. 1994;17:1782-1792.
33. Swartz JF, Jones JL, Jones RE, Fletcher R. Conditioning prepulse of biphasic defibrillator waveforms enhances refractoriness to fibrillation wavefronts. *Circ Res*. 1991;68:438-449.
34. Jones JL, Jones RE, Milne KB. Refractory period prolongation by biphasic defibrillator waveforms is associated with enhanced sodium current in a computer model of the ventricular action potential. *IEEE Trans Biomed Eng*. 1994;41:60-68.
35. Jones JL, Tovar OH. The mechanism of defibrillation and cardioversion. *Proc IEEE*. 1996;84:392-403.

36. Daubert JP, Frazier DW, Wolf PD, Franz MR, Smith WM, Ideker RE. Response of relatively refractory canine myocardium to monophasic and biphasic shocks. *Circulation*. 1991;84:2522-2538.
37. Tomassoni G, Newby K, Deshpande S, Axtell K, Sra J, Akhtar M, Natale A. Defibrillation efficacy of commercially available biphasic impulses in humans. Importance of negative-phase peak voltage. *Circulation*. 1997;95:1822-1826.
38. Jones JL, Balasky G, Jones RE. Triphasic defibrillator waveforms decrease arrhythmias in myocardial cells. *Circulation*. 1986;74:II-185.
39. Chapman PD, Wetherbee JN, Vetter JW, Troup PJ. Comparison of monophasic, biphasic, and triphasic truncated pulses for non-thoracotomy internal defibrillation. *J Am Coll Cardiol*. 1988;11:57A.
40. Huang J, KenKnight BH, Rollins DL, Smith WM, Ideker RE. Defibrillation with triphasic waveforms. *Pacing Clin Electrophysiol*. 1997;20:1056.
41. Huang J, KenKnight BH, Smith WM, Ideker RE. Improved defibrillation efficacy with triphasic waveforms. *Circulation*. 1997;96:I-580.
42. Blair HA. On the intensity-time relations for stimulation by electric currents. II. *J Gen Physiol*. 1932;15:731-755.
43. Sweeney RJ, Gill RM, Jones JL, Reid PR. Defibrillation using a high-frequency series of monophasic rectangular pulses: observations and model predictions. *J Cardiovasc Electrophysiol*. 1996;7:134-143.
44. Swerdlow CD, Fan W, Brewer JE. Charge-burping theory correctly predicts optimal ratios of phase duration for biphasic defibrillation waveforms. *Circulation*. 1996;94:2278-2284.
45. Wharton JM, Wolf PD, Smith WM, Chen P-S, Frazier DW, Yabe S, Danieleley N, Ideker RE. Cardiac potential and potential gradient fields generated by single, combined, and sequential shocks during ventricular defibrillation. *Circulation*. 1992;85:1510-1523.
46. Zhou X, Daubert JP, Wolf PD, Smith WM, Ideker RE. Epicardial mapping of ventricular defibrillation with monophasic and biphasic shocks in dogs. *Circ Res*. 1993;72:145-160.
47. Shibata N, Chen P-S, Dixon EG, Wolf PD, Danieleley ND, Smith WM, Ideker RE. Epicardial activation following unsuccessful defibrillation shocks in dogs. *Am J Physiol*. 1988;255:H902-H909.

48. Frazier DW, Wolf PD, Wharton JM, Tang ASL, Smith WM, Ideker RE. Stimulus-induced critical point: Mechanism for electrical initiation of reentry in normal canine myocardium. *J Clin Invest*. 1989;83:1039-1052.
49. Walcott GP, Walcott KT, Knisley SB, Zhou X, Ideker RE. Mechanisms of defibrillation for monophasic and biphasic waveforms. *Pacing Clin Electrophysiol*. 1994;17:478-498.
50. Efimov IR, Cheng Y, Van Wagoner DR, Mazgalev T, Tchou PJ. Virtual electrode-induced phase singularity: a basic mechanism of defibrillation failure. *Circ Res*. 1998;82:918-925.
51. Kao CY, Hoffman BF. Graded and decremental response in heart muscle fibers. *Am J Physiol*. 1958;194:187-196.
52. Knisley SB, Smith WM, Ideker RE. Effect of field stimulation on cellular repolarization in rabbit myocardium: Implications for reentry induction. *Circ Res*. 1992;70:707-715.
53. Sweeney RJ, Gill RM, Steinberg MI, Reid PR. Ventricular refractory period extension caused by defibrillation shocks. *Circulation*. 1990;82:965-972.
54. Dillon SM. Optical recordings in the rabbit heart show that defibrillation strength shocks prolong the duration of depolarization and the refractory period. *Circ Res*. 1991;69:842-856.
55. Cohen IS, Falk RT, Kline RP. Voltage-clamp studies on the canine purkinje strand. *Proc Roy Soc B*. 1982;217:215-236.
56. Plonsey R, Barr RC. Inclusion of junction elements in a linear cardiac model through secondary sources: Application to defibrillation. *Med Biol Eng Comput*. 1986;24:137-144.
57. Krassowska W, Frazier DW, Pilkington TC, Ideker RE. Potential distribution in three-dimensional periodic myocardium: Part II. Application to extracellular stimulation. *IEEE Trans Biomed Eng*. 1990;37:267-284.
58. Fast VG, Rohr S, Gillis AM, Kléber AG. Activation of cardiac tissue by extracellular electrical shocks. Formation of 'secondary sources' at intercellular clefts in monolayers of cultured cells. *Circ Res*. 1998;82:375-385.
59. Sepulveda NG, Roth BJ, Wikswo JP Jr. Current injection into a two-dimensional anisotropic bidomain. *Biophys J*. 1989;55:987-999.
60. Knisley SB. Transmembrane voltage changes during unipolar stimulation of rabbit ventricle. *Circ Res*. 1995;77:1229-1239.

61. Wikswo JP Jr, Lin S-F, Abbas RA. Virtual electrodes in cardiac tissue: A common mechanism for anodal and cathodal stimulation. *Biophys J*. 1995;69:2195-2210.
62. Knisley SB, Baynham TC. Line stimulation parallel to myofibers enhances regional uniformity of transmembrane voltage changes in rabbit hearts. *Circ Res*. 1997;81:229-241.
63. Saypol JM, Roth BJ. A mechanism for anisotropic reentry in electrically active tissue. *J Cardiovasc Electrophysiol*. 1992;3:558-566.
64. Lin S-F, Roth BJ, Echt DS, Wikswo JP. Quatrefoil reentry in myocardium: An optical imaging study of the induction mechanism. *Pacing Clin Electrophysiol*. 1998;21:854.
65. Trayanova N. Discrete versus syncytial tissue behavior in a model of cardiac stimulation—I: Mathematical formulation. *IEEE Trans Biomed Eng*. 1996;43:1129-40.
66. Gillis AM, Fast VG, Rohr S, Kleber AG. Spatial changes in transmembrane potential during extracellular electrical shocks in cultured monolayers of neonatal rat ventricular myocytes. *Circ Res*. 1996;79:676-690.
67. White JB, Walcott GP, Pollard AE, Ideker RE. Myocardial discontinuities: A substrate for producing virtual electrodes to increase directly excited areas of the myocardium by shocks. *Circulation*. 1998;97:1738-1745.
68. Waldecker B, Brugada P, Zehender M, Stevenson W, Wellens HJJ. Dysrhythmias after direct-current cardioversion. *Am J Cardiol*. 1986;57:120-123.
69. Stoeckle H, Nellis SH, Schuder JC. Incidence of arrhythmias in the dog following transthoracic ventricular defibrillation with unidirectional rectangular stimuli. *Circ Res*. 1968;23:343-348.
70. Yabe S, Smith WM, Daubert JP, Wolf PD, Rollins DL, Ideker RE. Conduction disturbances caused by high current density electric fields. *Circ Res*. 1990;66:1190-1203.
71. Peleska B. Cardiac arrhythmias following condenser discharges and their dependence upon strength of current and phase of cardiac cycle. *Circ Res*. 1963;13:21-32.
72. Lesigne C, Levy B, Saumont R, Birkui P, Bardou A, Rubin B. An energy-time analysis of ventricular fibrillation and defibrillation thresholds with internal electrodes. *Med Biol Eng*. 1976;14:617-622.

73. Dahl CF, Ewy GA, Warner ED, Thomas ED. Myocardial necrosis from direct current countershock: Effect of paddle size and time interval between discharge. *Circulation*. 1974;50:956-961.
74. Tacker WA, Jr., Geddes LA, VanVleet JF. Cardiac damage produced by defibrillation. In: *Electrical Defibrillation*. Boca Raton, Fla: CRC Press; 1980:137-153.
75. Tovar O, Tung L. Electroporation of cardiac cell membranes with monophasic or biphasic rectangular pulses. *Pacing Clin Electrophysiol*. 1991;14:1887-1892.
76. Tung L. Electrical injury to heart muscle cells. In: Lee RC, Cravalho EG, Burke JF, eds. *Electrical Trauma: The Pathophysiology, Manifestation, and Clinical Management*. Cambridge: University of Cambridge Press; 1992:361-400.
77. Zhou X, Smith W, Rollins D, Ideker R. Transmembrane potential changes caused by shocks in guinea pig papillary muscle. *Am J Physiol*. 1996;271:H2536-H2546.
78. DeBruin KA, Krassowska W. Electroporation and shock-induced transmembrane potential in a cardiac fiber during defibrillation strength shocks. *Ann Biomed Eng*. 1998;26:584-596.
79. Krassowska W. Effects of electroporation on transmembrane potential induced by defibrillation shocks. *Pacing Clin Electrophysiol*. 1995;18:1644-1660.
80. Catherine M, Spencer K, Pagan-Carlo L, Smith R, Buettner G, Kerber R. Direct current shocks to the heart generate free radicals: an electron paramagnetic resonance study. *J Am Coll Cardiol*. 1996;28:1598-1609.
81. Teissié J, Rols M-P. An experimental evaluation of the critical potential difference inducing cell membrane electroporation. *Biophys J*. 1993;65:409-413.
82. Plonsey R, Barr RC. Effect of microscopic and macroscopic discontinuities on the response of cardiac tissue to defibrillating (stimulating) currents. *Med Biol Eng Comput*. 1986;24:130-136.
83. Wijffels M, Kirchhof C, Boersma L. Atrial fibrillation begets atrial fibrillation, A study in awake chronically instrumented goats. *Circulation*. 1995;92:1954-1968.
84. Luo C-H, Rudy Y. A dynamic model of the cardiac ventricular action potential. I. Simulations of ionic currents and concentration changes. *Circ Res*. 1994;74:1071-1096.
85. Trayanova N, Skouibine K, Aguel F. The role of cardiac tissue structure in defibrillation. *Chaos*. 1998;8:221-233.

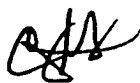
APPENDIX
ANIMAL USE APPROVAL

THE UNIVERSITY OF ALABAMA AT BIRMINGHAM

Office of the Executive Vice President and Provost
Institutional Animal Care and Use Committee
MEMORANDUM

DATE: October 1, 1996

TO: IDEKER, RAYMOND E.

FROM: Clinton J. Grubbs, PhD 
Chairman, Institutional Animal Care and Use Committee

SUBJECT: Notice of Approval

Title: CARDIA MAPPING OF VENTRICULAR DEFIBRILLATION

Agency: NIH

Committee Action Date: September 25, 1996

IACUC Protocol Number: 9603195

Species: DOG/GUINEA PIG

Stress Level: B

This application was reviewed and approved by the University of Alabama at Birmingham Institutional Animal Care and Use Committee (IACUC). Animal use is scheduled for review one year from the Committee Action Date noted above.

This institution has an Animal Welfare Assurance on file with the Office for Protection from Research Risks (Assurance Number A3255-01) and is registered as a Research Facility with the United States Department of Agriculture. Its animal care and use program is accredited by the Association for the Assessment and Accreditation of Laboratory Animal Care (AAALAC International).

As a condition of approval, the IACUC required the following modification(s) of this application:

- ☐ *Change in agent, dosage, route of administration, or schedule of administration*
- ☐ *Change in method or schedule of sample collection*
- ☐ *Change in pre- or postoperative care*
- ☐ *Change in endpoint*
- ☐ *Additional training for personnel*
- ☐ *Monitoring by Animal Resources personnel or by IACUC members*
- ☐ *Additional information or clarification*
- ☐ *See attached*
- ☒ *None*

Please forward this notice to the appropriate granting agency.

If you have any questions, call the IACUC office at 924-7692.

The University of Alabama at Birmingham
B10 Volker Hall • 1717 Seventh Avenue South
Birmingham, Alabama 35294-0019 • (205) 934-3553 • FAX (205) 934-1188



Recycled Recyclable

THE UNIVERSITY OF ALABAMA AT BIRMINGHAM

Office of the Executive Vice President and Provost
Institutional Animal Care and Use Committee
MEMORANDUM

DATE: July 2, 1997

TO: Ideker, Raymond

FROM: Clinton J. Grubbs, PhD
Chairman, Institutional Animal Care and Use Committee

SUBJECT: Notice of Approval

Title: Atrial Fibrillation/Defibrillation Project

Agency: Lilly

Committee Action Date: June 26, 1997

IACUC Protocol Number: 9703705

Species: Dogs/Sheep/Goats

Stress Level: B/B/B

The use of animals in the above referenced application was reviewed and approved by the University of Alabama at Birmingham Institutional Animal Care and Use Committee (IACUC). As part of this review, the following changes were required and have been satisfactorily addressed:

- ☐ Change in agent, dosage, route of administration, or schedule of administration
- ☐ Change in method or schedule of sample collection
- ☐ Change in pre- or postoperative care
- ☐ Change in endpoint
- ☐ Additional training for personnel
- ☐ Additional information or clarification
- ☐ See attached
- ☒ None

Animal use is scheduled for review one year from the Committee Action Date noted above.

This institution has an Animal Welfare Assurance on file with the Office for Protection from Research Risks (Assurance Number A3255-01) and is registered as a Research Facility with the United States Department of Agriculture. The animal care and use program is accredited by the Association for the Assessment and Accreditation of Laboratory Animal Care (AAALAC International).

Please forward this notice to the appropriate granting agency.

If you have any questions, call the IACUC office at 934-7692.

CJG/en

The University of Alabama at Birmingham
B10 Volker Hall • 1717 Seventh Avenue South
Birmingham, Alabama 35294-0019 • (205) 934-3553 • FAX (205) 934-1188



*updated
spread sheet
10/14/99*

NOTICE OF APPROVAL

DATE: September 29, 1999

TO: Raymond Ideker, MD, PhD
VH-B140 0019
FAX: 975-4720

FROM: Clinton J. Grubbs, PhD, Chairman *C.J.G.*
Institutional Animal Care and Use Committee

SUBJECT: Atrial Fibrillation/Defibrillation/Ablation Project, (Guidant), 990904512

On September 29, 1999, the University of Alabama at Birmingham Institutional Animal Care and Use Committee (IACUC) reviewed the animal use proposed in the above referenced application. It approved the use of the following species and numbers of animals:

Species	Use Category	Number in Category
Dogs	B	48
Sheep	B	80

Animal use is scheduled for review one year from September 29, 1999. Approval from the IACUC must be obtained before implementing any changes or modifications in the approved animal use.

Please keep this record for your files, and forward the attached letter to the appropriate granting agency.

Refer to Animal Protocol Number (APN) 990904512 when ordering animals or in any correspondence with the IACUC or Animal Resources Program (ARP) offices regarding this study. If you have concerns or questions regarding this notice, please call the IACUC office at 934-7692.

Institutional Animal Care and Use Committee
B10 Volker Hall
1717 7th Avenue South
205.934.7692
Fax 205.934.1188
iacuc@uab.edu

The University of
Alabama at Birmingham
Mailing Address:
VH B10
1530 3RD AVE S
BIRMINGHAM AL 35294-0019

**GRADUATE SCHOOL
UNIVERSITY OF ALABAMA AT BIRMINGHAM
DISSERTATION APPROVAL FORM
DOCTOR OF PHILOSOPHY**

Name of Candidate James Bradley White

Major Subject Physiology and Biophysics

Title of Dissertation An Analysis of Components Influencing the Outcome of

Defibrillation Shocks

I certify that I have read this document and examined the student regarding its content. In my opinion, this dissertation conforms to acceptable standards of scholarly presentation and is adequate in scope and quality, and the attainments of this student are such that he may be recommended for the degree of Doctor of Philosophy.

Dissertation Committee:

Name	Signature
<u>Dr. Raymond E. Ideker</u> , Chair	<u>Raymond E. Ideker</u>
<u>Dr. Kathleen H. Berecek</u>	<u>Kathleen H. Berecek</u>
<u>Dr. Jack M. Rogers</u>	<u>Jack M. Rogers</u>
<u>Dr. James A. Schafer</u>	<u>James A. Schafer</u>
<u>Dr. Gregory P. Walcott</u>	<u>Gregory P. Walcott</u>

Director of Graduate Program

Dean, UAB Graduate School

Date

11/19/99

William Seligson
Jean Loden